

# Investigation of "Whole Tree" Combustion in a Packed-Bed.

by

**ABDOULAYE OUEDRAOGO**

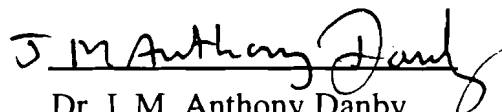
A dissertation submitted to the Graduate Faculty of  
North Carolina State University  
in partial fulfillment of the  
requirements for the Degree of  
Doctor of Philosophy


Department of Mechanical and Aerospace Engineering


Raleigh

1994

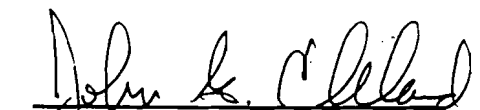
APPROVED By:

  
Dr. J. M. Anthony Danby

  
Dr. R. R. Johnson

  
Dr. M. N. Ozisik

  
Co-chair of Advisory Committee

  
Co-chair of Advisory Committee

## DEDICATION

This work is dedicated to my wife, ZOURATA OUEDRAOGO and son

CHECK ABBAS TEWENDE for their love and understanding.

## BIOGRAPHY

Mr. A. OUEDRAOGO holds a Licence de Physique (1977) de l' Université Chech Anta Diop de DAKAR (west Africa), a Maitrise de Recherche es Sciences Physiques Appliquées (1978) and a Diplome D' Etudes Approfondies (D.E.A.) D' Energie Solaire (1980) from the same University. Prior to joining (1987) the Institut de Mathematique et Physique now the Faculte des Sciences et Techniques de l' Université de OUAGADOUGOU (west Africa), Mr. A. OUEDRAOGO has work as managing officer for SOLAR POMPS (6 units of 1 KW Rankine Cycle type Pumps, known as Thermodynamics pumps and 1 Photovoltaic Pump of 4.5 KW) and latter earned (1986) a Master of Science in Mechanical Engineering Degree from the Department of Mechanical Engineering of the University of TUSKEGEE (U.S.A.) where he has investigated the use of bio-fuels in farm equipments.

## ACKNOWLEDGEMENTS

The author wishes to express his deepest appreciation and thanks to Dr. James C. Mulligan and Dr. John G. Cleland, Co-chairmen of his advisory committee, who have given their time generously in guiding and reviewing all the work.

The author wishes to thank Dr. M. N. Ozisik for exposing him to many new topics and for serving in his advisory committee.

The author also wishes to thank Dr. R. R. Johnson for fruitful discussions and for serving on his advisory committee.

The author also wishes to thank Dr. J. M. Anthony Danby for serving on his advisory committee.

The author would gratefully like to acknowledge the financial support and encouragement of the African-American Institute through the AFGRAD Fellowship.

Finally, the author wishes to thank his Parents and Parents-in-law for their understanding and encouragement, Idrissa Ouedraogo and Ron E. Burke for their constant support.

## TABLE OF CONTENTS

	Page
LIST OF FIGURES.....	ix
LIST OF TABLES.....	xii
<b>1. A quasi-steady shrinking core analysis of wood</b>	
<b>    combustion.....</b>	<b>1</b>
1.1 Abstract.....	2
1.2 Introduction.....	2
1.3 Shrinking core model.....	5
1.3.1 Equations of the shrinking core model.....	6
1.4 Modeling of the mass transfer coefficient	
and char layer thickness.....	9
1.4.1 Modeling of the mass transfer coefficient.....	9
1.4.2 Modeling of the char layer thickness.....	11
1.5 Model validation.....	13
1.6 Conclusion.....	15
1.7 References.....	31

1.8	Nomenclature.....	32
1.9	Appendix.....	33
1.9.1	Code for a single fuel element combustion model.....	34
2.	A quasi-steady state shrinking core model of "whole tree" combustion in a countercurrent fixed-bed reactor.....	43
2.1	Abstract.....	44
2.2	Introduction.....	44
2.3	Model development.....	46
2.3.1	Burning rate submodel.....	46
2.3.2	Conservation equations in the solid phase.....	49
2.3.3	Conservation equations in the gas phase.....	51
2.4	Results and discussion.....	53
2.5	Conclusion.....	55
2.6	References.....	78
2.7	Nomenclature.....	79
2.8	Appendix.....	82
2.8.1	Code for the quasi-steady model.....	83

3. Transient moving boundary shrinking core model of "whole tree" combustion in a countercurrent fixed-bed reactor.....	91
3.1 Abstract.....	91
3.2 Introduction.....	92
3.3 Upper region modeling : Preheat submodel.....	94
3.4 Solid phase combustion.....	97
3.4.1 Shell combustion submodel.....	97
3.4.2 Core drying and pyrolysis submodel.....	99
3.4.3 Core-shell interface modeling.....	100
3.5 Gas phase combustion.....	100
3.6 Numerical method : Finite Difference Approximation.....	101
3.6.1 Internal nodes.....	102
3.6.2 Convective boundary nodes.....	104
3.6.3 Centerline nodes.....	104
3.6.4 Interface nodes.....	105
3.6.5 Determination of the time step.....	105
3.6.6 Bed spatial grid.....	106
3.7 Continuous Mapping Variable Grid Method : <i>CMVGM</i> .....	106
3.8 Results and discussion.....	110
3.8.1 Preheat profile.....	110
3.8.2 <i>CMVGM</i> solution of the combustion model.....	111
3.9 Conclusion.....	113
3.10 References.....	127

3.11 Nomenclature..... 128

3.12 Appendix..... 132

    3.12.1 *CMVGM* code..... 133



## LIST OF FIGURES

		Page
Fig. 1.1	Fuel element model.....	17
Fig. 1.2	Energy balance at the char surface.....	18
Fig. 1.3	Energy balance at the core surface.....	18
Fig. 1.4	Fractional mass loss.....	19
Fig. 1.5	Normalized radial shrinking rate.....	20
Fig. 1.6	Burnout time of 10 mm cubic particles.....	21
Fig. 1.7	Variation of burnout time with radius.....	22
Fig. 1.8	Effect of moisture on burnout time.....	23
Fig. 1.9	Burnout time of small particles.....	24
Fig. 1.10	Moisture effect on average shrinking rate.....	25
Fig. 1.11	Char layer thickness of small particles.....	26
Fig. 1.12	Char layer thickness of 10 cm long chunkwood.....	27
Fig. 1.13	Surface temperature of 10 cm long chunkwood.....	28
Fig. 1.14	Surface temperature of 10 cm long chunkwood, $\alpha = 72\%$ .....	29
Fig. 1.15	Effect of moisture on particles burnout time.....	30
Fig. 2.1	"Whole tree" burn fuel conversion sequence.....	58
Fig. 2.2	"Whole tree" burn power plant.....	59
Fig. 2.3	Fuel cell.....	49
Fig. 2.4	Moisture effect on residence time.....	60
Fig. 2.5	Effect of fuel elements size on residence time.....	61
Fig. 2.6	Moisture effect on combustion zone depth.....	62

Fig. 2.7	Effect of fuel elements size on combustion zone depth.....	63
Fig. 2.8	Residence time of small particles.....	64
Fig. 2.9	Combustion zone depth of small particles.....	65
Fig. 2.10	Moisture effect on average shrinking rate.....	66
Fig. 2.11	Gas temperature, $R_o = 0.1016$ m, $\alpha = 100\%$ , $\gamma = 80\%$ .....	67
Fig. 2.12	Surface temperature, $R_o = 0.1016$ m, $\alpha = 100\%$ , $\gamma = 80\%$ .....	68
Fig. 2.13	Surface and gas temperatures, $R_o = 0.1016$ m, $\alpha = 80\%$ , $\gamma = 80\%$ ..	69
Fig. 2.14	Surface and gas temperatures, $R_o = 0.1016$ m, $\alpha = 100\%$ , $\gamma = 80\%$ ..	70
Fig. 2.15	Surface and gas temperatures, $R_o = 0.1016$ m, $\alpha = 100\%$ , $\gamma = 100\%$ ..	71
Fig. 2.16	Surface and gas temperatures, $R_o = 0.1016$ m, $\alpha = 100\%$ , $\gamma = 80\%$ . mc = 50%.....	72
Fig. 2.17	Surface and gas temperatures, $R_o = 0.1016$ m, $\alpha = 100\%$ , $\gamma = 80\%$ mc = 60%.....	73
Fig. 2.18	Oxygen concentration.....	74
Fig. 2.19	Normalized radial shrinking rate.....	75
Fig. 2.20	Effect of superficial gas velocity on residence time.....	76
Fig. 2.21	Effect of superficial gas velocity on combustion zone depth.....	77
Fig. 3.1	Interface and nearest core and shell nodes.....	119
Fig. 3.2	Computational domain : Variable fuel and bed grids.....	120
Fig. 3.3	Preheat profiles. $R_o = 0.1016$ m, mc = 33.3 %.....	121
Fig. 3.4	Preheat profiles. $R_o = 0.2540$ m, mc = 33.3 %.....	122
Fig. 3.5	Core and shell temperature profiles. $R_o = 0.1016$ m.....	123
Fig. 3.6	Core and shell temperature profiles. $R_o = 0.2540$ m.....	124
Fig. 3.7	Selected temperature profiles, $R_o = 0.1016$ m.....	125



## LIST OF TABLES

	Page
Table 1.1 Constant thermal properties.....	16
Table 2.1 Characteristics of the bed.....	56
Table 2.2 Constant thermal properties.....	57
Table 3.1 Constant thermal properties.....	114
Table 3.2 Bed depth of the two models.....	115
Table 3.3 Burnout time of the two models.....	116
Table 3.4 Oxygen concentration and preheated gas temperature at the bottom of the bed.....	117
Table 3.5 Heat of pyrolysis $h_p$ (KJ/Kg) as a function of fuel properties.....	118

# 1 A quasi-steady shrinking core analysis of wood combustion.\*

---

\* A short version of this work was submitted for publication in *Combustion and Flame*, (1994).

## 1.1 Abstract

A shrinking core model of the combustion of individual chunkwood and particle wood elements is developed and validated by comparison with literature data. The model is formulated on the physical evidence that large wood specimens inserted into a hot environment lose weight mostly over a relatively thin outside layer, while the interior (core) remains relatively undisturbed. The modeling of the complete process requires a correlation of the turbulent heat and mass transfer coefficients which includes the effects of transpiration of volatilized organic compounds and moisture, geometry, and shrinking radius. The fuel element burnout time is shown to be a function of fuel properties, moisture content and size. Drier and smaller elements burn faster while moisture is shown to slow the shrinking rate due to the cooling effects of transpiration and the latent heat of evaporation.

## 1.2 Introduction

Early analysis of wood decomposition and combustion were almost entirely concerned with pyrolysis reactions and the kinetics of small water-free samples because of the lack of data in these areas. The physics and heat transfer aspects were usually lumped into an apparent activation energy and frequency factor, and the entire decomposition process modeled following a first-order Arrhenius reaction. The temperature was obtained by solving the classical heat conduction equation with the heat of reaction as a source term. This approach, however, has been proven in recent years to be an oversimplification of the sequence of processes which actually occur, particularly for large samples. As the external surface of wood is exposed to a heat flux, the solid heats up at first mostly by transient conduction, although there is evidence of moisture migration and perhaps even convection in this phase. When the surface is hot enough, it starts to pyrolyze into volatiles and residual char. At a certain stage in the heating process, a network of cracks and fissures develops on the surface and propagates into the wood in association with the pyrolysis wave. The gases produced in the early pyrolysis flow back through the char layer, which becomes a zone of secondary reactions and heat exchange.

In the unfissured zone, volatile products are somehow trapped, increasing the internal pressure. A portion of the volatiles and moisture are forced toward the interior where vapors may condense and eventually re-evaporate as the pyrolysis front progresses. The process is seen to be extremely complex and, therefore, it has become customary to attempt to include such effects as transient diffusion and conduction, internal convection, heat generation and radiation energy, along with the Arrhenius decomposition, in the formulation of a burning model. Contrary to early formulations, it is now common practice to consider wood pyrolysis and combustion as a heat and mass transfer constrained process, either alone or combined with chemical kinetics. In fact, for large particles confined in a hot environment, the reaction rate is so great that the reaction itself is localized at the external surface of the fuel element and mass transfer becomes the rate controlling factor.

Blackshear and Kanury [1.1] used the similarities between the burning of cellulosic material in air and the burning of fuel-soaked wicks employing  $\text{CH}_3\text{OH}$ , whose driving force is known, to infer the heat and mass transfer coefficients of  $\alpha$ -cellulose cylinders. The mass flux is expressed in diffusion form as the product of the mass transfer coefficient and the driving force. It was found that the mass transfer coefficient, which is formulated as a product of a constant mass transfer coefficient without blowing and a driving force, is dependent upon the thickness of the pyrolyzing solid and time.

Maa and Bailie [1.2] are believed to be the first to apply the shrinking core model to the description of the pyrolysis of cellulosic material. The pyrolysis is assumed to take place at the surface of an unreacted shrinking core which is surrounded by a layer of material that has been pyrolyzed. The char in the char layer is assumed to be inert and does not undergo reaction. Hence, the reaction is taken to occur at the interface between the two solid regions. It is assumed that the thickness of the pyrolyzing zone is negligible and there is a sharp interface between the unreacted central core and the outer char layer. The unreacted core is modeled following the Arrhenius first-order decomposition equation. The temperature profile is obtained by solving the classical heat conduction equation with the addition of the bulk flow term with the shrinking core characteristics.

Saastamoinen and Richard [1.3] have also used a shrinking core formulation and obtained a total combustion time as a sum of the combustion time with infinitely fast chemical reaction and the combustion time with infinitely fast diffusion rate. The equation used for the diffusion coefficient is similar to that of Blackshear and Kanury but is expressed in terms of the mass flux, which is itself a function of the diffusion coefficient. Hence, unless an independent correlation can be found, no apparent closure exists for these relations.

Ragland et al. [1.4] followed a similar concept in modeling chunkwood, although the burning rate formulation was based on mass transfer considerations alone. The heat transfer equation used is a replica of the early models. The mass transfer equation was modeled following the evaporation of a single sphere in forced convection, hence is only a function of the fuel radius and flow characteristics. For unspecified reasons, however, the radius was kept constant as the fuel element shrinks, consequently the mass transfer coefficient remains constant for prescribed flow characteristics. The model is reported to predict the experimental findings of a constant shrinking rate of 1.8 mm / min. The burning rate is shown to depend on the chunkwood size but independent of its initial moisture content.

In this paper the shrinking core model is developed further and applied to the case of combustion of chunkwood and particle wood elements. The basic concept of an unreacted core is well established and assumed here. Additional assumptions will be discussed in the following sections. The present work differs from previous studies in that attention is focused primarily on the following elements:

- 1) The development of an appropriate mass transfer coefficient and its explicit correlation as a function of the transpiration of volatilized organic compounds and moisture, geometry and shrinking radius.
- 2) The quantitative evaluation of the fuel element moisture content on the burnout time.
- 3) The appropriate correlation of the heat transfer coefficient.



4) The complete modeling of the shrinking char layer and the possible replacement of the general thermal equations by quasi-steady balance equations at the char and core surfaces.

The work is divided into three main parts. First, a more complete theoretical basis of the shrinking core model is formulated. Secondly, the char layer thickness and the mass transfer coefficient are correlated using the experimental results of Ragland et al. [1.4] on the combustion of chunkwood and Simmons and Ragland [1.5] on the combustion of small cubes. Third, the results are compared with those of previous investigators.

### 1.3 Shrinking core model

Experimental observations have shown [1.6] that large cylindrical logs inserted into a hot environment lose weight over a relatively thin outside layer while the interior (core) remains relatively undisturbed. The logs lose weight due to transpiration of volatilized organic compounds and water vapor through their surface, leaving behind a char layer which also shrinks while reacting with oxygen in heterogeneous combustion. The decomposition and combustion of cellulosic material may then be regarded as the superposition of two physical processes. First, the thermal decomposition process, which is related to the accumulation and propagation of heat by conduction and convection. This process occurs with the passage of a pyrolysis wave and results in the internal release of volatiles and water vapor. Second, the combustion process, which consists of heterogeneous combustion of a surface char layer as well as the combustion of gaseous products (volatiles). The heat release then in turn sustains the combustion.

While physical evidence shows that pyrolysis and combustion processes of large porous fuel elements occur simultaneously [1.6], many investigators, have formulated models on the assumption of separate and distinct phases. Mukunda et al. [1.7] modeled the combustion of dried wooden spheres assuming two separate regimes. These were first, the flaming regime during which the spheres lose weight exclusively due to the loss of volatiles, followed by a glowing regime describing the surface combustion of porous char. The effects of blowing of volatiles and moisture (transpiration) are usually ignored

[1.4,1.7], or not explicitly accounted for [1.1-1.3]. The mass transfer coefficient proposed by Ragland et al. [1.4] is in fact a mass transfer coefficient without blowing and while it may be an approximation, it is not adequate in describing the simultaneous process of decomposition and combustion of cellulosic materials. Likewise, neither Blackshear and Kanury [1.1] nor Saastamoinen and Richard [1.3] explicitly correlated the overall mass transfer coefficient to account for both the effects of transpiration and oxygen diffusion. In analyzing the glowing combustion even for fuel particles as small as coal, Yoon et al. [1.8] began speaking of the concept of the three phases of drying, pyrolysis and combustion which, in reality, overlap.

To model the complete process, consider the motionless one dimensional fuel element sitting in a gravity-free environment shown in Figure 1.1 An unreacted shrinking core of radius  $r_w$  is surrounded by a char layer of thickness  $b_c$  and a gas film. The pyrolysis layer is assumed thin and, for simplicity the secondary reactions comprising the process of "cooking" and internal pressure build-up are ignored. Also, the heat of reaction of pyrolysis is neglected [1.9]. Because of differences in geometry between the model and actual three dimensional fuel elements, a geometry correction factor  $K$  is introduced to account primarily for end and corner effects on the overall transfer coefficients. The model fuel element is conceived from actual fuel elements [1.4] of yellow poplar and black spruce wood chunks of 7.5 cm radius and 5, 7.5 and 10 cm length, and 10 mm cubes of sugar pine [1.5]. The conditions of modeling of the heterogeneous combustion have been clearly postulated by Walker, Rusinko and Austin [1.10] in the three-temperature-zone theory. It is assumed in our model, however, that when the fuel elements are inserted into the hot environment, their surface temperature reaches instantly a quasi-steady state condition with the subsequent formation of a char layer. This excludes, of course, the short initial phase of transient warming to ignition.

### 1.3.1 Equations of the shrinking core model

Following Ragland et al. [1.4], the rate of mass loss may be written as

$$\frac{dm}{dt} = -i A \dot{m} \quad (1.1)$$

where  $m$  is the mass of the fuel element,  $A$  is the external surface area,  $i$  represents the stoichiometric index and  $\dot{m}''$  is the surface mass flux.

Defining the free stream oxygen concentration as  $C_\infty$  and the concentration at the fuel surface by  $C_s$ , the mass flux may be expressed in a form similar to that of Blakshear and Kanury [1.1], as the product of the overall mass transfer coefficient (the oxygen mass transfer coefficient modified by transpiration) and the driving force

$$\dot{m}'' = h_D (C_\infty - C_s) \quad (1.2)$$

The reaction rate at the surface is a function of the concentration of the oxidizer, which depends itself on the actual kinetics of the mechanism at the surface. If we assume this functional relationship to be of the form  $f(C_s)$ , then under stationary conditions, the reaction rate at the surface must be equal to the rate at which the reactant reaches the interface by diffusion [1.11]. That is,

$$\dot{m}'' = f(C_s) \quad (1.3)$$

Now, if the reaction is taken to be of first-order, Equation (1.3) may be explicitly written as

$$\dot{m}'' = K_p C_s \quad (1.4)$$

where  $K_p$  is the rate of chemical reaction. Combining equations (1.2) and (1.4) yields

$$\dot{m}'' = \frac{K_p h_D}{K_p + h_D} C_\infty \quad (1.5)$$

In their model, Saastamoinen and Richard [1.3] have computed the burnout time as a function of both the chemical reaction rate and diffusion rate. But if we assume the kinetic rate to be faster than the diffusion rate [1.12], which implies that  $K_p \gg h_D$  or that the process is controlled solely by diffusion, it is seen that

$$\dot{m}'' = h_D C_\infty \quad (1.6)$$

Substituting equation (1.6) into (1.1) yields

$$\frac{dm}{dt} = -i A h_D C_\infty \quad (1.7)$$

Furthermore, experimental evidence has shown that in a diffusion controlled environment the product of the heterogeneous char combustion is CO, and the conversion of CO to CO<sub>2</sub> takes place externally in the gas phase (gas film) [1.11]. The stoichiometric index, defined as the number of grams of fuel that burns with one gram of oxidizer, is then equal to (12/16). Finally, equation (1.7) becomes

$$\frac{dm}{dt} = -\left(\frac{12}{16}\right) A h_D C_\infty \quad (1.8)$$

We then make the approximation that the burnoff of the char layer may well offer a good estimate of the total burnout time of the fuel element. That is, we assume that the total mass of the solid that burns represents the fixed carbon, i.e.

$$i \dot{m}'' = \dot{m}_{char}''$$

Thus equation (1.8) is written as

$$\frac{dr}{dt} = -\left(\frac{12}{16}\right) h_D C_\infty / \rho_c \quad (1.9)$$

where  $r$  is the outside radius and  $\rho_c$  the char density. Neglecting the ash layer and writing the burning rate as a sum of the unreacted core shrinking rate and the diffusion limited char-oxygen surface reaction rate in Figure 1.1, it is seen that

$$\frac{dm}{dt} = \rho_c \frac{dv}{dt} + (\rho_w - \rho_c) \frac{dv_w}{dt} \quad (1.10)$$

where  $v$  is the volume of the fuel element. Applying equation (1.10) to the spherical fuel element in Figure 1.1 and expanding and rearranging yields

$$\frac{dm}{dt} = 4 \Pi [\rho_c r^2 \frac{dr}{dt} + (\rho_w - \rho_c)(r - b_c)^2 \frac{dr_w}{dt}] \quad (1.11)$$

where  $b_c$  is the char thickness,  $r_w = r - b_c$  the core radius, and the core density is expressed as [1.13]

$$\rho_w = S_g (1 + mc) \rho_{water}$$

$S_g$  is the specific density of wood and  $mc$  its moisture content (on wet basis) expressed in percent. The solution of these equations requires explicit relationships for the overall mass transfer coefficient and the char layer thickness.

## 1.4 Modeling of the mass transfer coefficient

### and char layer thickness

#### 1.4.1 Modeling of the mass transfer coefficient

As suggested by Blackshear and Kanury [1.1] the external boundary layer thickness and diffusional characteristics are constantly modified by the effects of blowing. Hence, the overall mass transfer coefficient is assumed to have the same form as in reference [1.1], wherein experimental results indicated the driving force is a function of the fuel elements size and time. The Reynolds number is assumed sufficiently high so that the mass transfer is turbulent. In an experimental study of the hydrodynamic and heat-transfer behavior of equilibrium and near-equilibrium turbulent boundary layers subject to blowing, Kays and Moffat [1.14] proposed the following correlation to described the effect of blowing:

$$\frac{St}{St_o} |_{R_{ex}} = \frac{b}{e^b - 1} \quad (1.12)$$

where  $St$  and  $St_0$  are the Stanton number with and without blowing measured at the same Reynolds number  $Re_x$ ,  $b$  is the blowing parameter. Applying these results to the fuel element in Figure 1.1 and using the experimental results of Simmons and Ragland [1.5] and Ragland et al. [1.4], the overall mass transfer coefficient may be correlated using a relation slightly different from that of Kays and Moffat to account for the physical differences between the two problems. That is

$$\frac{h_D}{h_D^*} = \frac{K b_1}{e^{b_2} - 1} \quad (1.13)$$

where  $b_1 = .766 mc r_o / r$  and  $b_2 = .573 mc r_o / r$

and the mass transfer coefficient without blowing  $h_D^*$  [1.15] is given as

$$h_D^* = 2.06 D Re_D^{.425} / 2r$$

This relationship is seen to be similar to the mass transfer coefficient in the Ragland's model [1.4], which is

$$h_D = D (2 + .6 Re^{1/2} Sc^{1/3}) / 2r \quad (1.14)$$

At high Reynolds number, the constant term (i.e. 2.) in this equation is negligible.

In equation (1.13),  $K$  is a geometry correction factor,  $D$  the molecular diffusivity,  $Re_D$  the Reynolds number,  $mc$  the moisture content of the logs, and  $r_o$  and  $r$  the initial and outside radii. The Schmidt number is taken to be equal to one. For cases of dried fuel elements, the mass transfer coefficient collapses to a corrected value of its no-blowing counterpart.

$$h_D = 2.75 K D Re_D^{.425} / 2r \quad (1.15)$$

The heat transfer coefficient is correlated from the mass transfer coefficient as

$$h = h_D \rho C \quad (1.16)$$

where  $\rho C$  is the volumetric heat capacity of air at the gas film temperature. The transpiration gases are assumed ideal. We still need an explicit relation for the char layer thickness which will be shown to be a function of the surface temperature of the fuel elements and the rate at which the pyrolysis front progresses.

## 1.4.2 Modeling of the char layer thickness

A quasi-steady state condition is assumed within the fuel elements. The core temperature is taken to be uniform and equal to the ambient temperature. Clearly, this assumption is justified during most of the combustion process due to the size of the fuel elements. It certainly becomes critical near the end of the combustion, but it is believed that this will not significantly affect the determination of the burnout time (defined as the time of a given percentage of initial weight loss). This assumption also ensures that the surface temperature remains the only unknown.

An energy balance at the char surface, figure 1.2, labeling  $V$  and  $V_w$  respectively the regression velocities of the core and char and  $A_w$  and  $A$  their surface areas, yields

$$[\rho_c + \alpha \rho_v] H_{as} VA - hA (T_s - T_\infty) - \rho_w V_w [\epsilon_c C_{p_c} + \epsilon_v C_{p_v} + \epsilon_m C_{p_m}] (T_s - T_i) A_w = \frac{k_c (T_s - T_i)}{b_c} A_c + q'' \quad (1.17)$$

where 
$$H_{as} = \frac{[\rho_c H_c + \alpha \rho_v H_v]}{\rho_c + \alpha \rho_v} \beta$$

and 
$$\left(\frac{A}{A_w}\right) = \left(\frac{r}{r - b_c}\right)^2 \quad V_w = -\frac{dr_w}{dt} \quad V = -\frac{dr}{dt}$$

Recall that under boundary layer diffusion control, the char goes only to incomplete combustion at the char-gas interface. Also it is known that of all the volatiles released, sometimes only a fraction  $\alpha$  burn incompletely at the gas-solid interface and the re-

mairder escapes to the gas phase. Hence,  $H_{as}$  represents the average incomplete heat of combustion of the char and volatiles at the interface.

In equation (1.17), the first term on the left represents the total heat released by the combustion, the second term is the convected energy between the combustion front and the gas phase, and the third term represents the internal convected energy through the char towards the unreacted core. The first and second terms on the right are respectively the heat transported by thermal conduction away from the combustion zone and the radiative exchange between the surface of the solid media and the furnace walls, assuming the flue-gas to be non-participative. Basically the equation expresses the fact that the net heat exchange between the gas and solid phase represents the enthalpy of combustion of the char and volatiles. To keep the formulation simple, the existence of thermal equilibrium between the two phases is assumed.

Now consider the energy balance at the core surface, figure 1.3. The energy entering the core is assumed sufficient enough to heat it up to pyrolysis with the subsequent transpiration of organic compounds and moisture due to the phase change of active material to pyrolysis gas ( $hfg_v$ ) and liquid water to water vapor ( $hfg_m$ ).

$$q_w V_w A_w [ \epsilon_v hfg_v + \epsilon_m hfg_m ] = \frac{k_c (T_s - T_i)}{b_c} A_c \quad (1.18)$$

As it is, equations (1.17) and (1.18) represent a quasi-steady state formulation of a moving boundary type problem since the core-char interface changes its position continuously due to pyrolysis with the subsequent phase-change of active matters and moisture respectively to volatiles and water vapor. The core being at uniform temperature throughout, only the surface temperature is unknown. Hence, the problem is a one-phase problem (ablation) sometimes referred to as a "Stefan problem".

Combining equations (1.17) and (1.18) yields the surface temperature  $T_s$ . The thermal radiation term has been neglected compared to the other thermal quantities. Hence,



$$T_s - T_i = \frac{[\rho_c + \alpha \rho_v] H_{as} V \left( \frac{A}{A_w} \right) + h \left( \frac{A}{A_w} \right) (T_\infty - T_i) - \rho_w V_w (\epsilon_v hfg_v + \epsilon_m hfg_m)}{h \left( \frac{A}{A_w} \right) + \rho_w V_w \sum_{j=1}^3 \epsilon_j C_{pj}} \quad (1.19)$$

where  $j = m, c, v$ .

Now after some manipulations in equation (1.18) where  $A_c$  is the log-mean area and neglecting higher order terms,  $b_c$  is obtained. It is clearly seen that the char layer thickness is a function of the surface temperature and the core shrinking rate. That is,

$$b_c = \frac{k_c (T_s - T_i)}{\rho_w V_w (\epsilon_v hfg_v + \epsilon_m hfg_m) + \frac{k_c (T_s - T_i)}{r}} \quad (1.20)$$

## 1.5 Model validation

In their experiments, Ragland et al. [1.4] measured a char layer thickness of 3 mm and 15 mm respectively for green and air-dried chunkwood of 15 cm diameter. For practical purposes then, a solution for a thin char layer approximation may be sufficient. Under this assumption, the core and surface recession velocities are assumed to have approximately the same magnitude. However, both this assumption and the uniform core temperature approximation may become critical towards the end of the combustion. We also assume constant thermal properties and negligible radiation transfer.

Instead of a classical moving boundary type solution, the thin char layer approximation is solved by a simple iterative procedure using the constant thermal properties given in table 1.1 Logs of radius equal to 0.2540 m (10 inches) down to particles of 0.10 mm radius have been tested at various moisture content and selected results are presented. Whenever possible, these results are compared with literature data. All the volatiles are assumed to go to incomplete combustion at the char surface (i.e.,  $\alpha = 1$ ).

Figure 1.4 shows a plot of the fractional mass loss of 15 cm diameter wood chunks (10 cm long) at 20 and 75 % moisture for both the present model and the model used by Ragland and al. to investigate their experimental data. The burnout time was said to be

32 min for both values of moisture but this value is shown to fall approximately between the values of our model. This is clearly shown in Figure 1.5, where the averaged experimental radial shrinking rate is plotted together with our model curve. This averaging process seems to have precluded the observation of any difference between the experimental data at the two moistures and may have smoothed out any moisture effect. Recognizing the difficulties of properly accounting for the complete burnout time of the chunkwood after a 30 % initial mass loss, the investigators concluded that it appears that moisture has little effect on the rate of combustion at the conditions of these tests. Also by neglecting the blowing effect and keeping the mass transfer coefficient constant in equation (1.9), one would naturally expect to get a constant shrinking rate (1.8 mm / min here) regardless of the initial moisture content of the fuel elements.

Using additional data, the burnout time of small cubic particle elements of 10 mm size at 15 and 240 % moisture is plotted in Figure 1.6. Here again, the model shows good agreement with the experimental data of Simmons and Ragland [1.5] and it is clearly stated by the authors that the presence of moisture does slow the mass loss rate. If we let the fuel elements shrink indefinitely or longer than needed, they would seem to have the same burnout time. We should keep in mind, however, that the burnout time is an asymptotic value which for practical purposes should be clearly defined as the time corresponding to a mass loss of 99 %, since it will not make sense on physical grounds to have a solid media whose mass shrinks to zero.

The validated mass transfer coefficient is then used to investigate further the effect of fuel elements size and moisture content on the burnout time  $t_b$ . As was anticipated, the burnout time is function of the diameter of the logs for a given moisture content, Figure 1.7. It is also shown in Figure 1.8 to be both a function of the fuel element size and moisture content contrary to earlier publications [1.4]. The thicker and greener elements take longer to burnout. Also, for a given log the burnout time is not rigorously a simple linear function of its moisture content. As a matter of fact, the burnout time varies from 40 to 60 min for logs of 0.1016 m (4 inches) radius at 15 and 75 % moisture respectively, but increases approximately threefold between the same moisture for logs of 0.2540 m (10 inches) radius. Thus, the effects of moisture are more sensible for large size fuel elements than for small ones. It is known that free-water molecules are easily

removed, while bound water molecules in the inner trunks especially when the diameters are large, become harder to remove. These smooth variations become somehow erratic for small samples, Figure 1.9. This was certainly expected and is speculated to be caused by both the uniform core temperature assumption and the thin char layer approximation.

Finally, moisture definitely slows the shrinking rate, which is shown to vary from approximately 2 mm / min at 20 % moisture content to 1.25 mm / min at 70 % moisture content for a chunkwood of 0.1016 radius Figure 1.10. As predicted by the model, Figure 1.11 and 1.12 (moisture content equal 33.3 %) show that  $b_c$  varies not only with the log radius but also shrinks with time while reacting with oxygen. The same best fit value of 0.60 for  $K$  has been used for all chunkwood samples, and a slightly lower value of 0.40 for the cubic particles, due to the difference between the two shapes. The surface temperature of the 15 cm diameter chunkwood, Figure 1.13, is quite similar to that found by Ragland et al. [1.4] especially for lower values of  $\alpha$  (72 %), figure 1.14. The model not only predicts the burnout time of chunkwood and cubic particles but also the burnout time of particles as small as 0.10 mm radius. Figure 1.15 shows that it takes about 1 min to combust particles of 10 mm radius (the same burnout time approximately is obtained for the 10 mm cubic particles in Figure 1.6) while 0.10 mm particles burn instantly.

## 1.6 Conclusion

The overall mass transfer coefficient correlation in this study is shown to be the central element of the shrinking core model. Under boundary layer diffusion control, the external boundary layer thickness and diffusional characteristics are constantly modified by the effects of blowing. Hence, for green wood specimens, the cooling effects of transpiration of organic compounds and moisture and the latent heat of evaporation do slow the burning rate contrary to earlier publications. These chilling effects are found to increase with the amount of moisture content and fuel elements size. The model is simple and yet reliable enough to predict adequately the burnout time of chunkwood and particle fuel elements of different sizes and shapes. Additionally, the model may be used as well to investigate the combustion of coal of different sizes and moisture content.

Table 1.1 Constant thermal properties

Properties	Values	Units	References
$C_{\infty}$	0.049	$\text{Kg/m}^3$	1.4
$C_{pc}$	0.670	$\text{KJ/Kg}^{-\circ}\text{K}$	1.16
$C_{pm}$	4.20	$\text{KJ/Kg}^{-\circ}\text{K}$	
$C_{pv}$	1.1	$\text{KJ/Kg}^{-\circ}\text{K}$	1.16
$D$	$3.15 \times 10^{-4}$	$\text{m}^2/\text{sec}$	1.4
$hfg_m$	2250	$\text{KJ/Kg}$	
$hfg_v$	200	$\text{KJ/Kg}$	
$H_c$	31,100	$\text{KJ/Kg}$	1.17
$H_v$	13,500	$\text{KJ/Kg}$	1.18
$K_c$	$0.41 \times 10^{-4}$	$\text{KW/m}^{-\circ}\text{K}$	1.16
$Re_D$	17,400r	-	1.4
$\rho_c$	95	$\text{Kg/m}^3$	1.4
$S_g$	0.46	-	1.4
$T_i$	25	$^{\circ}\text{C}$	
$T_{\infty}$	1200	$^{\circ}\text{C}$	1.4

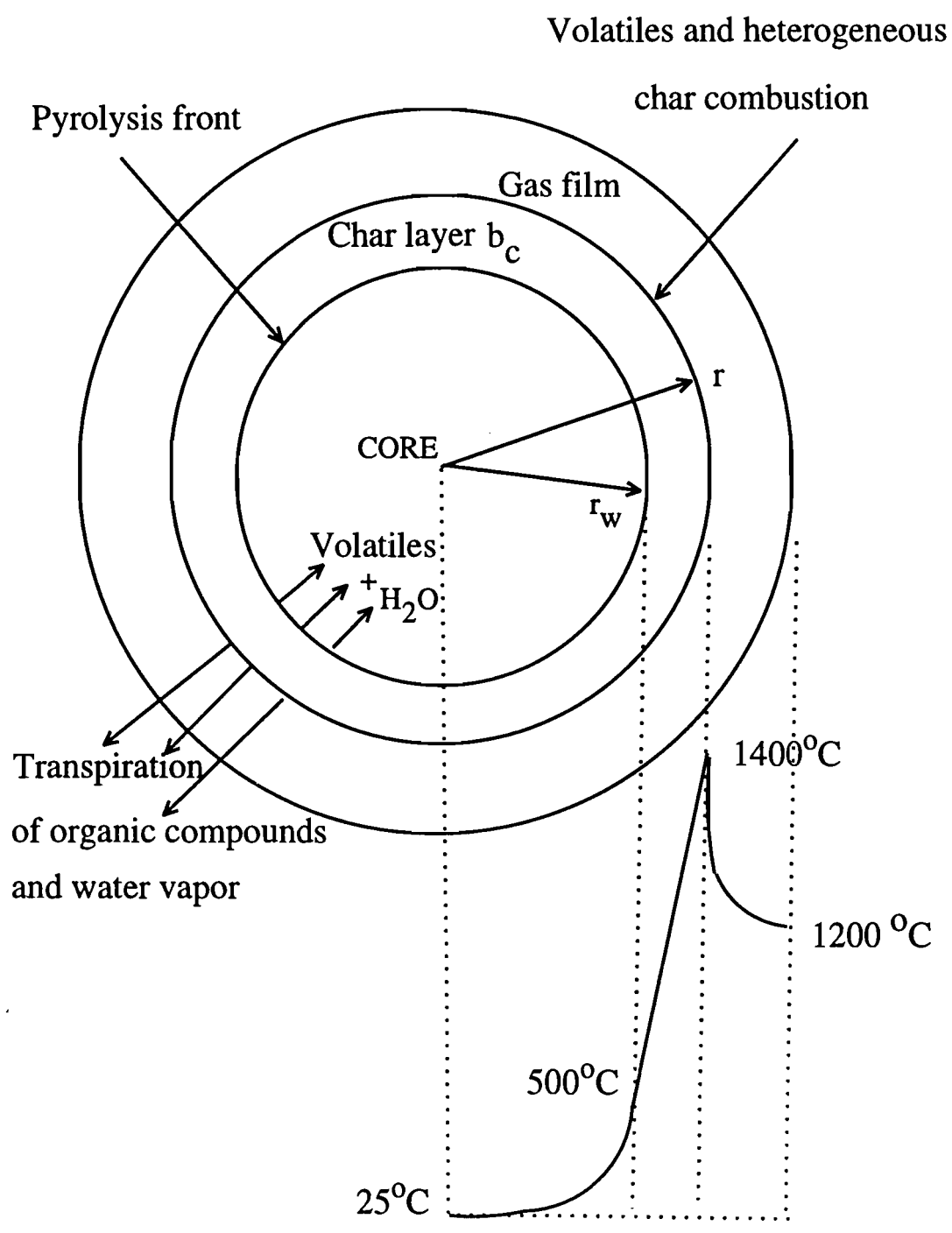


Fig. 1.1 : Fuel element model

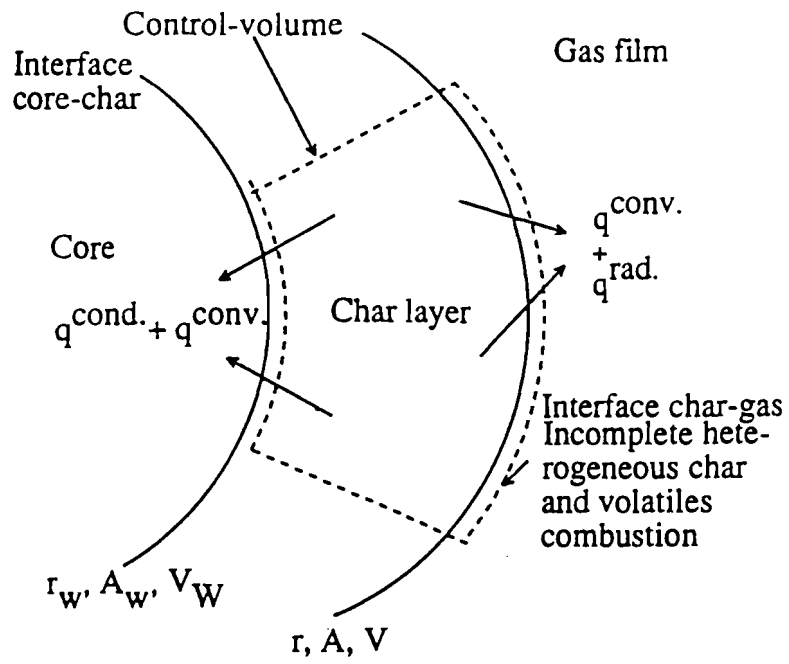


Fig. 1.2 : Energy balance at the char surface

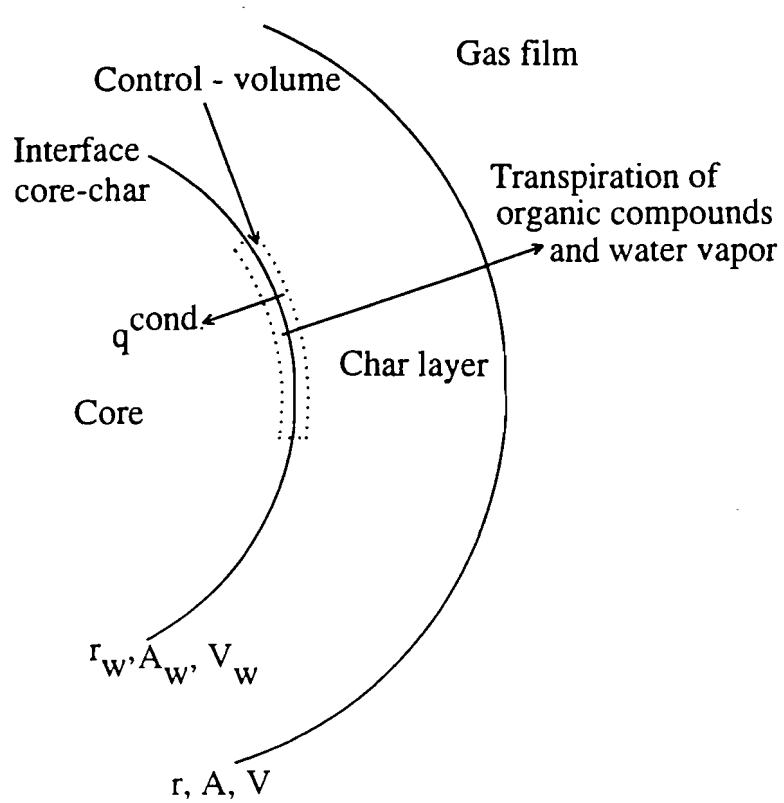


Fig.1.3 : Energy balance at the core surface

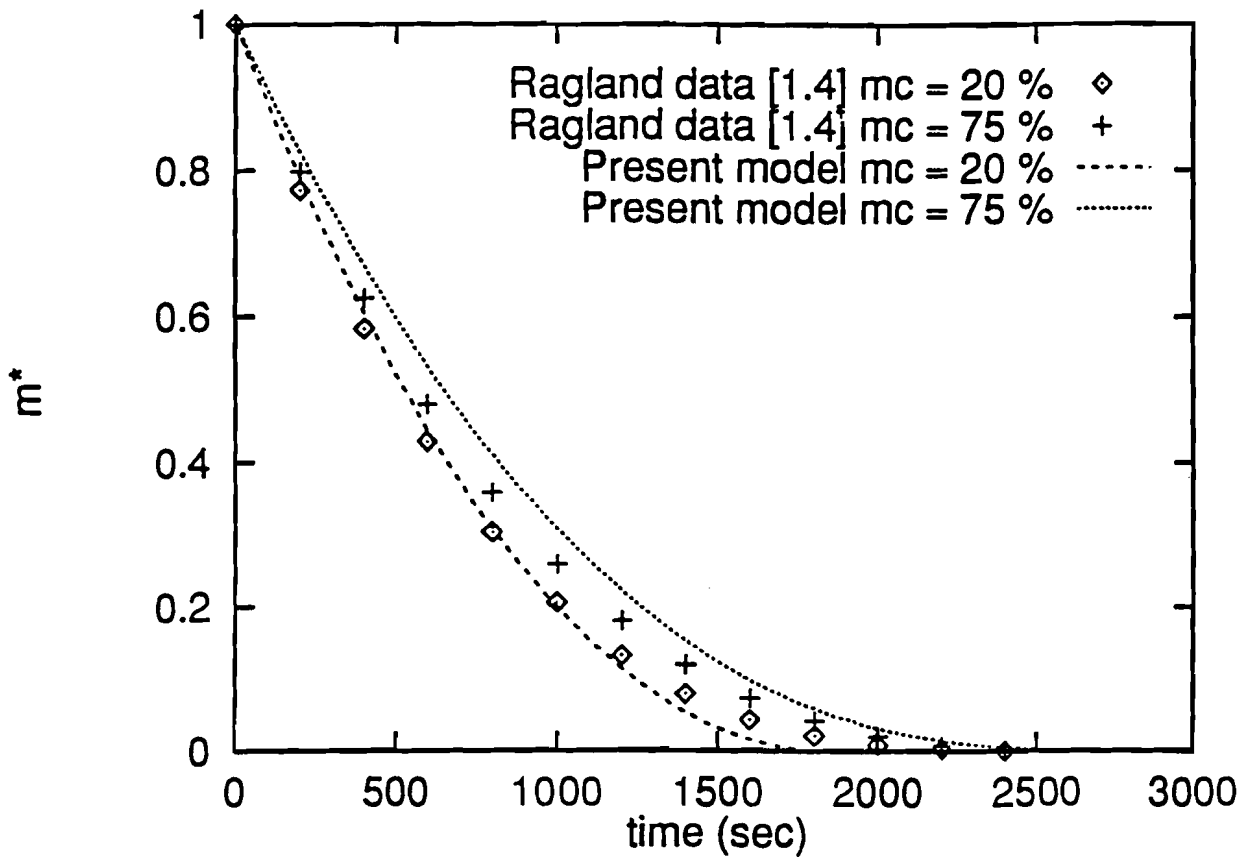


Fig. 1.4 : Fractional mass loss

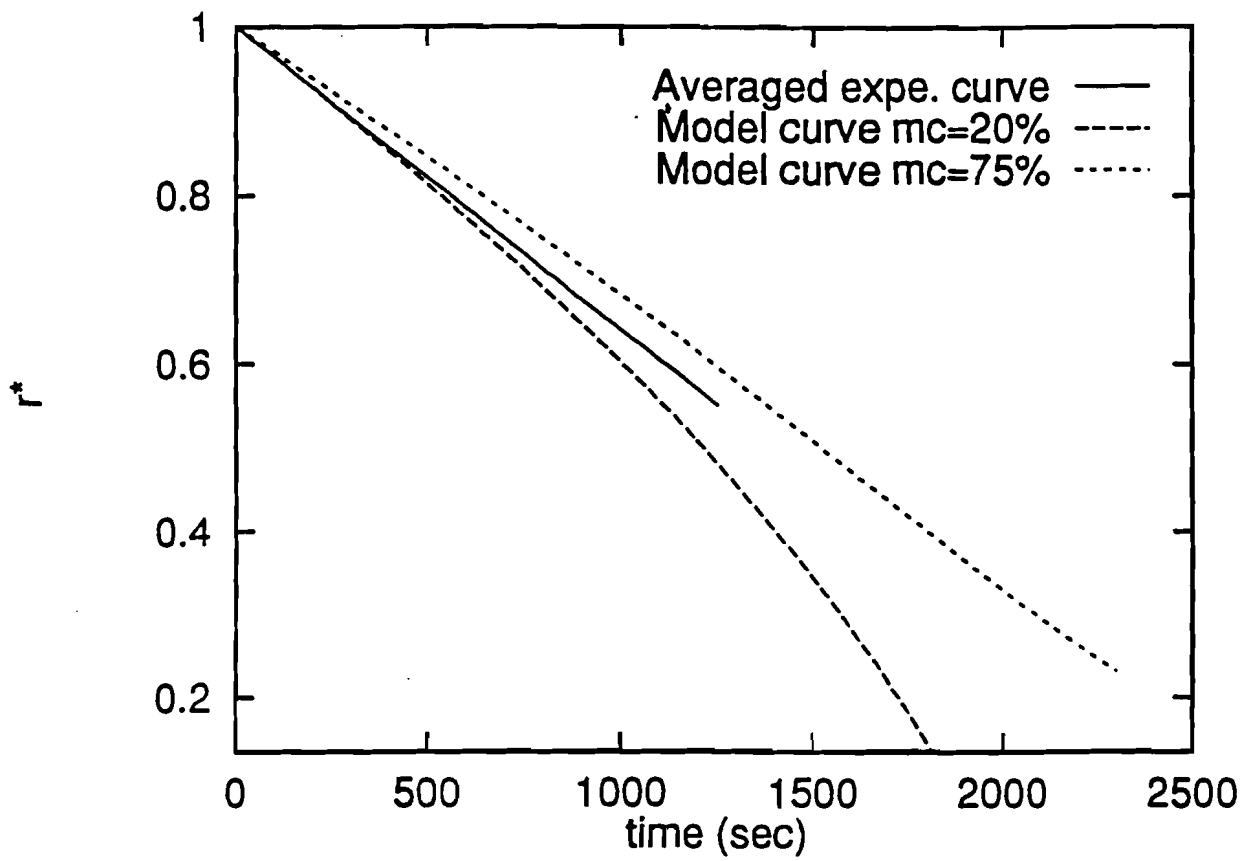


Fig. 1.5 : Normalized radial shrinking rate



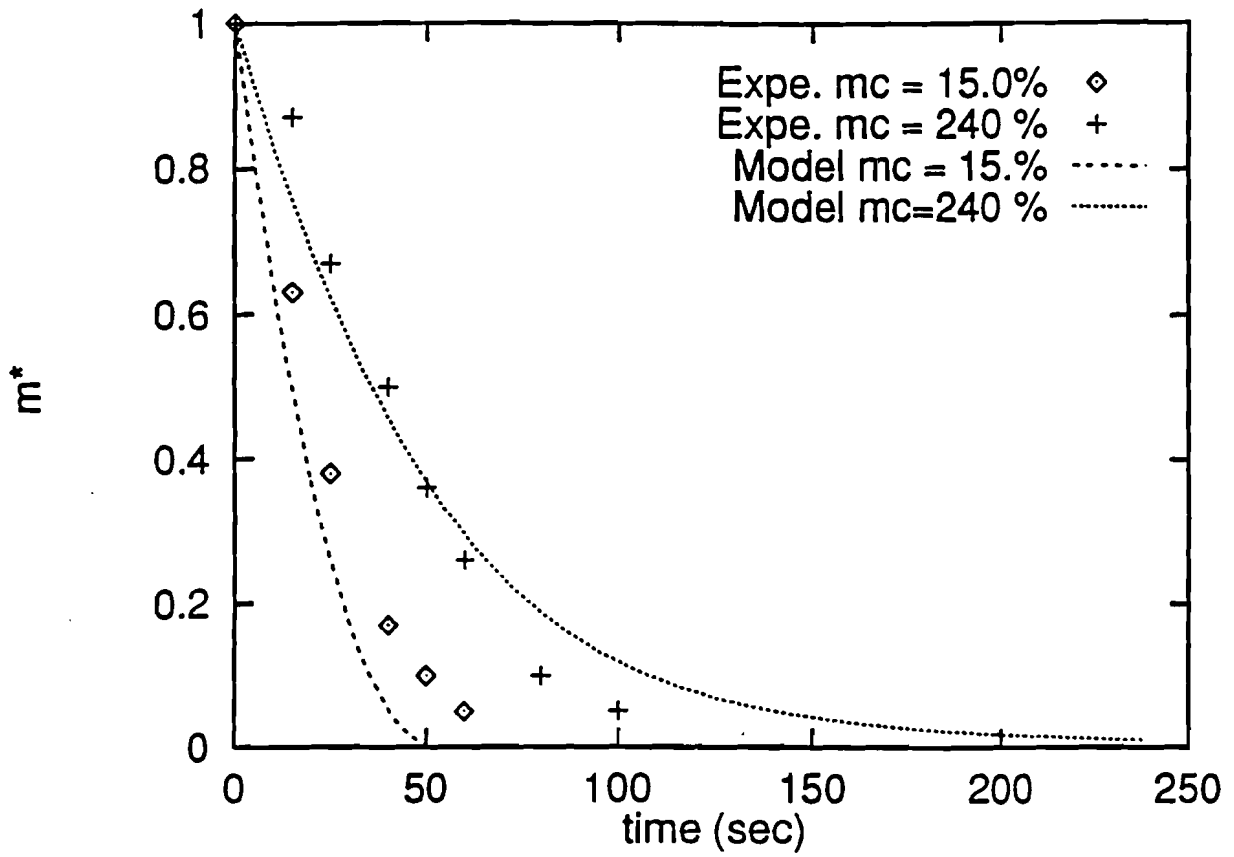


Fig. 1.6 : Burnout time of 10 mm cubic particles

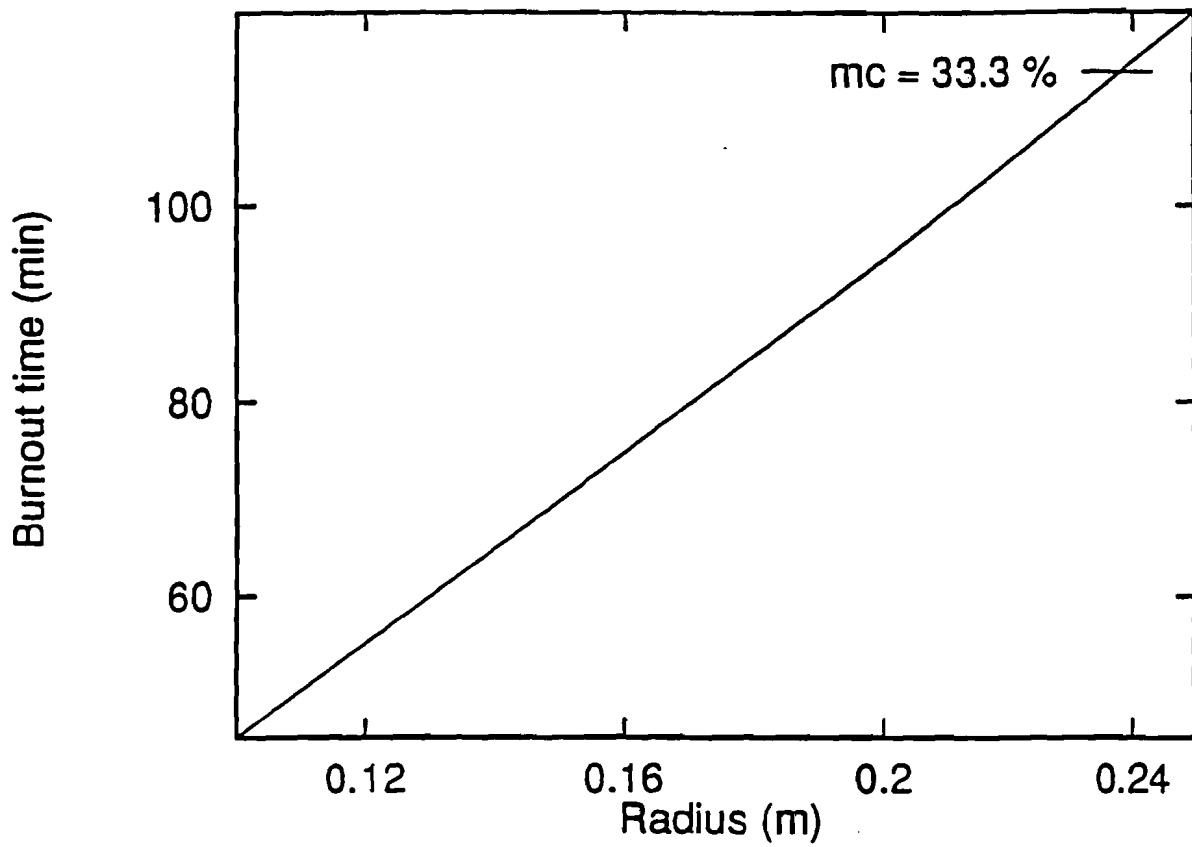


Fig. 1.7 : Variation of burnout time with radius

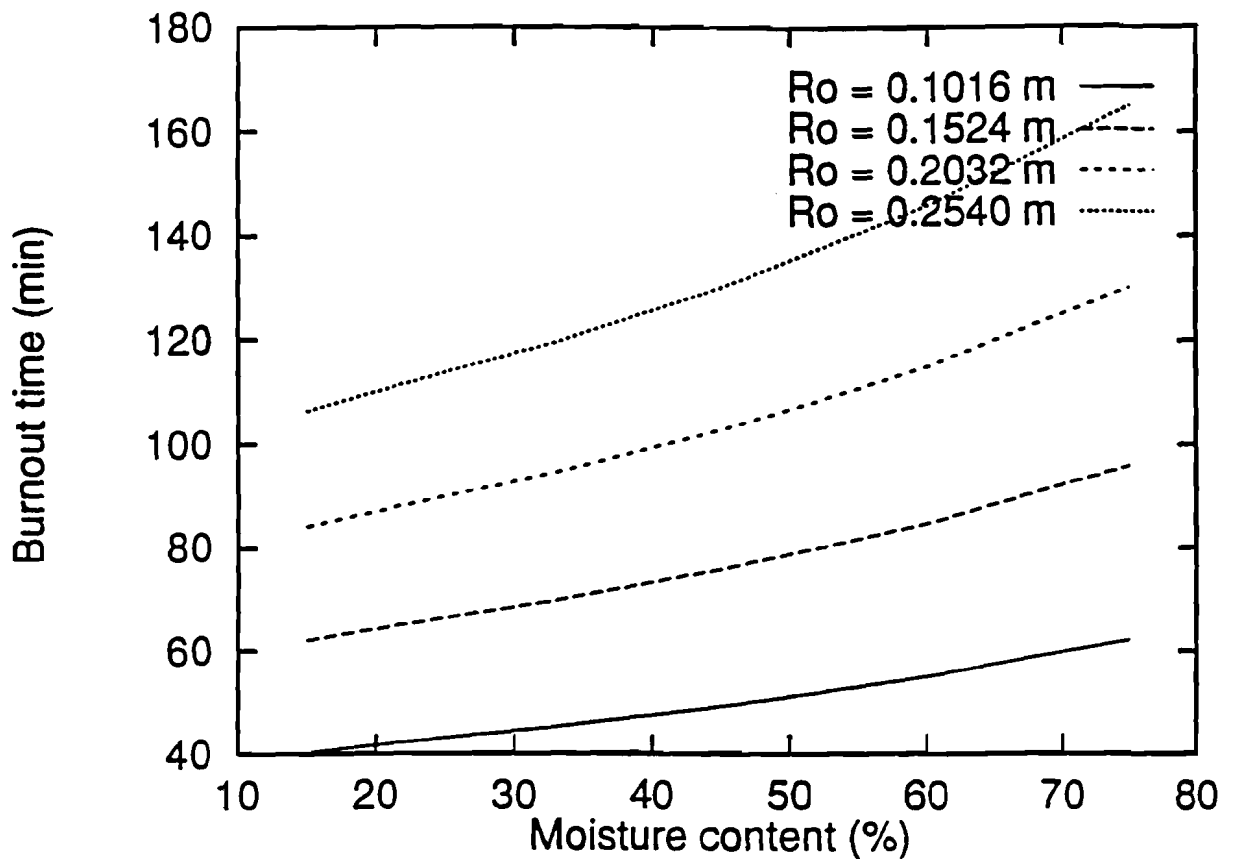


Fig. 1.8 : Effect of moisture on burnout time

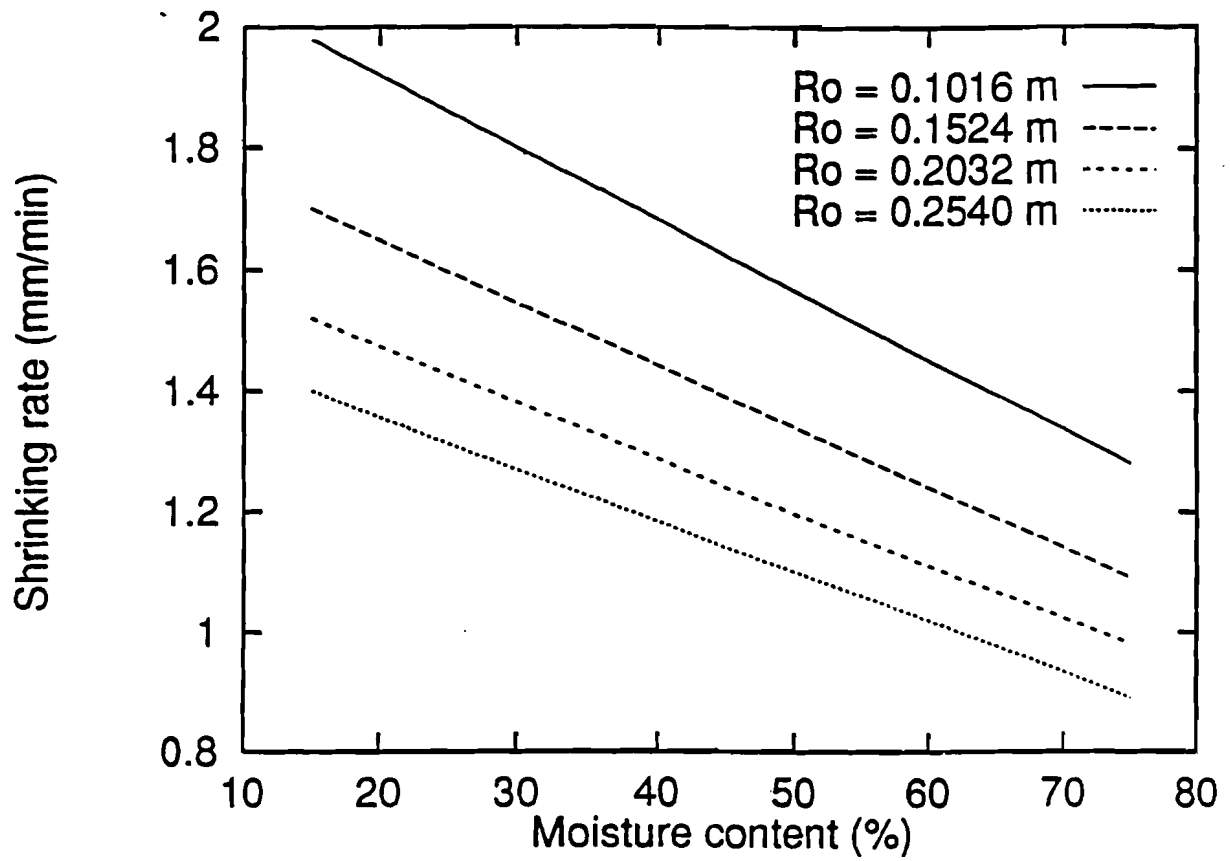


Fig. 1.10 : Moisture effect on average shrinking rate

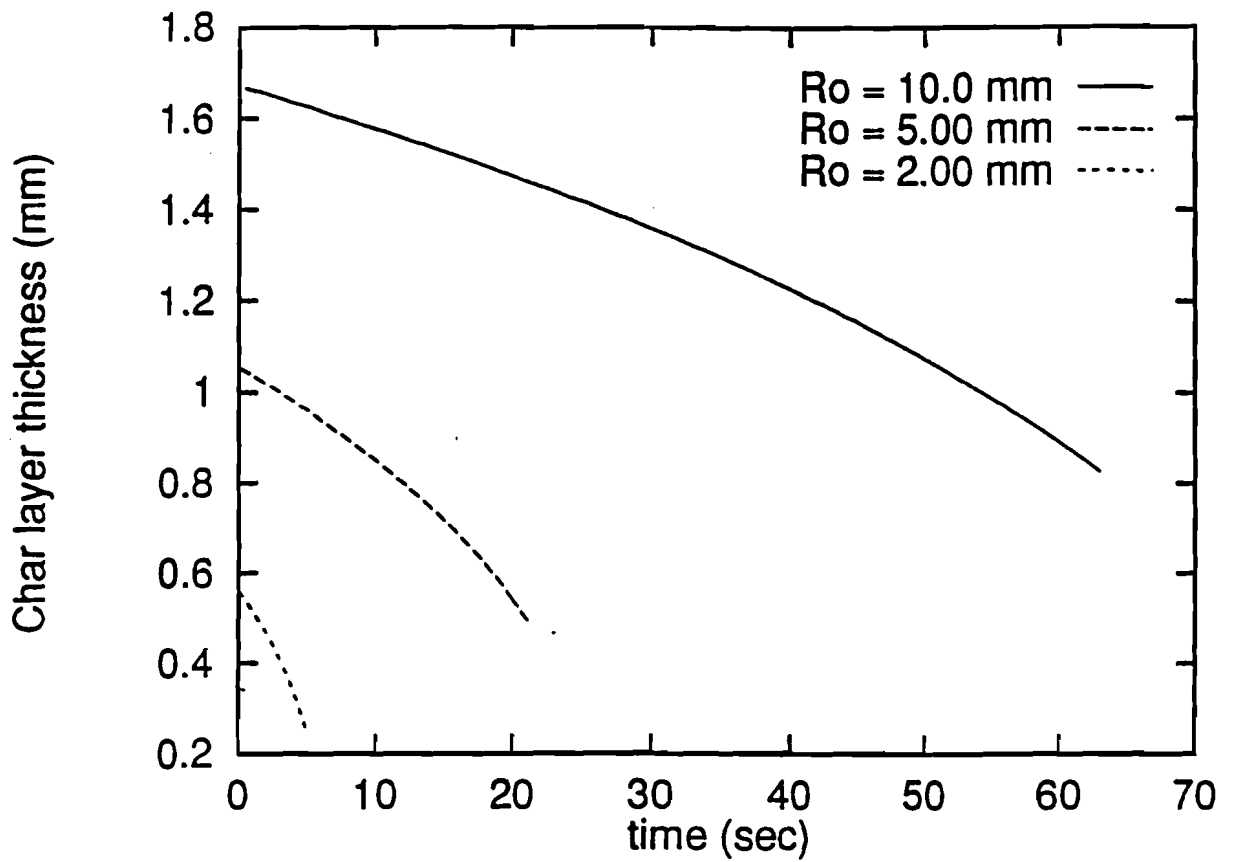


Fig. 1.11 : Char layer thickness of small particles

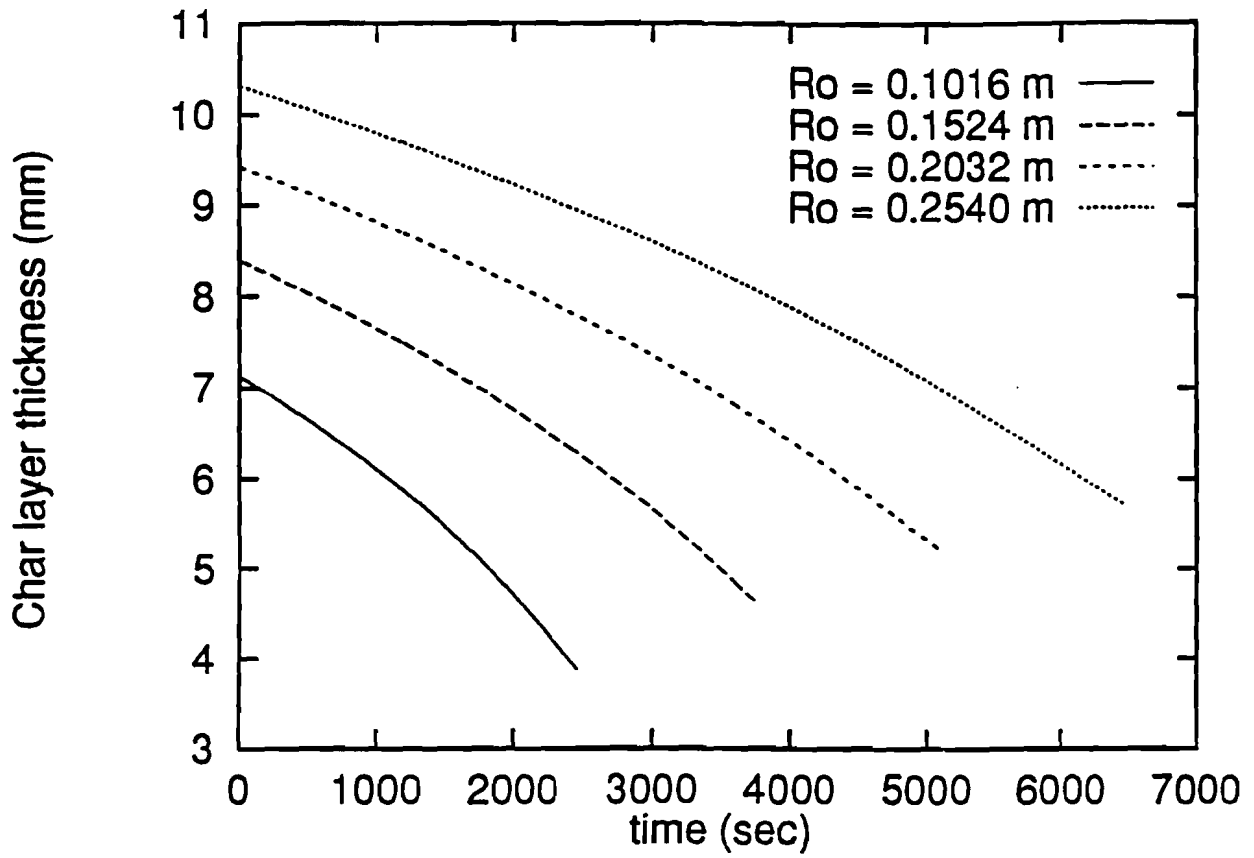


Fig. 1.12 : Char layer thickness of 10 cm long chunkwood

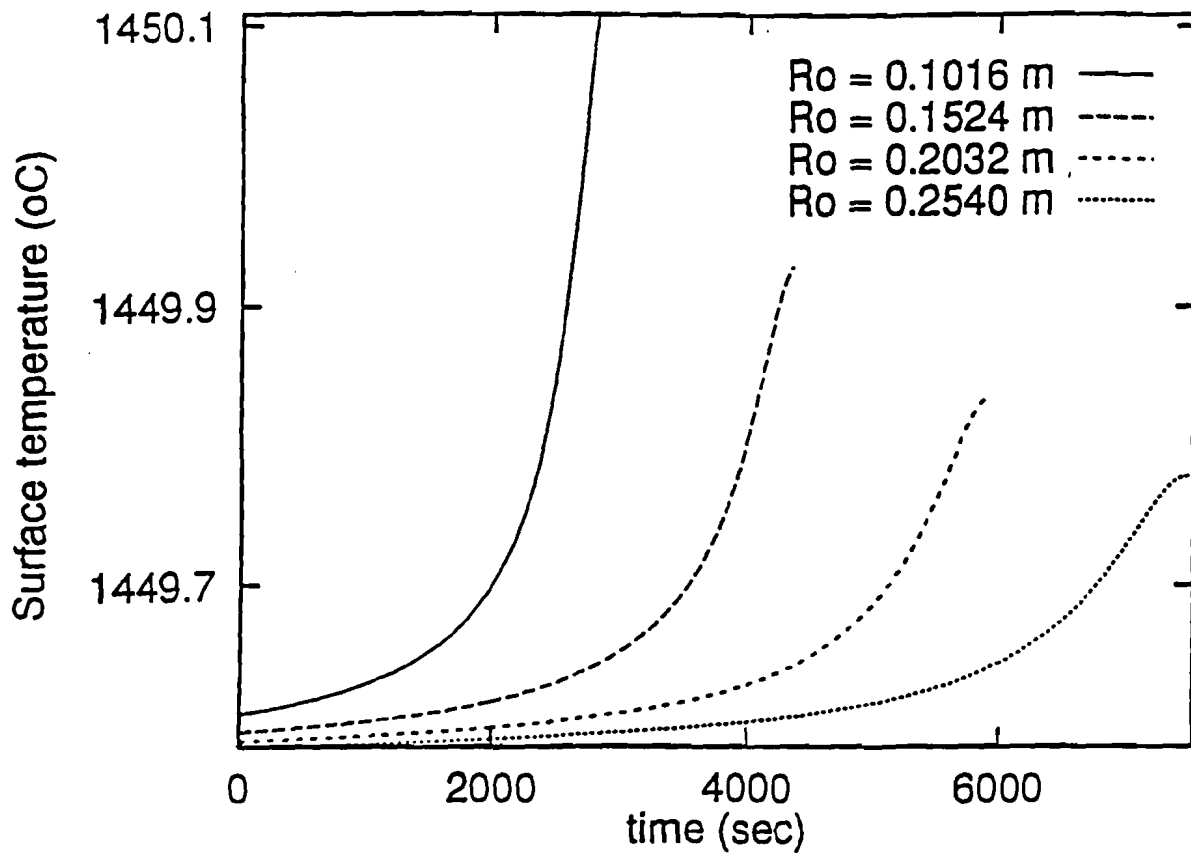


Fig. 1.13 : Surface temperature of 10 cm long chunkwood

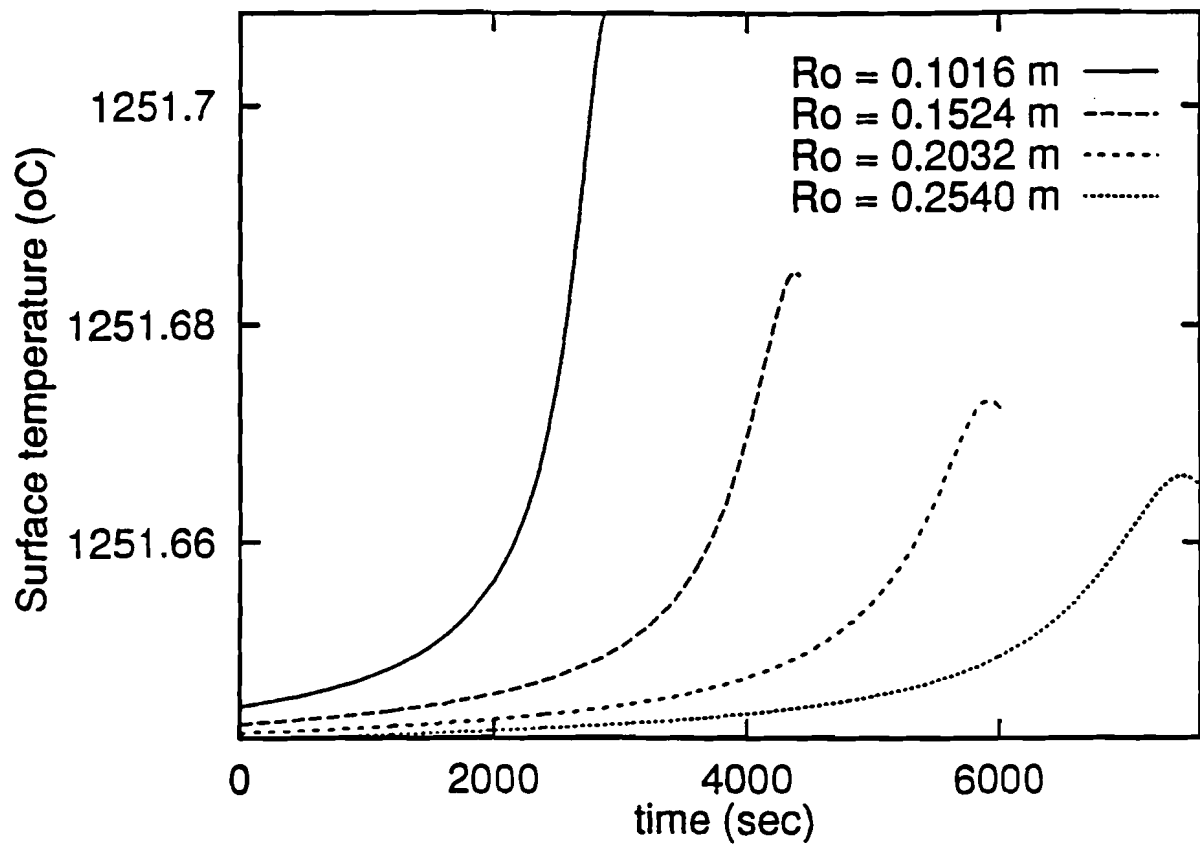


Fig. 1.14 : Ts of 10 cm long chunkwood,  $\alpha = 72 \%$



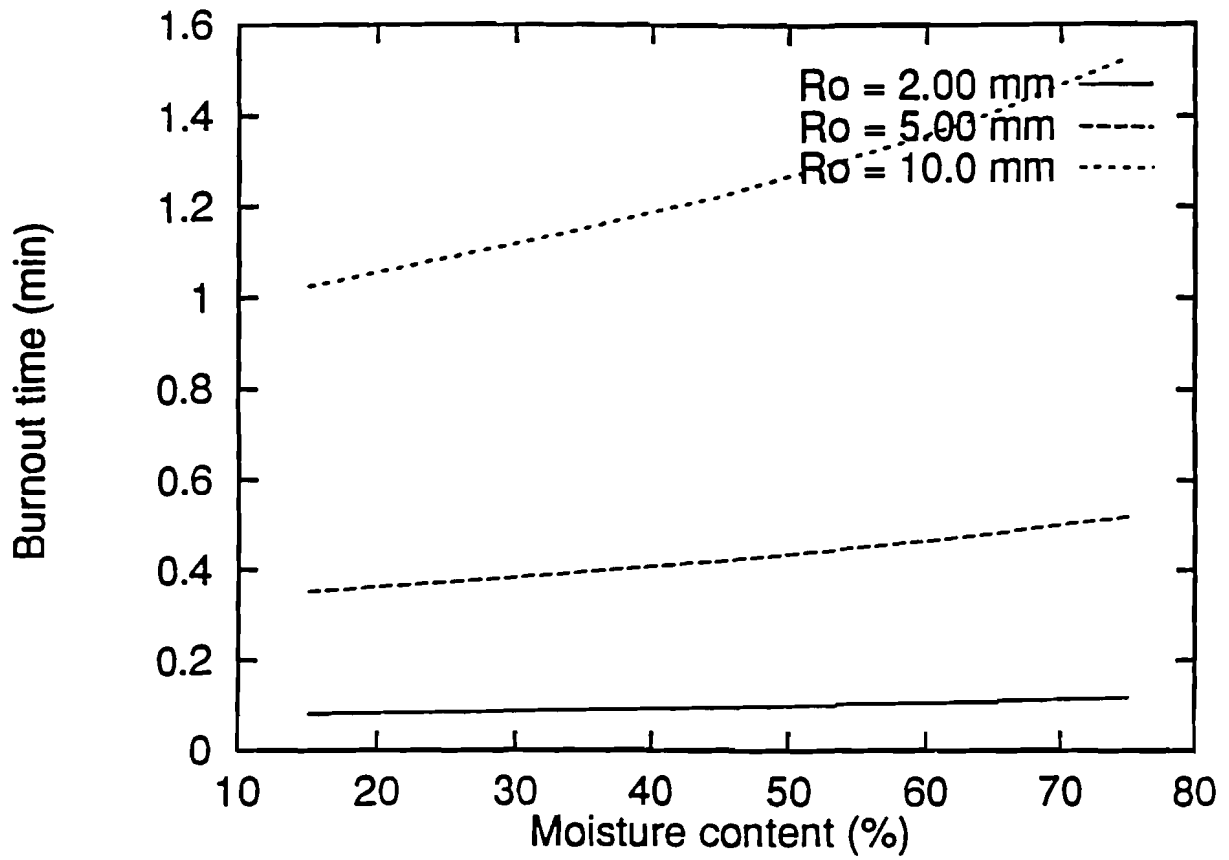


Fig. 1.15 : Effect of moisture on particles burnout time

## 1.7 References

- 1.1 P. L. Blackshear Jr and A. M. Kanury. Heat and mass transfer to, from and within cellulosic solids burning in air. Tenth Symposium (International) on Combustion, 911-923, 1965.
- 1.2. P. S. Maa and R. C. Bailie. Influence of particle sizes and environment conditions on high temperature pyrolysis of cellulosic material. Comb. Sc. and Tech., 7:257-269, 1973.
- 1.3. J. Saastamoinen and J. Richard. Drying, pyrolysis and combustion of biomass particles. in Research in Thermochemical Biomass Conversion (A. V. Bridgwater and J. I. Kuester, Ed.), Elsevier Applied Science Publishers, 221-235, 1988.
- 1.4. K. W. Ragland, J. C. Boeger and A. J. Baker. A model of chunkwood combustion. Forest Products J., 38:27-32, 1988.
- 1.5. W. W. Simmons and K. W. Ragland. Single particle combustion and analysis of wood. in Fundamentals of Thermochemical Biomass Conversion (R. P. Overend, T. A. Milne and L. K. Mudge, Ed.), Elsevier Applied Science Publishers, 778-792, 1985.
- 1.6. E. L. Schaffer. An approach to the mathematical prediction of temperature rise within a semi-infinite wood slab subjected to high-temperature conditions. Pyrodynamics, 2:117-132, 1965.
- 1.7. H. S. Mukunda, P. J. Paul, U. Srinivasa and N. K. S. Rajan. Combustion of wooden spheres - Experimentals and model analysis. Twentieth Symposium ( International ) on Combustion, 1619-1628, 1984.
- 1.8. H. Yoon, J. Wei, and M. M. Denn. A model for moving-bed coal gasification reactors, AICHE J. 24:885-903, 1978.
- 1.9. A. Atreya, and I. S. Wichman. Heat and mass transfer during piloted ignition of cellulosic solids. J. of Heat Transfer, 111:719-725, 1989.

- 1.10. P. L. Walker Jr, F. Rusinko Jr and L. G. Austin. Gas reactions of carbon. in Advances in Catalysis (D. D. Eley, P. W. Selwood and P. B. Weisz, Ed.), Academic Press inc., vol. 9, 133-221, 1959.
- 1.11. D. A. Frank-Kamenetskii. Diffusion and Heat Transfer in Chemical Kinetics. Plenum Press, vol. 1, 56, 1969.
- 1.12. I. Glassman. Combustion. Academic Press, inc., vol. 2, 388, 1987.
- 1.13. W. Dinwoodie. Nature's cellular, polymeric fibre-composite. The Institute of Metals, vol. 1, 27, 1989.
- 1.14. W. M. Kays and R. J. Moffat. The behaviour of transpired turbulent boundary layers. in Studies in Convection ( B. E. lauder, Ed.), Academic Press, vol. 1, 223-319, 1975.
- 1.15. C. J. Geankoplis. Mass Transport Phenomena. Holt, Rinehart and winston, inc., vol. 1, 29, 1972.
- 1.16. K. Hsiang-Chen and A. S. Kalelkar. On the heat of reaction in wood pyrolysis. Combustion and flame, 20:91-103, 1973.
- 1.17. J. Diebold and J. Scahill. Ablative pyrolysis of biomass in solid-convective heat transfer environments. in Fundamentals of Thermochemical Biomass Conversion (R. P. Overend, T. A. Milne and L. K. Mudge, Ed.), Elsevier Applied Science Publishers, 539-555, 1985.
- 1.18. W. J. Parker. Prediction of the Heat Release Rate of Wood. Ph.D. Thesis. The George Washington University, 1988.

## 1.8 Nomenclature

A	external surface area ( $m^2$ )
b	blowing parameter
$b_c$	char thickness (m)

C	oxygen concentration (kg/m <sup>3</sup> )
C <sub>pj</sub>	specific heat of component j (KJ/kg <sup>0</sup> K)
D	molecular diffusivity (m <sup>2</sup> /sec)
h	heat transfer coefficient (KJ / m <sup>2</sup> -sec- <sup>0</sup> K)
h <sub>D</sub>	mass transfer coefficient (m/sec)
h <sub>D</sub> <sup>*</sup>	mass transfer coefficient without blowing (m/sec)
hfg <sub>m</sub>	enthalpy of phase change of liquid water (KJ/kg)
hfg <sub>v</sub>	enthalpy of phase change of active matter (KJ/kg)
H <sub>as</sub>	average heat of combustion at the interface (KJ/Kg)
H <sub>j</sub>	enthalpy of component j (KJ/kg)
i	stoichiometric index
K	geometry correction factor
K <sub>c</sub>	char conductivity (KW/m- <sup>0</sup> K)
K <sub>p</sub>	reaction rate constant (m/sec)
m	mass (kg )
$\dot{m}$	mass loss rate (kg/sec)
$\dot{m}''$	mass flux (kg/sec-m <sup>2</sup> )
r	outside radius (m)
r <sub>0</sub>	initial radius (R <sub>0</sub> in Figures) (m)
$\dot{r}$	rate of radius recession (m/sec)
t	time (sec)
T	temperature ( <sup>0</sup> C)
v	volume (m <sup>3</sup> )
V	velocity (m/sec)

## Dimensionless variables

Re <sub>D</sub>	Reynolds number
Re <sub>x</sub>	Reynolds number
Sg	specific gravity

St	Stanton number
St <sub>0</sub>	Stanton number without blowing

## Greek Letters

$\alpha$	fraction of the volatiles which burn to CO at char-gas interface
$\beta$	ratio of the heat of combustion of C to CO to that of C to CO <sub>2</sub>
$\epsilon$	mass fraction
$\rho$	density (kg/m <sup>3</sup> )

## Subscripts

b	burnout time
c	char
g	gas
i	initial (ambient)
j	components (c, m, v)
m	moisture
s	surface
v	volatiles
w	virgin wood
$\infty$	free-stream

## 1.9 Appendix



```

hc=31100.0d0
hv=13500.0d0
kc=.0000420d0
ti=25.0d0
tf=1200.0d0
cpv=1.10d0
cpm=4.20d0
cpc=.670d0
rocg=.3240d0
hfgv=200.0d0
hfgm=2250.0d0
rc=95.0d0
sg=.460d0
co=.0490d0
d=.0003150d0
ck=-(12.0d0/16.0d0)*co/rc

```

```

c*****

```

```

c      Input moisture content and additional data.

```

```

c      mc is the prescribed moisture content (say .15 for 15 %).
c      r and l are the radius and length (size for the cubic ele
c      ment) of the chunkwood.
c      step is the step size in time (may be as small as .005 for
c      r=.1mm and as big as 3. depending on the initial radius;
c      you may try values between 1. and 3. for r greater or equal
c      to .075m).
c      v is the volume of the cylindrical log or the cubic element
c      k (suggested value for the chunkwood is .60 and .40 for the
c      cubic element) is an empirical constant for the computation
c      of the mass and heat transfer coefficients.
c      tol is a shrinking limit (.001 for the chunkwood and .001
c      or .01 for the cubic element, depending on mc).
c      fe is the amount of volatiles that burns at the char-gas
c      interface fe is assumed equal to 1, but to obtain approxima
c      tely the same temperature as in reference (1.4), input fe =
c      72 %

```

```

pi=4.0d0*datan(1.0d0)

```

```

c-----

```

```

print*, '-----'

```

```

print*, 'input 1 if you want to run the CHUNKWOOD'

```

```

print*, 'and otherwise if running the CUBIC PARTICLE'

```

```

read*, nm

```



```

if(nm .eq. 1)then
print*, '-----'
print*, 'input mc,r,l,step,k,tol,fe'
read*,mc,r,l,step,k,tol,fe
ri=r
v=pi*l*r**2
c   the equivalent radius
r=((3.0d0/4.0d0)*(r**2)*l)**(1.0d0/3.0d0)
else
print*, '-----'
print*, 'input mc,l, step, k,tol,fe'
read*,mc,l,step,k,tol,fe
v=l**3
c   the equivalent radius
r=l*((3.0d0/(4.0d0*pi))**(1.0d0/3.0d0))
endif

c*****

c   rw is the density of wood.
c   ec,ev and em are the mass fraction of the char,volatile and
c   liquid water.
c   cq is a computational constant.
c   p1 and p2 are empirical constants for the computation of
c   the mass and heat transfer coefficients.

rw=1000.0d0*(1.0d0+mc)*sg
ec=rc/rw
em=mc/(1.0d0+mc)
ev=1.0d0-ec-em
cq=(2.060d0*k*d/2.0d0)*(17400.0d0)**(.4250d0)

p1=.004750d0/.00620d0
p2=.003550d0/.00620d0
hcl= (ec*hc + ev*hv*fe)*(.280d0)/(ec + ev*fe)

```

```

c-----
c   hd and h are the mass and heat transfer coefficients.
c   we start the iterations for the determination of the radius r.
   rs(1)=r
   i=2
1   do 10 j=i,i+2
      hd(j-1)=cq*rs(j-1)**(-.5750d0)*((p1*rs(1)*mc/rs(j-1))
&/ (dexp(p2*rs(1)*mc/rs(j-1))-1.0d0))
      if((rs(j-1) .lt. .0d0) .or. (hd(j-1) .lt. .0d0))then
         print*,'negative radius or mass transfer coefficient'
         print*,'you may check the time step'
         go to 2
      endif
      q1=rs(j-1)+step*ck*hd(j-1)
      f1=cq*q1**(-.5750d0)*((p1*rs(1)*mc/rs(j-1))
&/ (dexp(p2*rs(1)*mc/rs(j-1))-1.0d0))
      q2=rs(j-1)+step*ck*(f1+hd(j-1))/2.0d0
      f2=cq*q2**(-.5750d0)*((p1*rs(1)*mc/rs(j-1))
&/ (dexp(p2*rs(1)*mc/rs(j-1))-1.0d0))
      q3=rs(j-1)+step*ck*(f2+hd(j-1))/2.0d0
      f3=cq*q3**(-.5750d0)*((p1*rs(1)*mc/rs(j-1))
&/ (dexp(p2*rs(1)*mc/rs(j-1))-1.0d0))
      q4=rs(j-1)+step*ck*(f3+hd(j-1))/2.0d0
      rs(j)=q4
10  continue
c   output the normalized radial shrinking rate
      write(1,*)dfloat(i-1)*step,rs(i-1)/r

```

```

c-----
c   compute the surface temperature ts

c=dabs((rs(i-1)-rs(i)))/step
h=hd(i-1)*rocg
a1=h*(tf-ti)
b1=(ec + ev*fe)*hc1-ev*hfgv-em*hfgm+a1/(rw*c)
c1=ec*cpc+ev*cpv+em*cpm+h/(rw*c)

ts=ti+b1/c1

c   output the mass and heat transfer coefficients

write(2,*)dfloat(i-1)*step,hd(i-1),h

c   output the surface temperature

write(3,*)dfloat(i-1)*step,ts

```

```

c-----
c   compute the char layer thickness

d1=kc*(ts-ti)

e1=ev*hfgv+em*hfgm

do 20 j=i,i+2

u(j-1)=dabs(rs(j)-rs(j-1))/step

b(j-1)=d1/(rw*u(j-1)*e1+(d1/rs(j-1)))

bi=b(1)

if(b(j-1) .gt. rs(j-1))then

print*,'char thickness greater than the radius'
print*,'the model is no more valid'
print*,'you may check the inputs'
go to 2

endif

20 continue

c   output the char layer thickness

write(4,*)dfloat(i-1)*step,b(i-1)*1000.0d0

```

```

c-----
c   compute the fractional mass loss
c   mi is the initial mass

   g1=rc*(rs(i-1)**2)*((rs(i)-rs(i-1))/step)+(rw-rc)*((rs(i-1)
&-b(i-1))**2)*((rs(i)-rs(i-1))/step-(b(i)-b(i-1))/step)

   g2=rc*(rs(i)**2)*((rs(i+1)-rs(i))/step)+(rw-rc)*((rs(i)
&-b(i))**2)*((rs(i+1)-rs(i))/step-(b(i+1)-b(i))/step)

   mi=rw*v-4.0d0*pi*(r**3-(r-bi)**3)*(rw-rc)/3.0d0

   m(1)=mi

   m(i)=m(i-1)+2.0d0*pi*(g1+g2)*step

   mstar(1)=m(1)/mi

   mstar(i)=m(i)/mi

c*****
c   output the fractional mass loss mstar

   if((mstar(i) .gt. tol) .and. (mstar(i-1)-mstar(i)
&.gt. .0d0))then

   write(7,*)dfloat(i-2)*step,mstar(i-1)

c   compute the burnout time tb

   tb=dfloat(i-1)*step

   i=i+1

   go to 1

   endif

   tb=tb/60.0d0

c   compute the average shrinking rate (mm/min)

   sr=1000.0d0*(r-rs(i-1))/tb

   if(nm .eq. 1)then
write(8,*)ri

```

```

5    format(////////,
      & 20x,'the initial radius      (m)          =',f6.5)
      else
      write(8,15)1
15    format(////////,
      & 20x,'the size or length      (m)          =',f6.5)
      endif

      write(8,25)100.0d0*mc,tb,sr
25    format(/,
      & 20x,'the moisture content   (%)          =',f6.2,/,
      & 20x,'the burnout time        (min)         =',f10.6,/,
      & 20x,'the shrinking rate     (mm/min)      =',f6.2)

      print*,'-----'
      print*,'it is important to remember that the burnout time'
      print*,'tb (time to 99.99% or 99% mass loss) is an asymp '
      print*,'totic value which is best determined sometimes by'
      print*,'looking at the fractional mass loss curve'
      print*,'-----'
      print*,'the burnout time (min) '
      write(*,*)tb
      print*,'the shrinking rate (mm/min) '
      write(*,*)sr

      print*,'-----'

      if((tb .eq. .0d0) .or. (sr .eq. .0d0))then

      print*,'check the time step'

      print*,'-----'

      endif

2    end

```

c\$

2 A quasi-steady state shrinking core model of "whole tree" combustion in a countercurrent fixed-bed reactor.\*

---

\* A short version of this work was submitted for publication in *Combustion Science and Technology*, (1994).

## 2.1 Abstract

A one dimensional, fixed-bed model of "whole tree" combustion is developed and the results are compared with operating data from existing "whole tree" facilities. The fuel elements are assumed to be loaded uniformly from the top with a frequency of  $N$  rows / sec, countercurrent to the preheated air stream of superficial velocity  $V_s$ . The "whole tree" elements then migrate downward with a velocity  $V_f$ , modeled as a product of the typical row velocity and its characteristic depth. The mass loss rate is formulated in a quasi-steady state shrinking core submodel with a uniform core temperature approximation. The model is simple and yet reliable enough to predict adequately the burn-out time  $t_b$  and the depth of the combustion zone  $L_c$  of a 100 MW "whole tree" facility combusting 0.1016 m (4 inches) radius fuel at 33.3 % moisture content (wet basis). The model also handles relatively well the combustion of small particle specimens of the order of 0.10 mm radius. It shows that fuel elements properties (size, moisture content) strongly influence combustion characteristics, especially that higher moisture produces depressed flame temperature, longer  $t_b$ , and larger values of  $L_c$ .

## 2.2 Introduction

Biomass energy technology has shown substantial potential as an energy supply alternative and has received attention in recent years due to both a growing concern for the environment as well as the perception of a need to develop renewable energy sources. Bain and Overend [2.1] reported that after the Public Utilities Regulatory Policies Act (PURPA) of 1978, biomass electric power generation experienced a dramatic increase from less than 200 MWe in 1979 to approximately 6 GWe by 1989, with wood fired systems accounting for 88% of the total capacity. In addition to supplying power utilities, wood is also burned directly in residential stoves and many developing countries rely on biomass (especially wood) to provide much of their energy requirements. Biomass is virtually free of sulfur and thus minimizes the production of  $SO_2$  and acid rain when properly burned. The growth of biomass resources provides a sink for atmospheric  $CO_2$  that may offset the combustion emissions of  $CO_2$  from biomass electricity

production, hence providing a portion of the solution to global warming concerns. In addition, the development of a biomass electric industry may have other national advantages, by first reducing our dependence on foreign supplies and second by putting otherwise idle lands to use and providing a new market for farm products.

In recent years, a new approach in utilizing wood resources has been proposed wherein "whole tree" (without pre-processing operations such as chipping, etc.) are burned directly as a bed in a stoker boiler to produce electricity by steam turbine conversion. "Whole tree" burn, however, is more than just a novel combustion concept as it also includes improvement in such operations as fuel resource utilization, fuel drying, fuel handling, and heat recovery. It emphasizes hardwood tree species that are not acceptable to the pulp and paper industry and, therefore, not to most chip suppliers. Potentially, such units could be capable of operating less expensively if fuel throughput, air flow and other variables can be optimized.

A report by the Research Triangle Institute (RTI) [2.2] indicates that the first testing of the concept on a large scale took place in a municipal solid waste boiler in July 1985. More recent and larger scale "whole tree" burn combustion took place in 1986 in a converted coal-fired unit. Figure 2.1 shows the sequence of operations in a "whole tree" plant. Some of the advantages of the "whole tree" combustion provided by the early feasibility assessment and technologies comparison by the same Report are :

- minimized fuel preparation and handling
- combined fuel drying and storage
- allow for deep-bed combustion (potentially efficient countercurrent flow and high heat release rate).

The primary disadvantages are the uncertainties in terms of interaction of various components and in terms of large-scale operation.

Extensive work has been done over the years on countercurrent fixed-bed coal gasifiers. Complete literature review may be found in a report by Smoot [2.3] and the recent publication by Hobbs *et al.* [2.4]. Ragland and Purnomo [2.5] reported the performance of a downdraft woodchip packed bed combustor to power a gas turbine. Boiler technology is reasonably well established for woodchips and pulverized-coal firing. Additional modifications are required, however, for the design of "whole tree" fired boilers and



most investigations focus on the boiler efficiency (steam enthalpy produced per fuel heating value input) and heat release rate.

The objective of the present work is then to provide reliable basic data on "whole tree" residence time as a function of fuel elements properties (size, moisture content) and gas flow characteristics, for the design of wood fired boilers. The work is divided in two main parts. First, a one-dimensional "whole tree" fixed-bed combustion model is developed based on a shrinking core burning rate submodel and second, the results of the model whenever possible are compared with existing "whole tree" combustion facilities.

## 2.3 Model development

An under-fired "whole tree" fixed-bed, is loaded uniformly from the top in rows of  $N$  fuel elements at a frequency of  $V^*$  rows / sec which corresponds to a total fuel rate of 75 ton / hr. This fuel bed rests on a water-cooled fixed grate and is designed to fire a 100 MW "whole tree" power plant. For computational purposes, dimensions and characteristics shown in table 2.1, are assumed to be those of an actual unit described by the Research Triangle Institute (RTI) [2.2], Figure 2.2. The fuel elements are then subjected to an upward flow of preheated air stream at a theoretical requirement of 5.5 Kg of air per Kg of wet wood, with a superficial velocity  $V_s$  at a constant pressure of 1 atm. The "whole tree" elements migrate through the bed with velocity  $V_f$  while their initial radius  $r_o$  shrinks to  $r_f$  at the fixed grate. The distance traveled defines both the residence time and the depth of the combustion zone which are functions of fuel properties and gas flow characteristics. The bed is assumed to be one-dimensional, steady state, while quasi-steady state conditions are assumed within the fuel elements. The partial drying of the fuel elements, which takes place over the outside layers and occurs during the transient warming period is neglected compared to the total burnout time. The boiler startup, assumed to be accomplished in a 4 hr time is not modeled.

### 2.3.1 Burning rate submodel

It is reported by the RTI [2.2] that for large cylindrical logs, a popular conclusion is that the rate of combustion is basically heat and diffusion controlled rather than reaction

kinetics controlled. Oxygen must diffuse from the bed environment to the solids reaction site (solid-gas interface) and heat must diffuse from the combustion front into the "whole tree", raising their interior temperature. The increase of the inner temperature is followed by pyrolysis at around 500 °C. Moisture and volatiles also diffuse away from the pyrolysis front, possibly inward where they increase the interior pressure and temperature ("cooking") and outward where their cooling effect (blowing) produces depressed gas flame temperature inside the bed. It is believed that the best formulation for the combustion of large wood specimens is the shrinking core model, where it is understood that burnout is not accomplished until the combustion front reaches the center of the fuel elements. This combustion in the firing system of the "whole tree" power plant is divided into three stages, Figure 2.2. First, the tree elements burn in the bed with volatiles being released throughout the process. Second, a large fraction of the gases burn inside the bed while the remaining volatiles are combusted above the bed using overfire air. Third, char of final radius  $r_f$  and ashes fall through the grate openings.

The radial shrinking rate of the cylindrical elements may be expressed as [2.6]

$$\frac{dr}{dt} = -\left(\frac{12}{16}\right) h_D C / \rho_c \quad (2.1)$$

where  $r$  is the outside radius,  $C$  is the oxygen concentration inside the bed,  $\rho_c$  is the constant char density, and  $h_D$  is the overall mass transfer coefficient, i.e. the oxygen mass transfer coefficient modified by blowing. The actual mass transfer coefficient which includes the bed volume fraction is modified from that of a single chunkwood element, correlated in a recent study by Ouedraogo *et al.* [2.6]. The expression is

$$h_D = \frac{2.06 K D Re_D^{425}}{\epsilon_b (2r)} \frac{.766 mc r_o / r}{e^{(.573 mc r_o / r)} - 1}$$

where  $r$  and  $r_o$  are respectively the outside and initial radius,  $K$  is a geometry correction factor,  $D$  is the molecular diffusivity,  $\epsilon_b$  is the bed volume fraction, and  $mc$  is the fuel element moisture content (wet basis). The combustion is assumed complete when the element shrinks to approximately 99.99% of its initial mass. A residual char element of final radius  $r_f$  then falls through the grate. That is,

$$r_f = r_o (0.001)^{(0.5)}$$

Now shifting from a material time-rate derivative to a one-dimensional spatial-rate, yields

$$\frac{dr}{dt} = V_f \frac{dr}{dz} = -\dot{r} = \left(\frac{12}{16}\right) h_D C / \rho_c \quad (2.2)$$

where  $V_f$  is the migration velocity of the "whole tree" elements with respect to the top of the bed. Contrary to chunkwood, "whole tree" may be considered as infinite long cylinders. The shrinking core mass loss rate is formulated as the sum of the mass loss by the external char layer under heterogeneous combustion plus the mass loss by the core due to pyrolysis and loss of moisture. That is,

$$\frac{dm}{dt} = (2 \Pi r l) \left[ \rho_c \frac{dr}{dt} + (\rho_w - \rho_c) \left(1 - \frac{b_c}{r}\right) \frac{dr_w}{dt} \right] \quad (2.3)$$

where  $l$  is the length of the "whole tree",  $r_w$  and  $\rho_w$  are respectively the core radius and density and  $b_c$  is the char layer thickness. The core density [2.7] is given by

$$\rho_w = S_g (1 + mc) \rho_{water}$$

The migration velocity is modeled as the product of a typical row velocity  $V^*$  and the characteristic depth of a row  $L$ , figure 2.3.

$$V_f = V^* L$$

where  $\epsilon_s L^2 l = \Pi r^2 l$  and  $L = r \left(\frac{\Pi}{\epsilon_s}\right)^{(0.5)}$

The system loading rate would then be

$$\dot{N}_i = V^* N$$

where  $N = W/L$  is the number of fuel elements per row at the upper inlet plane of the bed. Hence,

$$\dot{N}_i = \left(\frac{V_f}{L}\right) \left(\frac{W}{L}\right) = \frac{V_f W}{L^2}$$

Since  $\dot{N}_i$  is a given constant, the migration velocity is

$$V_f = \left( \frac{\dot{N}_i \Pi}{W \epsilon_s} \right) r^2 = \frac{C^* r^2}{\epsilon_s}$$

where

$$C^* = \frac{\dot{N}_i \Pi}{W}$$

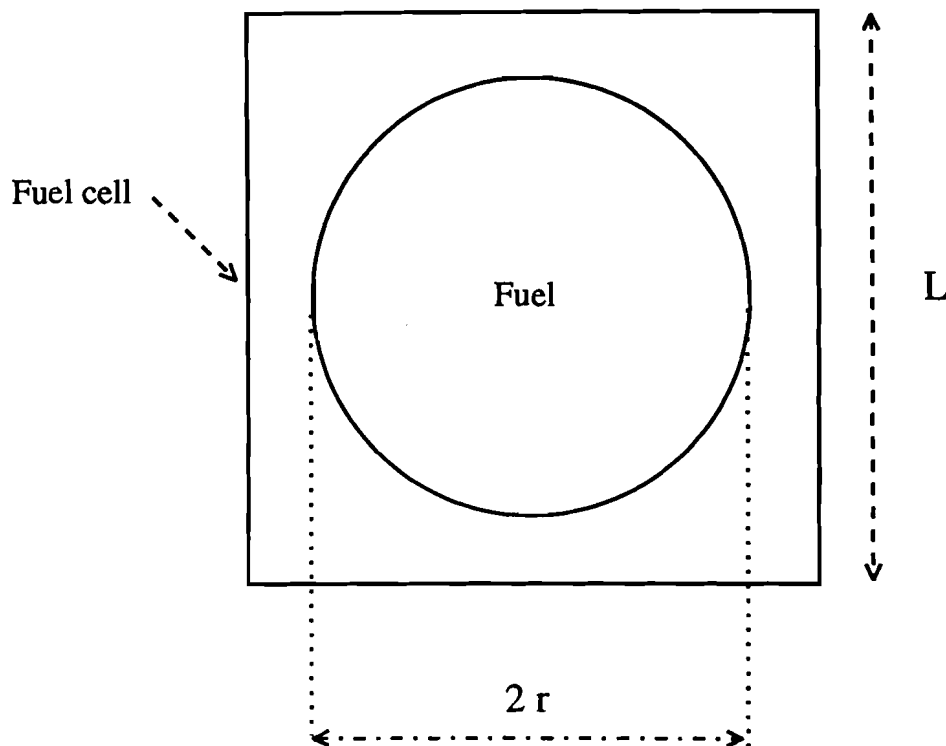


Fig. 2.3 : Fuel cell

### 2.3.2 Conservation equations in the solid phase

The char combustion is assumed to take place at constant density. The heterogeneous oxidation of carbon (char) can produce either CO or CO<sub>2</sub> as primary products, although CO is favored in diffusion controlled convective environment because oxygen molecules are in short supply at the solid-gas interface. Hence, it is assumed that a fraction  $\alpha$  of pyrolysis gases go to incomplete combustion (CO) at the char interface after their release. The combustion of both combustible (char and volatiles) is modeled with the assumption that they release the same <sup>proportional</sup> amount  $\beta$  of heat as the incomplete combustion of pure carbon to carbon monoxide.  $H_{as}$  then defines the average incomplete heat of combustion of the char and volatiles at the solid-gas interface. The core temperature is taken to be uniform and equal to ambient temperature.

Performing an energy balance at the char surface [2.6] yields the following equation

$$[\rho_c + \alpha \rho_v] H_{as} VA - hA (T_s - T_g) - \rho_w V_w [\epsilon_c C_{p_c} + \epsilon_v C_{p_v} + \epsilon_m C_{p_m}] (T_s - T_i) A_w = \frac{k_c (T_s - T_i)}{b_c} A_c + q' \quad (2.4)$$

where  $H_{as} = \frac{[\rho_c H_c + \alpha \rho_v H_v]}{\rho_c + \alpha \rho_v} \beta$  and  $h = h_D \rho_g C_{p_g}$

The heat transfer coefficient  $h$ , is correlated as the product of the mass transfer coefficient and the volumetric heat capacity of the gases,  $V$  and  $V_w$  represent respectively the char and core regression velocities,  $A$  and  $A_w$  their respective surfaces. This equation expresses the fact that to sustain the process, the rate of heat released by the combustion front should be equal to the rate of heat transfer away from it into the gas phase and into the pyrolyzing core.

A similar energy balance at the core surface [2.6] shows that the energy entering the core by conduction is sufficient enough to heat it up to pyrolysis with the subsequent phase change of liquid water to water vapor ( $hfg_m$ ) and active matter by pyrolysis ( $hfg_v$ ). That is,

$$\rho_w V_w A_w [\epsilon_v hfg_v + \epsilon_m hfg_m] = \frac{k_c (T_s - T_i)}{b_c} A_c \quad (2.5)$$

where  $A_c$  is the log-mean area between the core and char.

As it is seen, equations (2.4) and (2.5) represent a quasi-steady state formulation of a one phase moving boundary type problem since the core-char interface changes its position continuously and the core temperature is assumed constant during the process. Now combining equations (2.4) and (2.5), neglecting radiation and using appropriate relations for the surface areas

$$A = 2 \Pi r l$$

$$A = 2 \Pi r_w l$$

$$A = 2 \Pi \bar{r} l$$

where  $\bar{r} = (r_w + r) / 2 = r - b_c / 2$

and neglecting higher-order terms, we get the surface temperature  $T_s$  and the char layer thickness  $b_c$ . These are,

$$T_s - T_i = \frac{[\epsilon_c + \alpha \epsilon_v] \left(\frac{r}{r_w}\right) \left(\frac{r}{r_w}\right) H_{as} + h \left(\frac{r}{r_w}\right) (T_g - T_i) / (-\rho_w \dot{r}_w)}{h \left(\frac{r}{r_w}\right) / (-\rho_w \dot{r}_w) + \sum_{j=1}^3 \epsilon_j C_{p_j}} - \frac{(\epsilon_m h f g_m + \epsilon_v h f g_v)}{h \left(\frac{r}{r_w}\right) / (-\rho_w \dot{r}_w) + \sum_{j=1}^3 \epsilon_j C_{p_j}} \quad (2.6)$$

$$b_c = \frac{k_c (T_s - T_i)}{\rho_w V_w (\epsilon_v h f g_v + \epsilon_m h f g_m) + \frac{k_c (T_s - T_i)}{2r}} \quad (2.7)$$

### 2.3.3 Conservation equations in the gas phase

The products of the incomplete combustion at the char-gas interface (CO for the most part) and the fraction of volatiles that escapes early combustion, go to complete combustion in the gas phase. A sizable portion is burned inside the bed, and the remaining part is

combusted above the bed. It is assumed that the fraction of the total amount of gases produced that actually burn inside the bed is  $\gamma$ , the remaining is burned by secondary air above the bed of fuel. The gas phase then consists primarily of oxygen (air) and carbon monoxide and in a lesser extend of carbon dioxide, pyrolysis gases and water vapor. The preheated air, with maximum prescribed concentration at the bottom of the bed, moves in countercurrent to the flow of solid fuel and is assumed completely depleted of oxygen at the top of bed. Neglecting higher order terms, the following mass and heat balance equations are used to model the bed. The axial oxygen balance is

$$V_s \frac{dC}{dz} = - \dot{m}_{O_2}'' \left( \frac{A_s}{Vol} \right) \quad (2.8)$$

where the surface area-to-volume ratio of fuel ( $m^2$  fuel /  $m^3$  system)  $\left( \frac{A_s}{Vol} \right) = \frac{2 \epsilon_s}{r}$  and  $\dot{m}_{O_2}''$  is the oxygen surface mass flux given by

$$\dot{m}_{O_2}'' = - i \dot{m} / (2 \Pi r l) \quad (2.9)$$

where  $\dot{m}$  is the rate of mass loss. The bed solid fraction  $\epsilon_s$  and volume fraction  $\epsilon_b$  are respectively defined as

$$\epsilon_s = \frac{\rho_b}{\rho_w} \quad \epsilon_b = 1 - \epsilon_s$$

Neglecting radiation, the conservation of energy for the gas phase may be written as

$$\begin{aligned} \rho_g C_{p_g} V_s \frac{dT_g}{dz} = & - \rho_w \dot{r} \frac{2 \epsilon_s}{r} [ (\epsilon_c + \epsilon_v) \gamma H_{ag} \\ & - \sum_{j=1}^3 \epsilon_j C_{p_j} (T_s - T_i) - (\epsilon_v hfg_v + \epsilon_m hfg_m) ] \end{aligned} \quad (2.10)$$

where  $H_{ag}$  is the average complete heat of combustion of the gases

$$H_{ag} = \frac{[(\epsilon_c H_c + \alpha \epsilon_v H_v)(1 - \beta) + (1 - \alpha) \epsilon_v H_v]}{\epsilon_c + \epsilon_v}$$

This equation reflects the balance between the net heat of reaction and the change in enthalpy of the gases.

## 2.4 Results and discussion

Instead of solving the model equations by a classical moving boundary type solution, they are rather solved iteratively starting from the bottom of the bed, assuming a thin char layer approximation, Ouedraogo *et al.* [2.6], and constant thermal properties, table 2.2. A geometry correction factor  $K$  equal to 0.225 is introduced in the mass transfer equation to account primarily for end and corner effects. The initial oxygen concentration as well as the initial gas temperature are specified. The bed bulk density is also specified at the onset and a variable solid volume fraction is computed assuming that as the fuel elements shrink, a redistribution occurs inside the bed resulting in a changing value. Our computation, however, indicated this to have only a minor effect. At the fuel exit, the combustion is assumed completed and taken to correspond to a 99.99 % weight loss or approximately a 97 % radius reduction. The residual char and ash are assumed collected under the grate. The computation is carried out until the outside radius  $r$  equal to the initial radius  $r_0$  of the fuel elements at the top of the bed. Two types of model simulations were obtained. These were

1. Fixed bed characteristics and variable fuel size and / or moisture content.
2. Varied superficial gas velocity while holding the bed characteristics fixed.

Of particular importance for the design of wood boiler furnaces is the burnout time  $t_b$ , that is the actual residence time, and the combustion zone depth  $L_c$ . Figures 2.4 to 2.21 show selected results of our investigation for fuel elements of radius equal to 0.2540 m (10 inches), down to particles fuel of 0.10 mm radius. The burnout time and combustion zone depth are found to be a function of both the fuel element size and their moisture content, Figures 2.4 to 2.7. For small fuel elements, irregular patterns of these profiles are observed in figures 2.8 and 2.9, speculated to be due to the assumption of a uniform core temperature and a thin char layer. The difference in burnout time  $t_b$  comes from the



difference in average shrinking rate plotted in Figure 2.10. As a matter of fact, equation (2.1) shows that the shrinking rate is a function of not only the fuel element properties (size and moisture content), but also is a function of the oxygen concentration inside the bed. Fuel elements of 0.1016 m (4 inches) radius at 33.3 % moisture take approximately 40 min to burnout with a combustion zone depth of 3.26 m. These results are similar to those found in "whole tree" burn facilities of 100 MW investigated by the RTI [2.2].

In developing our model, the transient warm-up regime has been neglected compared to the total burnout time. The maximum temperatures reported accordingly are those of the actual combustion period. These temperatures are shown to be not only a function of the fuel element properties (size and moisture content) and flow characteristics ( $V_g$ ), but also a function of the amount of volatiles  $\alpha$  and maximum amount of gases  $\gamma$  that burn respectively at the char surface and inside the bed. Higher flame and surface temperatures are provided by the drier elements, while wet wood takes longer to burnout and produces depressed temperatures, Figures 2.11 and 2.12. This is so because a higher moisture means higher transpiration. Furthermore, a large portion of the heat generated must be used for phase change of the fuel moisture from liquid water to vapor. The effects of both the burning of volatiles at the solid-gas interface and the burning of the gases inside the bed are clearly shown in Figures 2.13 to 2.15 where the moisture content has been set equal to 33.3 %. It is seen that the temperatures increase with increasing  $\alpha$  and  $\gamma$  for a given moisture content. On the other hand, maintaining these parameters constant and increasing the moisture content (respectively at 50 and 60 %) once again confirms the adverse effect of moisture on the temperature, figures 2.16 and 2.17. Another singular effect is clearly shown in Figures 2.11 and 2.12 where at very large moisture (60 and 75%), the temperatures seem to "plateau" before increasing. Similar effect have been reported by Kanury [2.8] and said to be due to the deceleration of the local heating rate in the interior of the solid fuel when the coupling between thermal and mass diffusion occurs. The depletion of oxygen and the distribution of the fuel elements size (at 33.3 % moisture content) along the bed are indicated respectively by figures 2.18 and 2.19.

The model predicts rather adequately the temperature range reported by the RTI [2.2] which also found fuel moisture to significantly reduce boiler efficiency in the same "whole tree" burn facility. Drier fuel elements provide the best fuel input with increased heat release rate, smaller required furnace volume, and subsequently reduced boiler cost. But Schwleger [2.9] indicates that some experimental results have shown that less moisture is not always desirable. A moisture level possibly around 35 % is required to give optimum balance among drying costs, furnace and dryer performance, system efficiency, and problems such as dusting and explosions that are associated with handling dry, pulverulent fuels.

As expected, it is found that a drastic reduction in residence time and combustion zone depth is obtained with an increase of the superficial gas velocity, Figures 2.20 and 2.21.

## 2.5 Conclusion

The simplified "whole tree" fixed-bed model adequately predicts the burnout time, combustion zone depth and the temperature of a combustor of a 100 MW facility combusting 0.1016 m (4 inches) radius "whole tree" fuel elements. The proper determination of the burnout time allows a rigorous scaling of the volume of the boiler furnace and subsequently the calculations of the boiler heat release rate and efficiency. The shrinking core burning rate submodel is simple and yet reliable enough to show that the fuel elements moisture is an important variable in "whole tree" operations as it may affect directly boiler costs and efficiency. It is also instructive to see that the model can be applied, although with care, to the combustion of small particle fuel elements in the size of coal in a countercurrent fixed-bed.

Table 2.1. Characteristics of the bed

Properties	Values
CO (initial Oxygen concentration)	0.1365 Kg/m <sup>3</sup>
H (high)	4.572 m
L <sub>e</sub> (length)	9.144 m
L <sub>r</sub> (loading rate)	75.0 t/hr
m <sub>a</sub> (air flow rate)	5.5 Kg air / Kg fuel
ρ <sub>b</sub> (bulk density)	240 Kg/m <sup>3</sup>
S <sub>g</sub> (specific gravity)	0.64
T <sub>g</sub> (preheated temperature)	260 °C
W (width)	4.572 m

Table 2.2 Constant thermal properties

Properties	Values	Units	References
$C_{pc}$	0.670	KJ/Kg- $^{\circ}$ K	2.11
$C_{pm}$	4.20	KJ/Kg- $^{\circ}$ K	
$C_{pv}$	1.1	KJ/Kg- $^{\circ}$ K	2.11
D	$3.15 \times 10^{-4}$	m <sup>2</sup> /sec	2.10
$hfg_m$	2250	KJ/Kg	
$hfg_v$	200	KJ/Kg	
$H_c$	31,100	KJ/Kg	2.12
$H_v$	13,500	KJ/Kg	2.13
$K_c$	$0.41 \times 10^{-4}$	KW/m- $^{\circ}$ K	2.11
$\rho_c$	95	Kg/m <sup>3</sup>	2.10
$S_g$	0.64	-	2.2
$T_i$	25	$^{\circ}$ C	

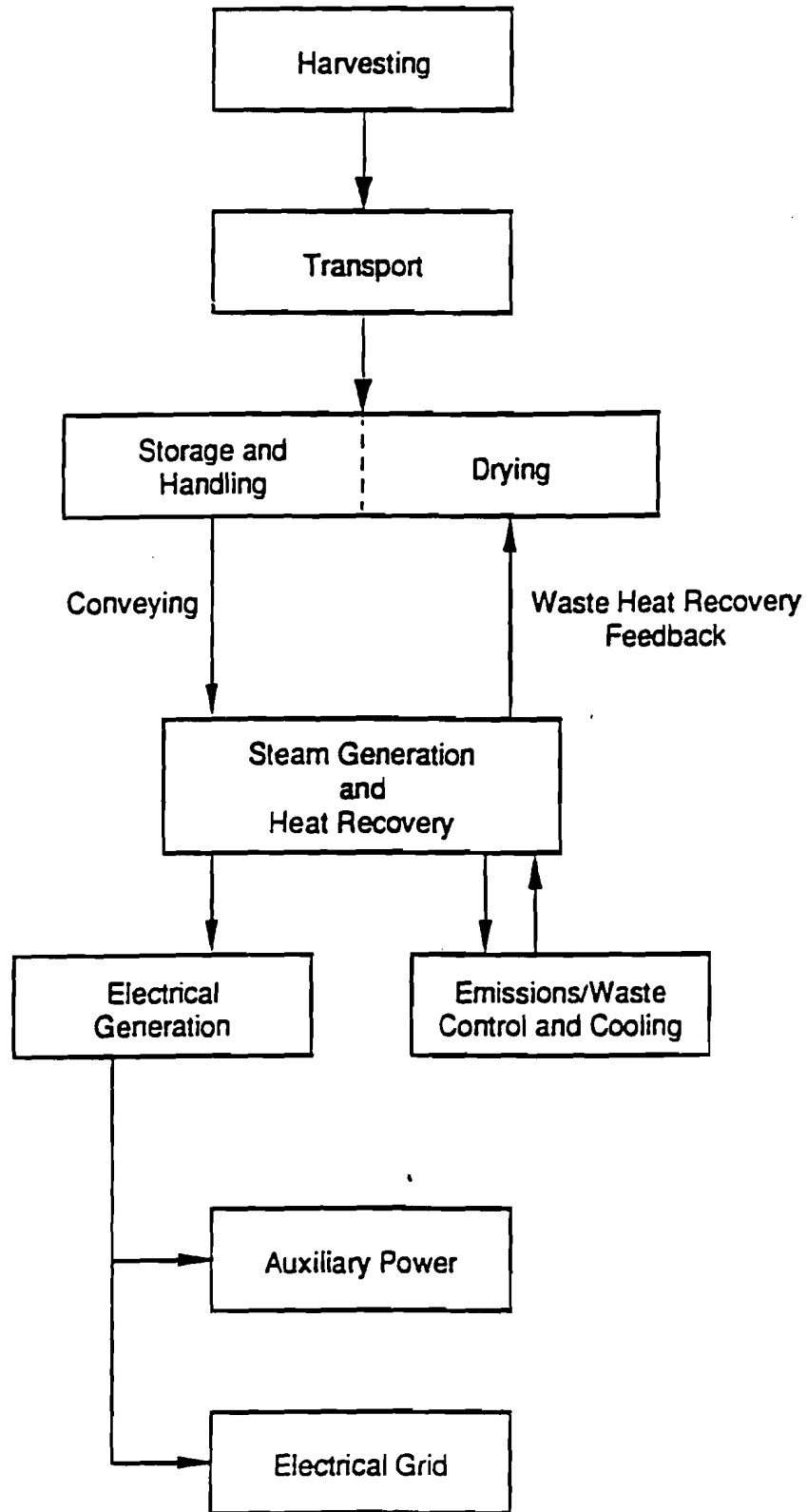


Fig. 2.1 : "Whole tree" burn fuel conversion sequence

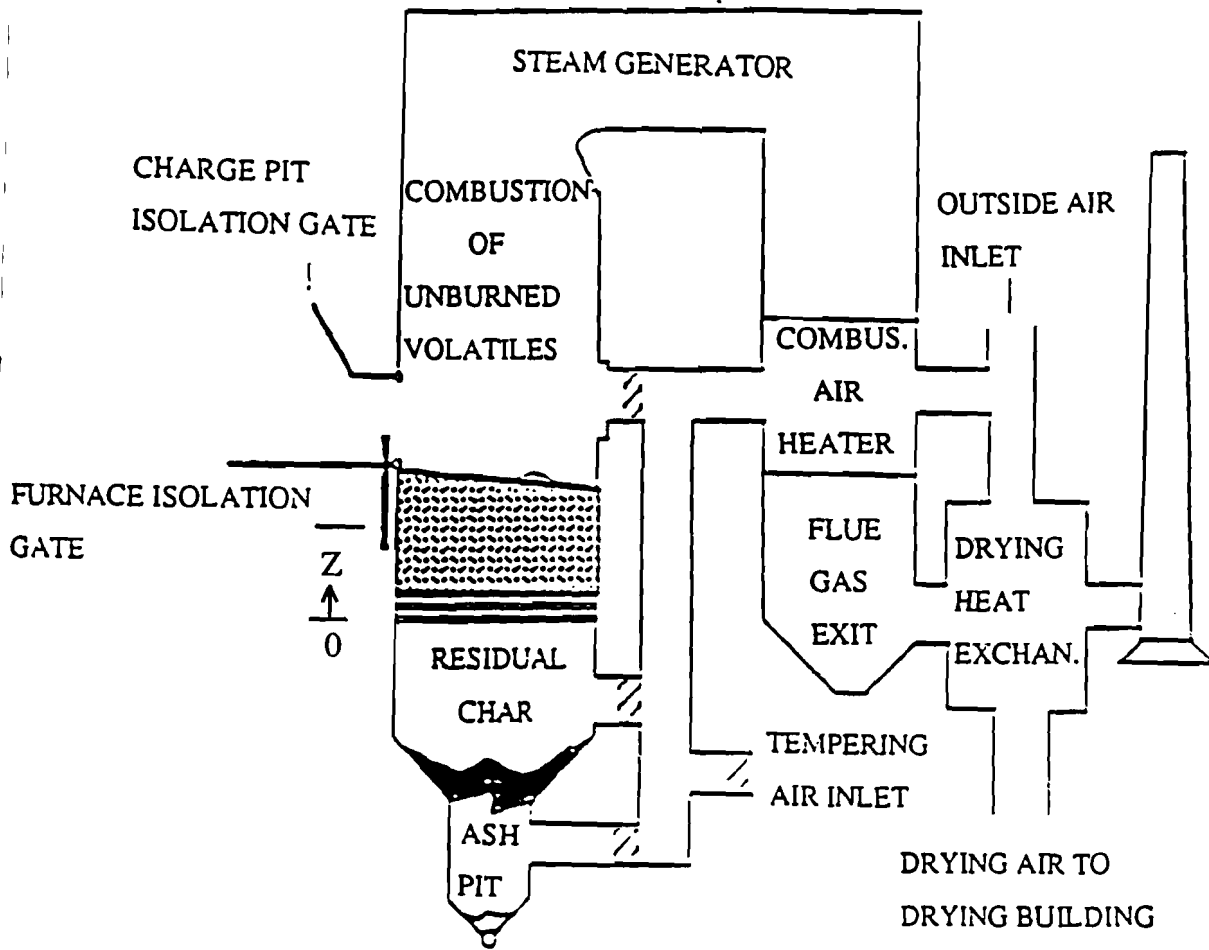


Fig. 2.2 : "Whole tree" burn power plant

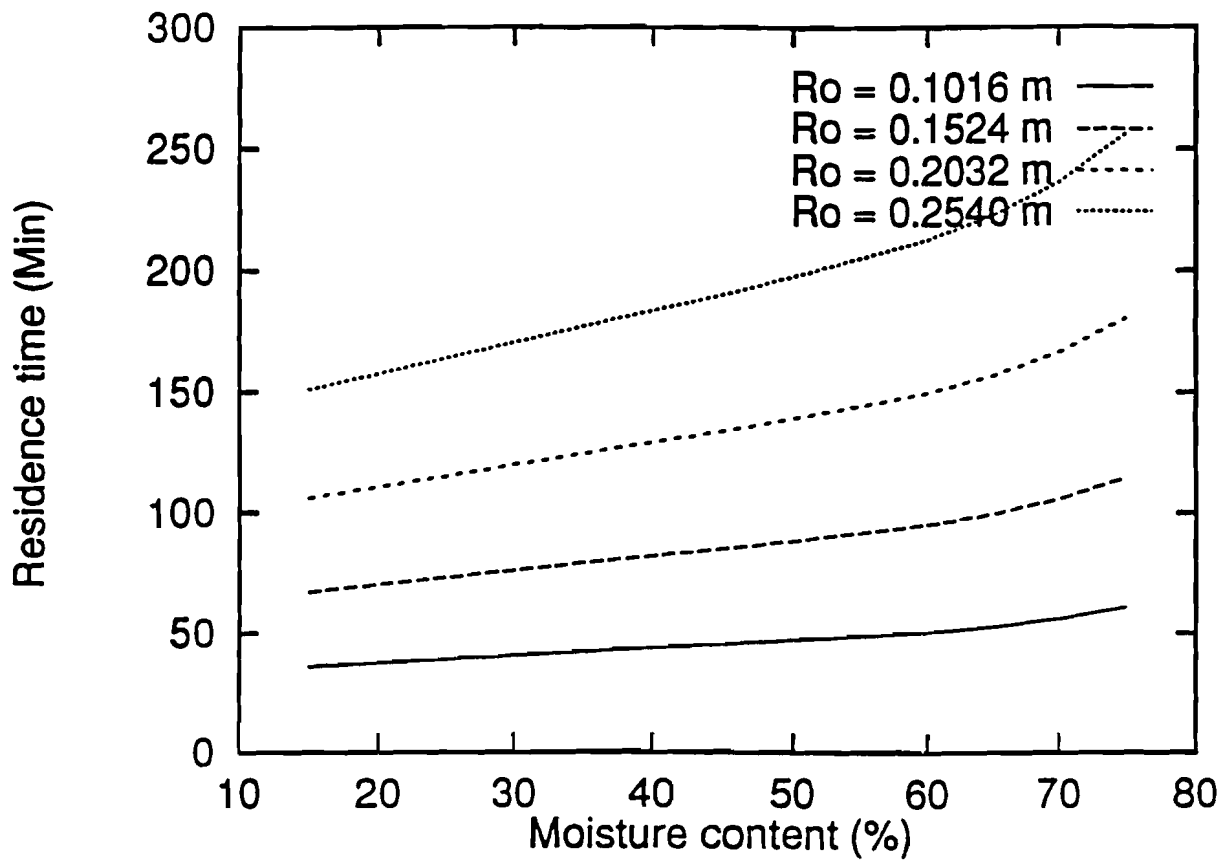


Fig. 2.4 : Moisture effect on residence time

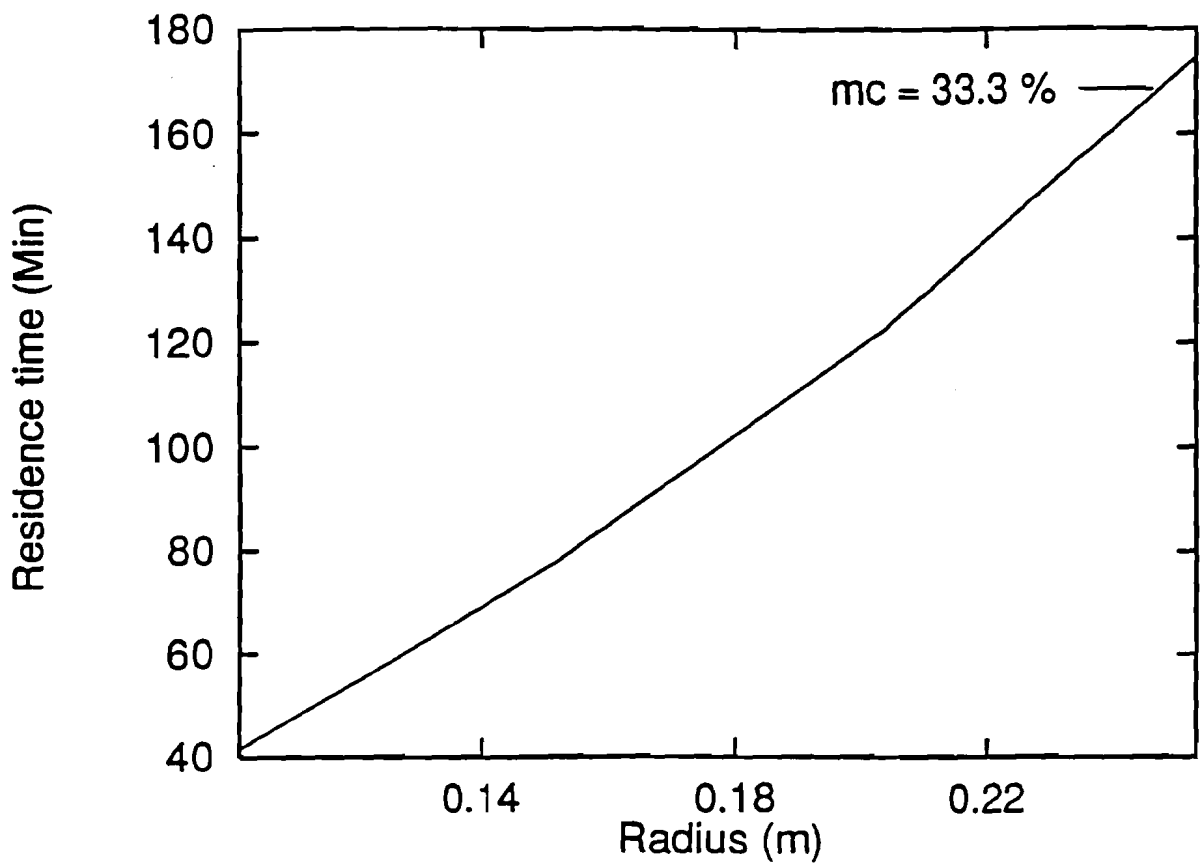


Fig. 2.5 : Effect of fuel elements size on residence time



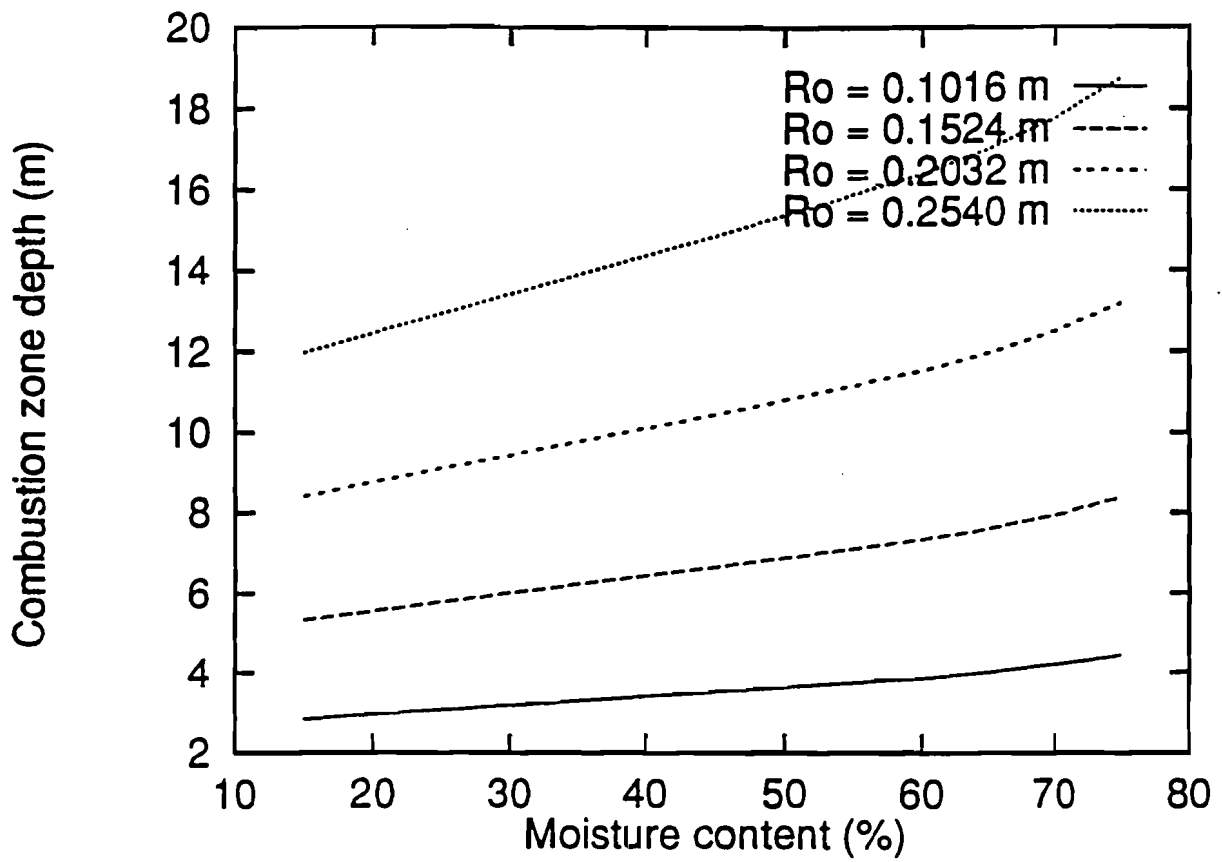


Fig. 2.6 : Moisture effect on combustion zone depth

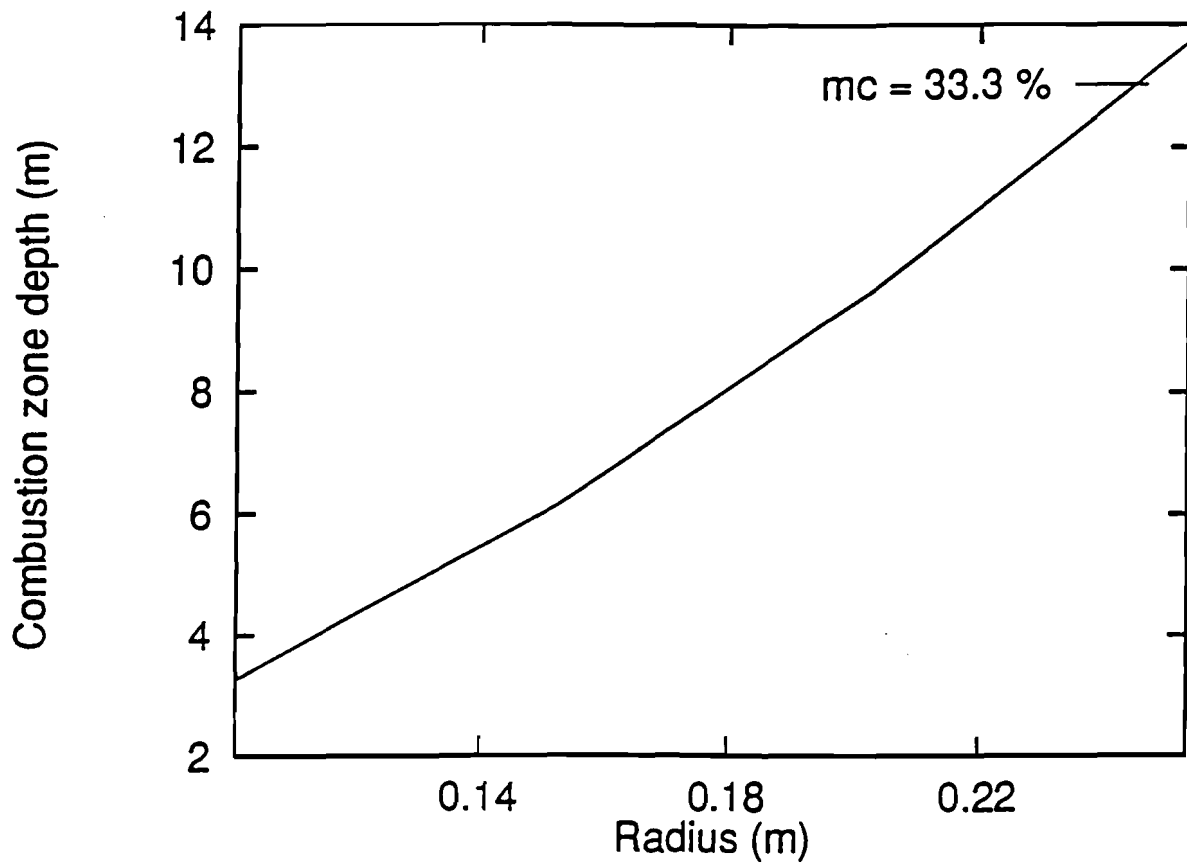


Fig. 2.7 : Effect of fuel elements size on  $L_c$

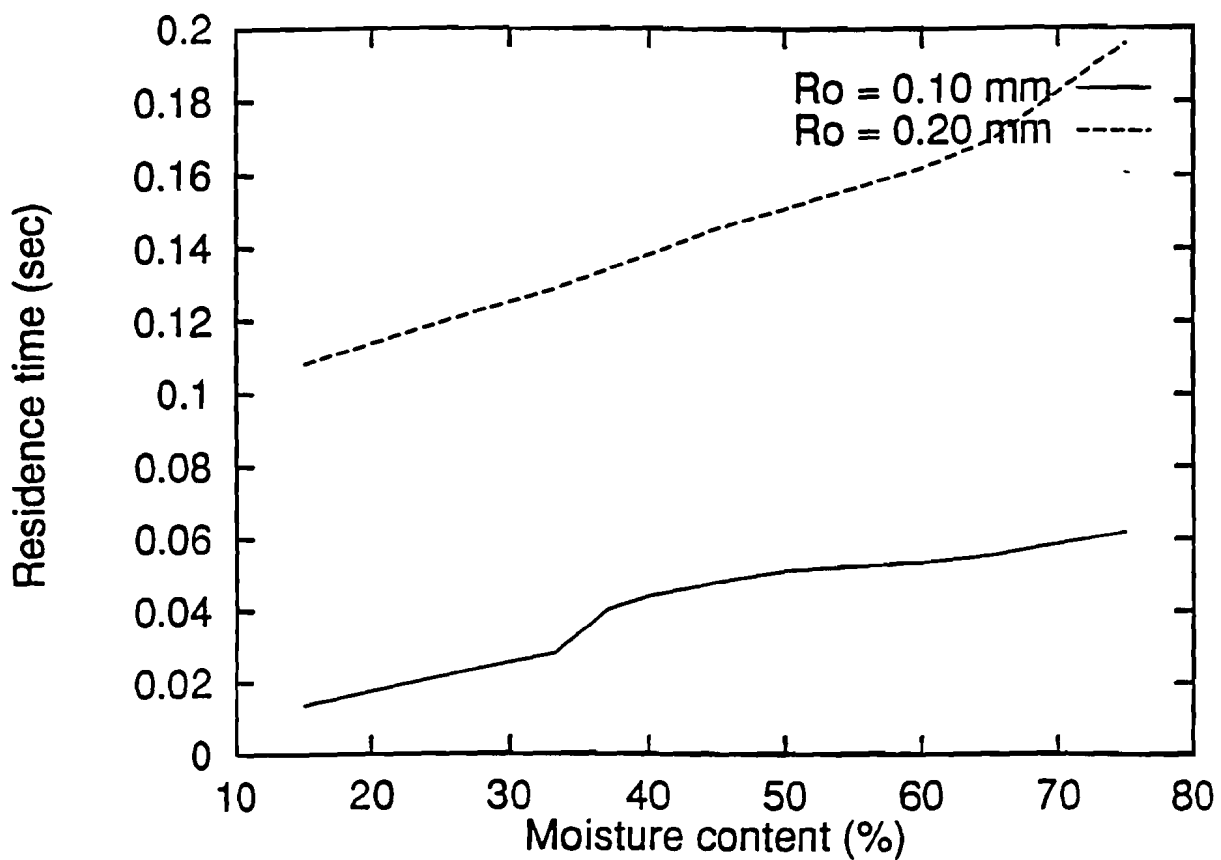


Fig. 2.8 : Residence time of small particles

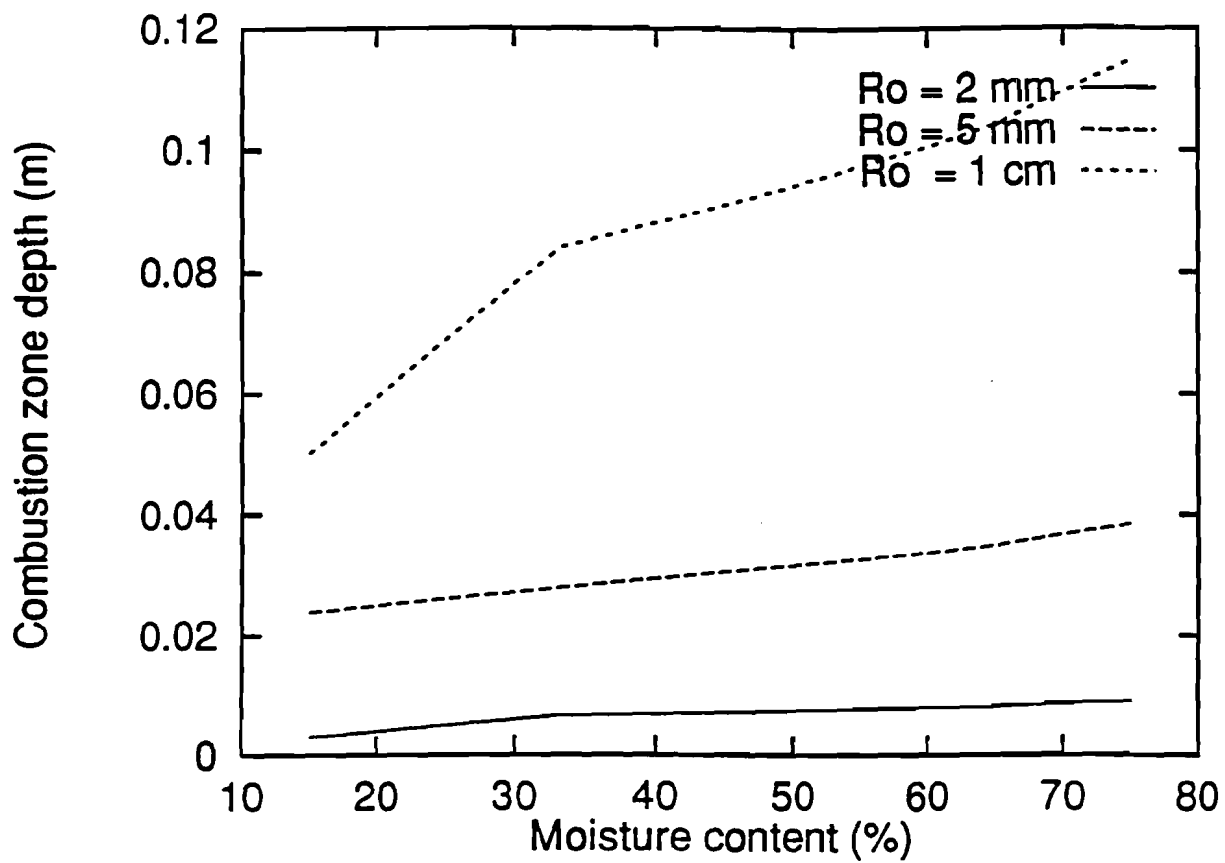


Fig. 2.9 : Combustion zone depth of small particles

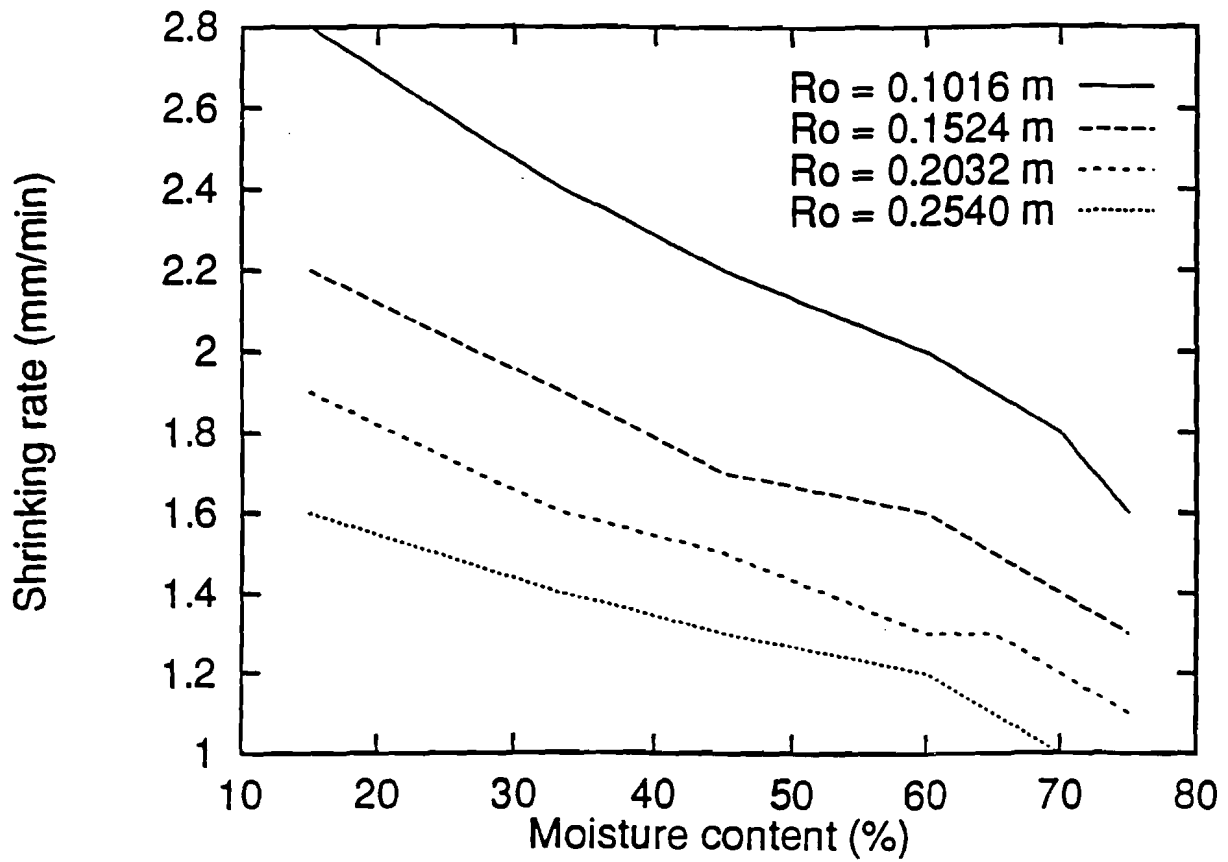


Fig. 2.10 : Moisture effect on average shrinking rate

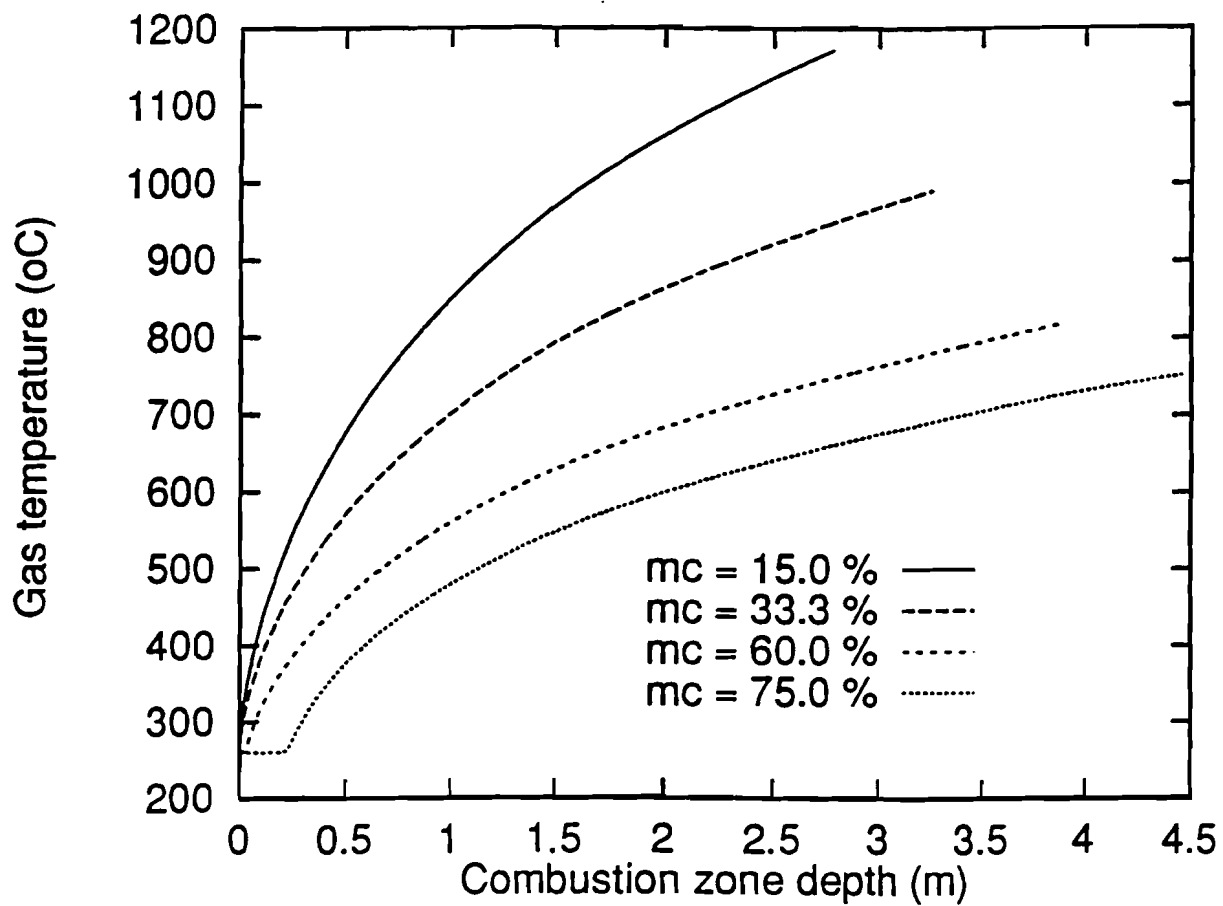


Fig. 2.11 :  $T_g$ ,  $R_o = 0.1016$  m,  $\alpha = 100\%$ ,  $\gamma = 80\%$

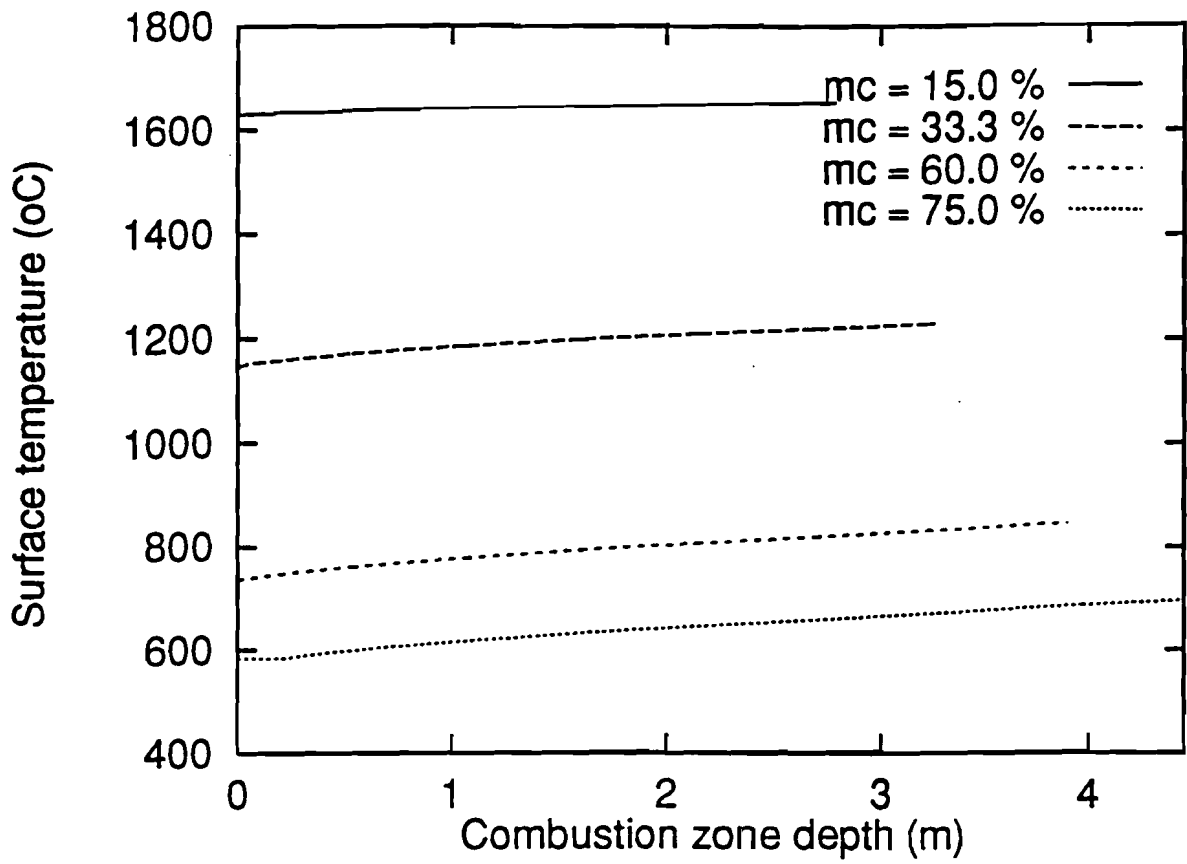


Fig. 2.12 :  $T_s$ ,  $R_o = 0.1016$  m,  $\alpha = 100\%$ ,  $\gamma = 80\%$

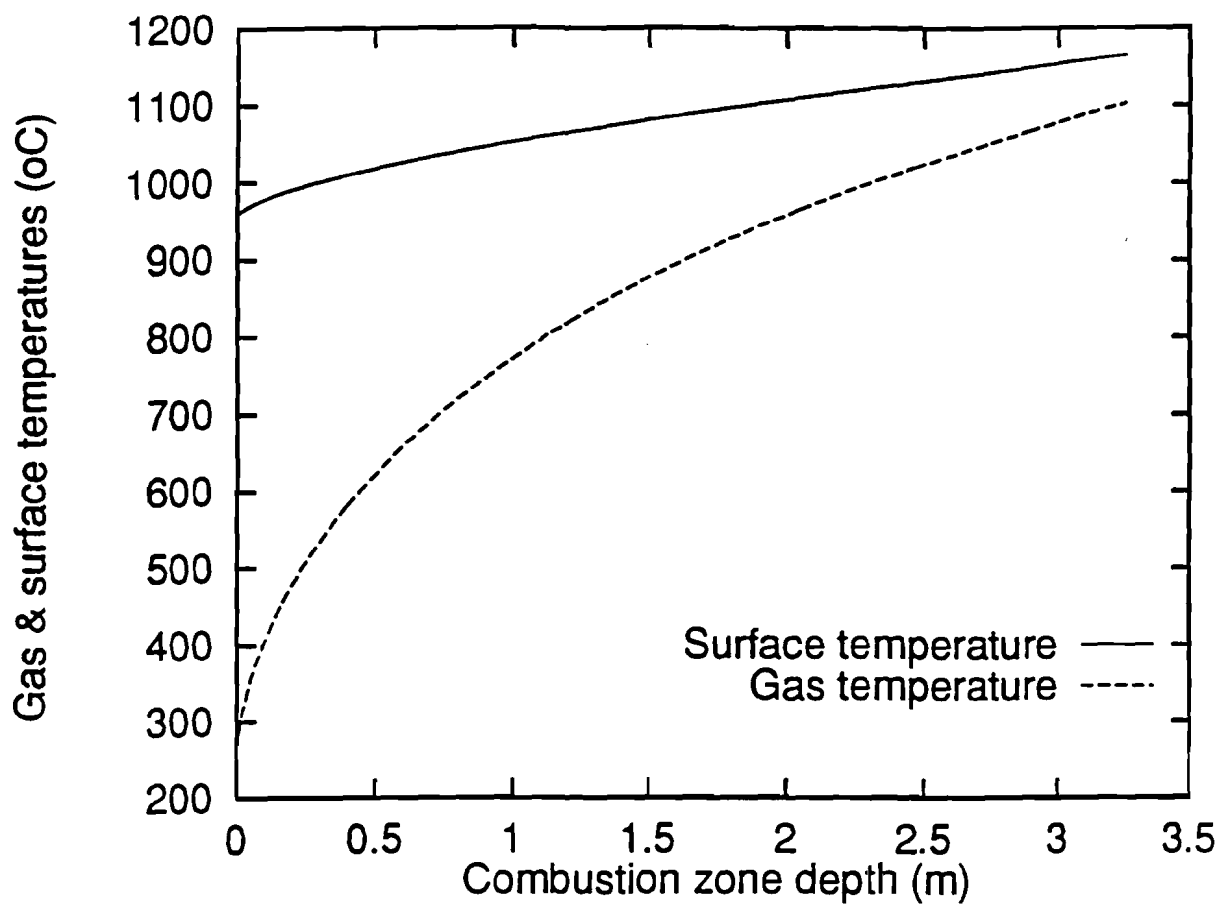


Fig. 2.13 :  $T_s$  and  $T_g$ ,  $R_o = 0.1016$  m,  $\alpha = 80\%$ ,  $\gamma = 80\%$



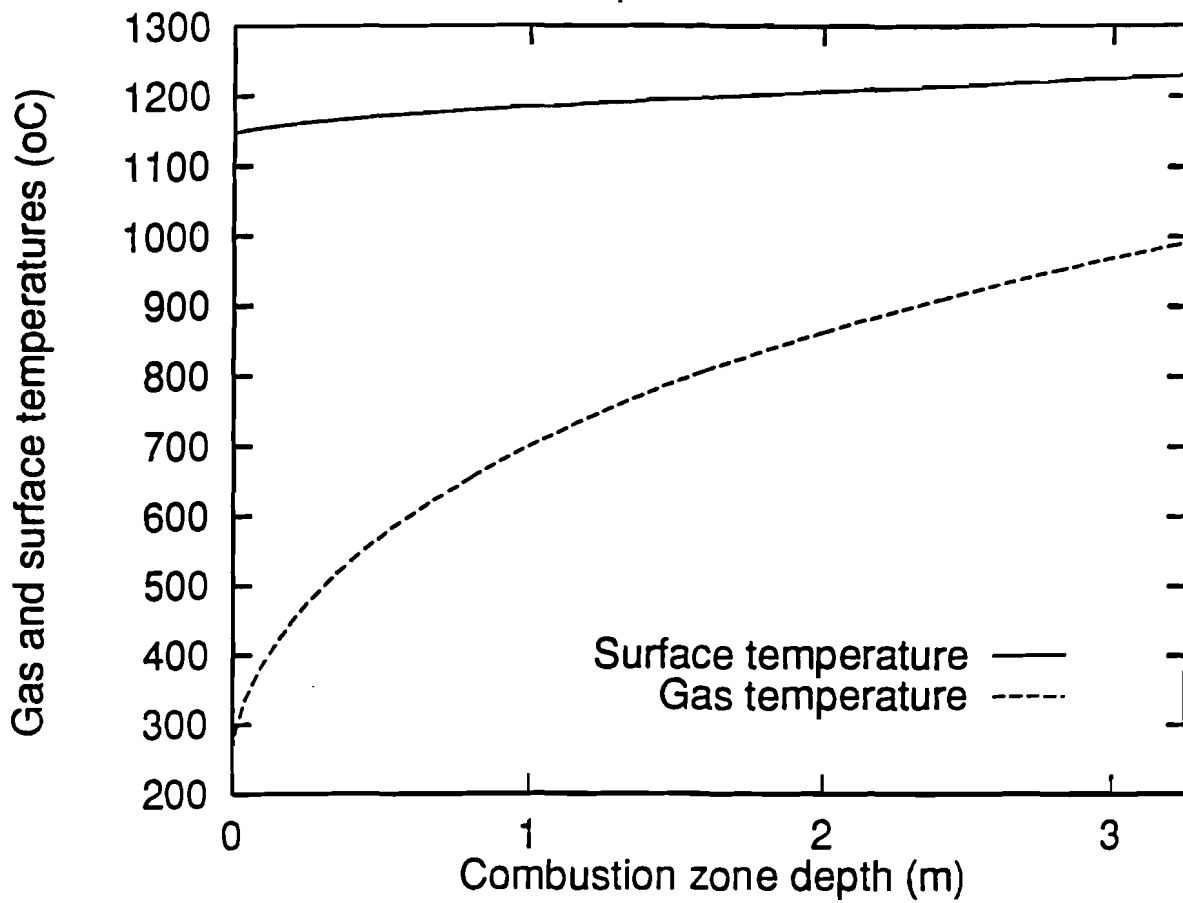


Fig. 2.14 :  $T_s$  and  $T_g$ ,  $R_o = 0.1016$  m,  $\alpha = 100\%$ ,  $\gamma = 80\%$

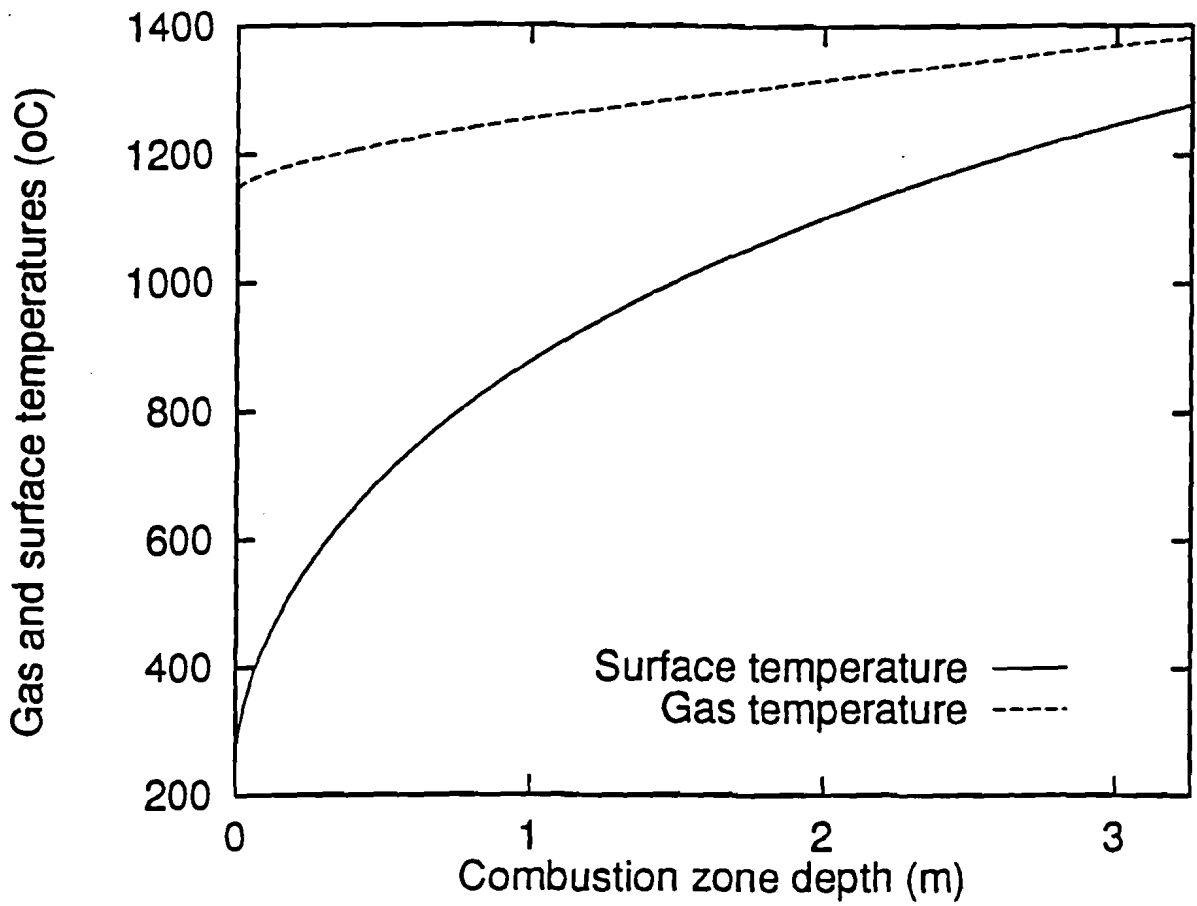


Fig. 2.15 :  $T_s$  and  $T_g$ ,  $R_o = 0.1016$  m,  $\alpha = 100\%$ ,  $\gamma = 100\%$

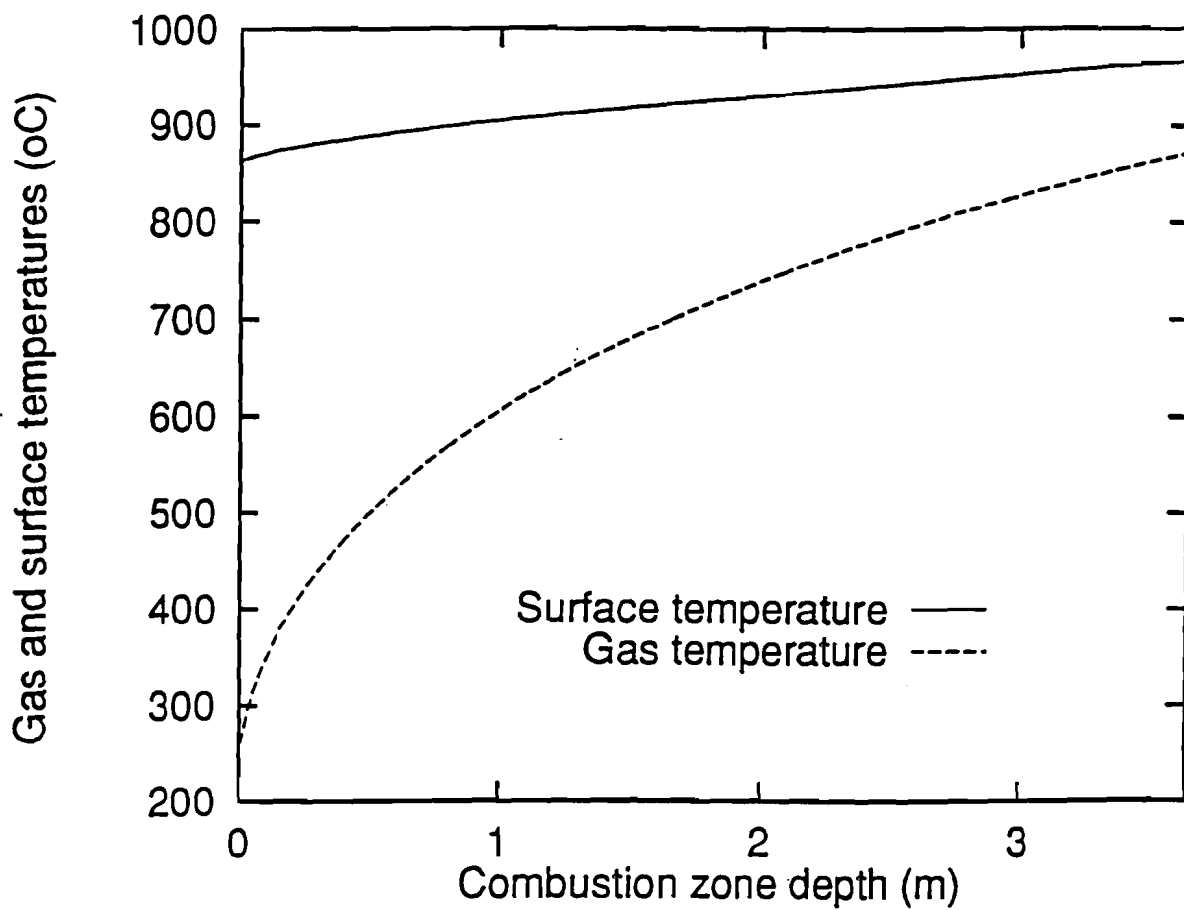


Fig. 2.16 :  $T_g$  and  $T_s$ ,  $R_0 = 0.1016$  m,  $\alpha = 100\%$ ,  $\gamma = 80\%$   
 $m_c = 50\%$

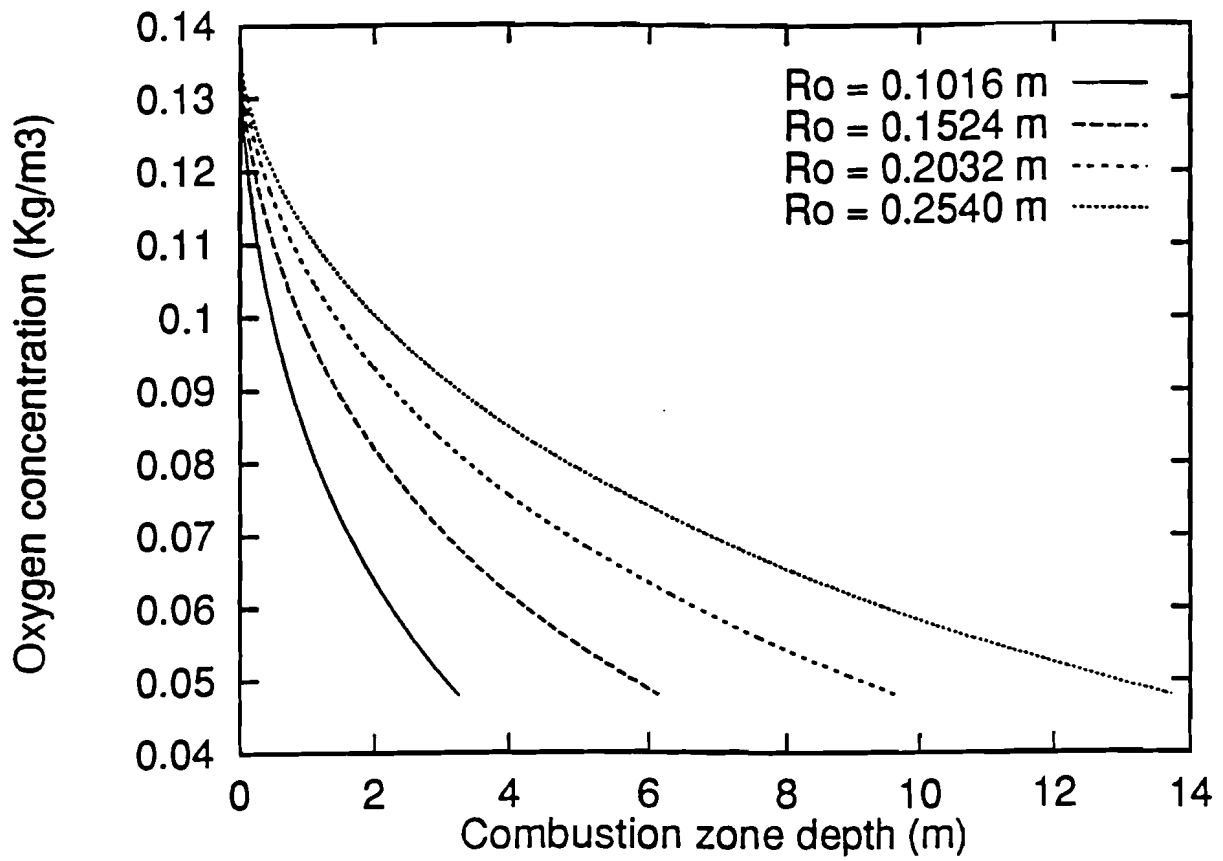


Fig. 2.18 : Oxygen concentration

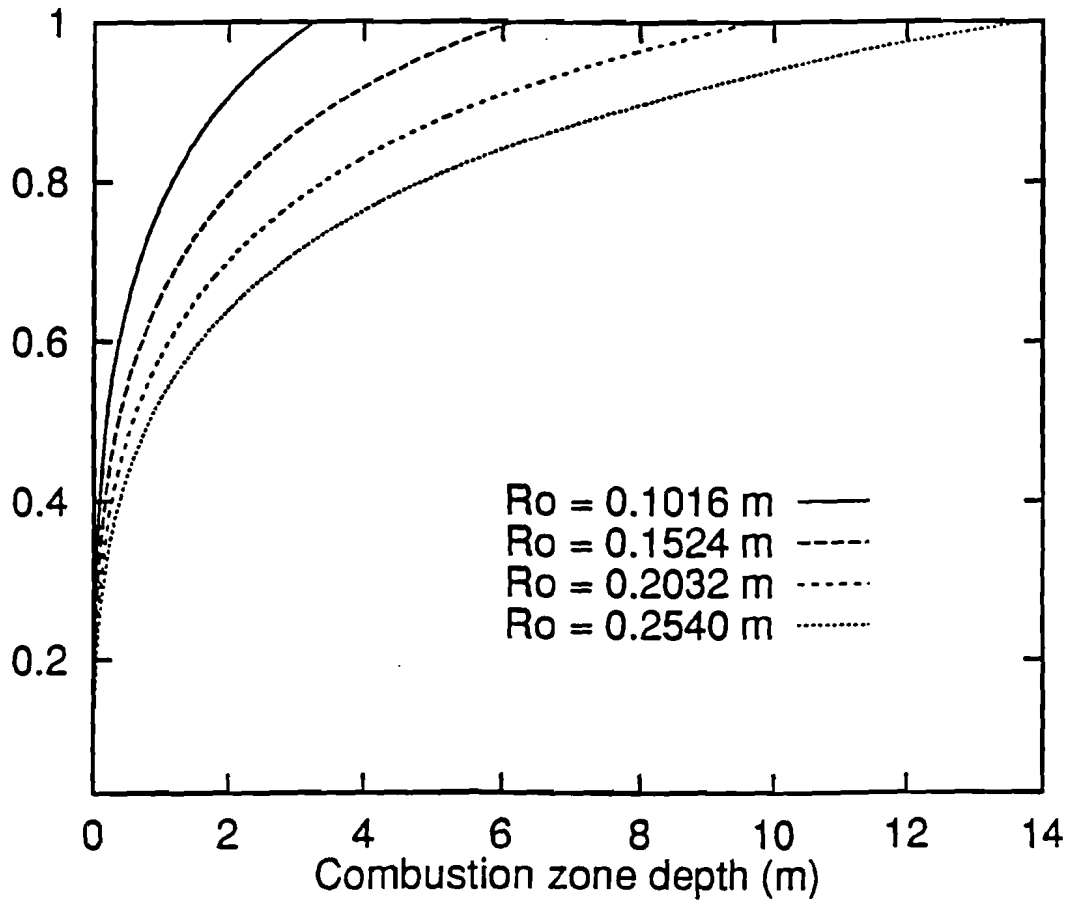


Fig. 2.19 : Normalized radial shrinking rate

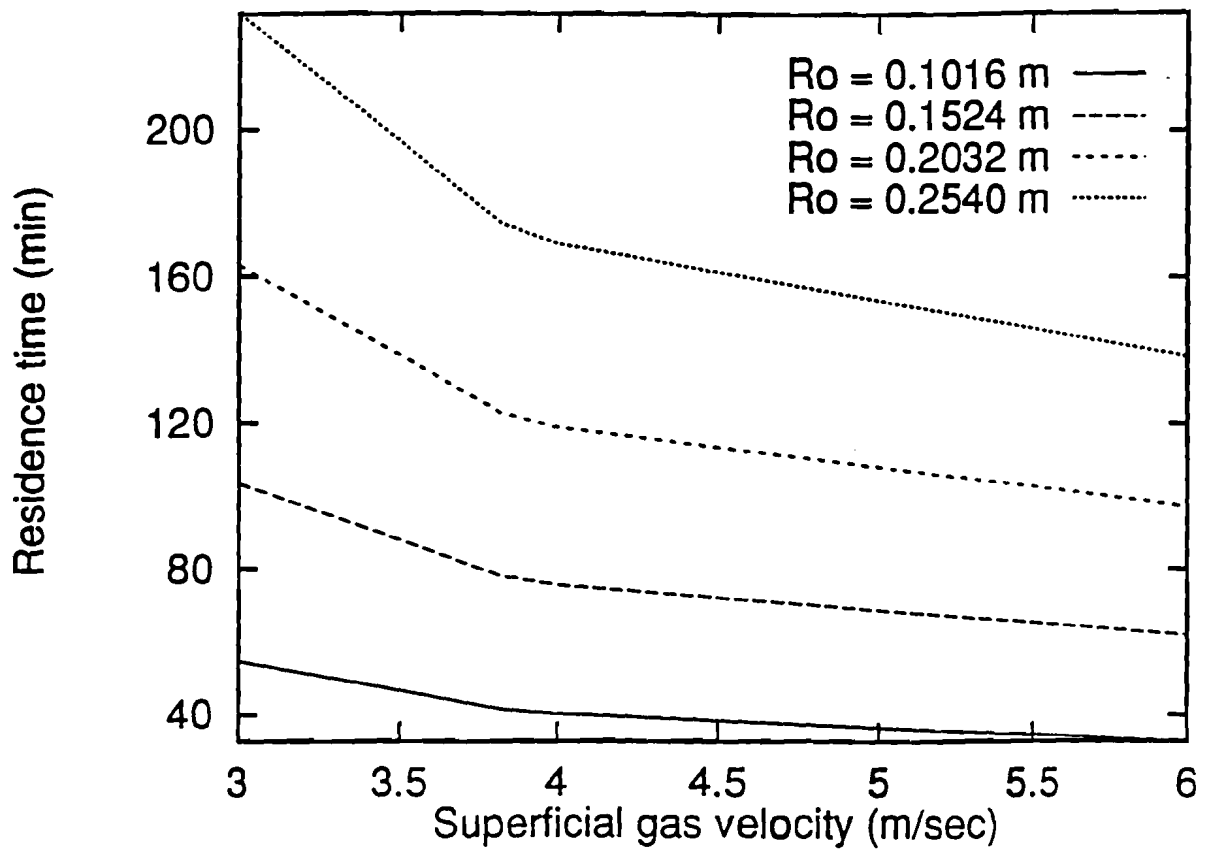


Fig. 2.20 : Effect of  $V_s$  on residence time

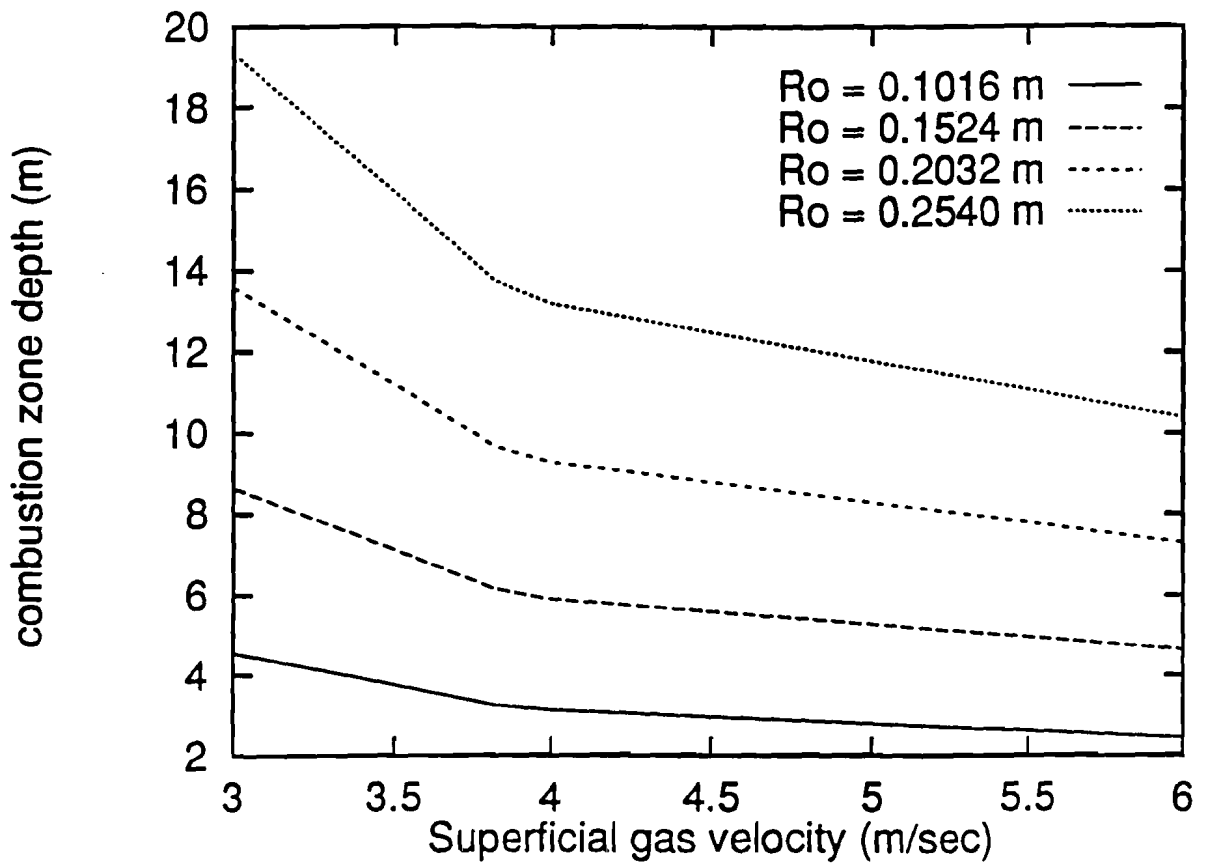


Fig. 2.21 : Effect of  $V_s$  on  $L_c$

## 2.6 References

- 2.1. R. L. Bain and R. P. Overend. Biomass Electric Technologies : Status and Future Development. in Advances in Solar Energy (K. W. Boer ed.), American Solar Energy Society inc. Boulder, Colorado, 7:449-494, 1992.
- 2.2. Draft Final Report, EPRI Project RP 2612-15. Contractor Research Triangle Institute, Research Triangle Park , NC 27709, 1991.
- 2.3 L. D. Smoot. Modeling of coal-combustion processes. Prog. Energy Combust. Sci. 10:229-272, 1980.
- 2.4 M. L. Hobbs, P. T. Radulovic and L. D. Smoot. Modeling fixed-bed coal gasifiers. AICHE J., 38:681-702, 1992.
- 2.5 K. W. Ragland and D. J. A. Purnomo. Pressured downdraft combustion of wood-chips. Twenty-Third Symposium (International) on Combustion, 1025-1032, 1990.
- 2.6 A. Ouedraogo, J. C. Mulligan and J. G. Cleland. A quasi-steady shrinking core analysis of wood combustion. Combustion and flame, (to be published), 1994.
- 2.7 J. Dinwoodie. Wood : Nature's cellular, polymeric fibre-composite. The Institute of Metals, 3-37, 1989.
- 2.8 A. M. Kanury. Thermal decomposition kinetics of wood pyrolysis. Combustion and Flame, 18:75-83, 1972.
- 2.9. B. Schwleger. Power from wood. A special Report. Power, 124(2):1-32.
- 2.10. K. W. Ragland, J. C. Boeger and A. J. Baker. A model of chunkwood combustion. Forest Products J. 38(2):27-32, 1988.
- 2.11. K. Hsiang-Chen and A. S. Kalelkar. On the Heat of Reaction in Wood Pyrolysis. Combustion and flame, 20:91-103, 1973.
- 2.12. J. Diebold and J. Scahill. Ablative Pyrolysis of Biomass in Solid-Convective Heat Transfer Environments. in Fundamentals of Thermochemical Biomass Conversion (R. P. Overend, T. A. Milne and L. K. Mudge, Ed.), Elsevier Applied Science Publishers, 539-555, 1985.



2.13. W. J. Parker. Prediction of the Heat Release Rate of Wood. Ph.D. Thesis, The George Washington University, 1988.

## 2.7 Nomenclature

A	external surface area ( $m^2$ )
$b_c$	char thickness (m)
C	oxygen concentration ( $kg/m^3$ )
$C_{pj}$	specific heat of component j ( $KJ/kg^{\circ}K$ )
D	molecular diffusivity ( $m^2/sec$ )
h	heat transfer coefficient ( $KJ / m^2\text{-sec-}^{\circ}K$ )
$h_D$	mass transfer coefficient (m/sec)
$hfg_m$	enthalpy of phase change of liquid water (KJ/kg)
$hfg_v$	enthalpy of phase change of active matter (KJ/kg)
H	height of the bed (m)
$H_{ag}$	average heat of combustion of gases inside the bed (KJ/Kg)
$H_{as}$	average heat of combustion at the interface (KJ/Kg)
$H_j$	enthalpy of component j (KJ/kg)
K	geometry correction factor
$K_c$	char conductivity ( $KW/m\text{-}^{\circ}K$ )
$l$	wood thickness (m)
L	cell dimension (m)
$L_c$	combustion zone depth (m)
$L_e$	length of bed (m)
$L_r$	bed loading rate (kg/hr)
m	mass (kg )
$\dot{m}$	mass loss rate (kg/sec)
N	number of fuel elements per row
$\dot{N}_i$	loading rate (log/sec)
r	outside radius (m)

$r_0$	initial radius ( $R_0$ in Figures) (m)
$\dot{r}$	rate of radius recession (m/sec)
$t$	time (sec)
$T$	temperature ( $^{\circ}\text{C}$ )
$V$	velocity (m/sec)
$V_f$	migration velocity (m/sec)
$V^*$	row frequency (row/sec)
$V_s$	superficial gas velocity (m/sec)
$W$	width of the bed (m)
$z$	bed coordinate (m)

## Dimensionless variables

$Re_D$	Reynolds number
$S_g$	Specific gravity

## Greek Letters

$\alpha$	fraction of the volatiles which burn to CO at char-gas interface
$\beta$	ratio of the heat of combustion of C to CO to that of C to $\text{CO}_2$
$\epsilon$	mass fraction
$\epsilon_b$	bed volume fraction
$\epsilon_s$	solid volume fraction
$\rho$	density ( $\text{kg/m}^3$ )
$\gamma$	fraction of the total gases that burn inside the bed

## Subscripts

$b$	burnout time
-----	--------------

c	char
g	gas
i	initial (ambient)
j	components (c, m , v)
m	moisture
s	surface
v	volatiles
w	virgin wood

## 2.8 Appendix

## 2.8.1 Code for the quasi-steady combustion model

```
c$$$$$$$$$$$$$$$$$$$$$$$$$$$$$$$$$$$$$$$$$$$$$$$$$$$$$$$$$$$$$$$$$$$$$$$$$$$$$$$$$$$$$$$$
```

```
c This program simulates a steady state one dimensional, fixed-bed model of "whole
c tree" combustion. Quasi-steady condition are assumed inside each fuel element.
```

```
c@@@@@@@@@@@@@@@@@@@@@@@@@@@@@@@@@@@@@@@@@@@@@@@@@@@@@@@@@@@@@@@@@@@@
```

```
c The fuel is loaded from the top of the bed with initial
c radius ri which shrinks to rf at the grate.
c The initial gas (air) temperature is taken to be tgi (oC)
c at a pressure of 1 atm.
c You may run the program for one prescribed moisture at a
c time (greater than 0% ).

c ALL UNITS ARE IN SI.
```

```
c*****
```

```
implicit double precision (a-h,o-z)

parameter(n=50000)

double precision r(n),co(n),tg(n),ts(n)
double precision f(n),g(n),rs(n),cs(n)
double precision rp(n),v(n),w(n),tgf(n)
double precision hd(n),h(n),tsf(n),bc(n)
double precision mc,k,lni,mi,lr,l
```

```
c*****
```

```
c Bed characteristics and wood properties
```

```
c sg is the specific gravity of the wood.
c rc is the density of the char.
c rg and cpg are the density and specific heat of air.
c rb is the bulk density.
c d is the molecular diffusivity.
c vs is the superficial gas velocity as computed from the
c air flow rate mi (5.5 lbair/lbfuel),the loading rate lr
c (75 tons/hr) and the bed cross-section area (wi*1).
c wi and l are the width and depth of the bed.
c ck1 is the negative stoichiometric ratio divided by rc.
c tol is a convergence criteria.
```

c-----

sg=.640d0  
rc=95.0d0  
rg=.650d0  
rb=240.0d0  
d=.0003150d0  
wi=4.5720d0  
l=9.1440d0  
mi=5.50d0  
lr=75.0d0\*907.20d0/3600.0d0  
vs=(mi\*lr)/(rg\*l\*wi)  
ck1=-(12.0d0/16.0d0)/rc  
tol=.0000010d0

c\*\*\*\*\*

c Thermal properties

c ti is the initial wood temperature.  
c cpv,cpm and cpc are respectively the specific heat of  
c the volatile,moisture(vapor) and char.  
c rocgv is the volumetric heat capacity of air.  
c hfgv and hfgm are the enthalpy of phase change of the volatile  
c and liquid water respectively.  
c hc is the enthalpy of combustion of the char  
c hv is the enthalpy of combustion of the volatiles  
c hc1 and hc2 turn out to be the complete and incomplete  
c heat of combustion of the gases inside the bed and the  
c char and volatiles at the char-gas interface.  
c

c-----

ti=25.0d0  
cpv=1.10d0  
cpm=4.20d0  
cpc=.670d0  
cpg=1.0340d0  
rocgv=rg\*cpg  
Hc =31100.0d0  
Hv =13500.0d0  
hfgv=200.0d0  
hfgm=2250.0d0

c\*\*\*\*\*

c Moisture content, initial conditions and additional data.

c mc is the moisture content (input say .15 for 15%).  
c r(1)=rf is the dimension of the radius as it falls through  
c the grate.

```

c   co is the concentration of oxygen at the bottom of the bed
c   k ( suggested value .225) ,c1 and c2 are empirical coeffi
c   cients for the mass and heat transfer coefficients.
c   vfo is the volume fraction of oxygen (21%).
c   dz is the grid size : suggested values ; for ri > .102 i.e
c   i.e.4" dz=.001 ; dz may be as low as .0000001 for ri =
c   .0001 m. In general look for faster convergence.
c   fe is the percentage of total gas ( CO + volatiles) that
c   actually burn inside the bed.

```

```
print*,'-----'
```

```

print*,'input the radius ri, moisture content mc, grid '
print*,'size dz and % of gas that actually burn inside the'
print*,'bed fe1 and fe2 the % of gas that actually burn'
print*,'incompletely at the solid-gas interface'

```

```
print*,'-----'
```

```
read*,ri,mc,dz,fe1,fe2
```

```

r(1)=ri*(.0010d0)**(.50d0)
vfo=.210d0
co(1)=rg*vfo
rs(1)=r(1)
cs(1)=co(1)
k=.2250d0
c1=.7660d0
c2=.5730d0

```

```
-----
```

```

c   alfa is an exponent used to introduce a correction factor
c   for the void fraction as we move upward along the bed.

```

```

tgi=260.0d0
tg(1)=tgi
alfa=.0d0

```

```
c*****
```

```

c   rw is the density of the wood.
c   ec,and ev are the mass fraction of the char, liquid water
c   and volatile.
c   lni is the loading rate (log/sec as computed from lr ).

```

```

rw=1000.0d0*(1.0d0+mc)*sg
ec=rc/rw
em=mc/(1.0d0+mc)
ev=1.0d0-ec-em
esi=rb/rw

```

```

    epsiloi=1.0d0-esi
    epsilo=epsiloi*(r(1)/ri)**(alfa)
    es=1.0d0-epsilo
    pi=4.0d0*datan(1.0d0)
    lni=lr/(pi*rw*1*ri**2)

c*****

    i=2

1    j=i

c    computational constants

    ck2=rw/(rg*cpg*vs)
    ck3=(12.0d0/16.0d0)*(2.0d0*es)*rw*ck1/vs
    ck4=((2.060d0*k*d/2.0d0)*(17400.0d0)**(.4250d0))/epsilo
    cc=pi*lni/wi
    q1=-ck1*ck4*es/cc
    q2=ck3*ck4
    q3=2.0d0*ck2*es
    Hc1=((ec*Hc + ev*Hv*fe2)*(.720d0) + ev*hv*(1.0d0-fe2))
    $*fe1/(ec + ev)
    Hc2=(ec*Hc + ev*Hv*fe2)*(.280d0)/(ec + ev*fe2)

c-----

c    we start the iteration for the radius and oxygen concen
c    tration by using the initial values specified above
c    (first step) the new values are introduced back into the
c    equations (step two ) and the result is averaged with
c    step one to give new values of r and co; we then check
c    for convergence.

c    since we start the computation from the bottom of the bed,
c    r=rf, we stop the program when r=ri (the initial radius).

c-----

    if((r(i-1) .eq. ri) .or. (r(i-1) .gt. ri))go to 4

2    f(j)=(rs(j-1)**(-2.5750d0))*cs(j-1)*(c1*mc*ri/rs(j-1))
    &/ (dexp(c2*mc*ri/rs(j-1))-1.0d0)

    g(j)=(rs(j-1)**(-1.5750d0))*cs(j-1)*(c1*mc*ri/rs(j-1))
    &/ (dexp(c2*mc*ri/rs(j-1))-1.0d0)

    if(j .eq. i)then

    rs(j)=r(i-1)+q1*dz*f(j)
    cs(j)=co(i-1)+q2*dz*g(j)

```



```

j=j+1

go to 2

else

rs(j)=r(i-1)+q1*dz*(f(i)+f(j))/2.0d0
cs(j)=co(i-1)+q2*dz*(g(i)+g(j))/2.0d0

c   check for convergence

   if((dabs(rs(j-1)-rs(j)) .gt. tol) .or. (dabs(cs(j-1)
&-cs(j)) .gt. tol)) then

j=j+1

go to 2

else

r(i)=rs(j)
co(i)=cs(j)
rs(i)=rs(j)
cs(i)=cs(j)

endif
endif

c*****

c   hd and h are the mass and heat transfer coefficients.

do 20 j=i-1,i

hd(j)=ck4*(r(j)**(-.5750d0))*(c1*mc*ri/r(j))
&/ (dexp(c2*mc*ri/r(j))-1.0d0)

h(j)=rocg*hd(j)

rp(j)=ck1*co(j)*hd(j)

20  continue

c*****

c   ts and tg are the surface temperature of the wood
c   and the gas temperature.
c   we use the same computational steps as above.

```

```

a1=(ec + ev)*Hc1
a2=ev*cpv+ec*cpc+em*cpm
a3=em*hfgm + ev*hfgv

b1=(ec + ev*fe2)*Hc2-ev*hfgv-em*hfgm
b2=1.0d0/rw

```

c we start the iteration for tg and ts

```

ts(1)=ti+(b1-b2*h(1)*(tg(1)-ti)/rp(1))/(a2-b2*h(1)/rp(1))
tsf(1)=ts(1)

```

```

ji=i
j=i

```

3 v(j)=rp(ji-1)\*(a1-a2\*(tsf(j-1)-ti)-a3)/r(ji-1)

```

if(j .eq. i)then

```

```

    tgf(j)=tg(i-1)-q3*dz*v(j)
    w(j)=(b1-b2*h(ji-1)*(tgf(j)-ti)/rp(ji-1))/(a2-b2*h(ji-1)
&/rp(ji-1))
    tsf(j)=ti+w(j)

```

```

    j=j+1
    ji=ji+1

```

```

go to 3

```

```

else

```

```

    tgf(j)=tg(i-1)-q3*dz*(v(i)+v(j))/2.0d0
    w(j)=(b1-b2*h(ji-1)*(tgf(j)-ti)/rp(ji-1))/(a2-b2*
&h(ji-1)/rp(ji-1))
    tsf(j)=ti+(w(i)+w(j))/2.0d0

```

```

    if((dabs(tgf(j)-tgf(j-1)) .gt. tol) .or. (dabs(tsf(j)
&-tsf(j-1)) .gt. tol))then

```

```

        j=j+1

```

```

go to 3

```

```

else

```

```

    tg(i)=tgf(j)
    ts(i)=tsf(j)

```

```

endif
endif

```

c output selected quantities

z=dfloat(i-2)\*dz

write(1,\*)z,r(i-1)/ri

write(2,\*)z,co(i-1)

write(3,\*)z,hd(i-1)

write(4,\*)z,h(i-1)

write(7,\*)z,tg(i-1)

write(8,\*)z,ts(i-1)

write(9,\*)r(i-1),hd(i-1)

epsilo=epsiloi\*(r(i)/ri)\*\*(alfa)

es=1.0d0-epsilo

i=i+1

go to 1

c\*\*\*\*\*

c we compute the shrinking rate sr and the burnout time tb  
c by Simpsons ' rule

4 xi0=r(1)\*\*2+r(i)\*\*2

xi1=.0d0

xi2=.0d0

do 30 j= 2,i-1

if(int(j/2)\*2 .eq. j)then

xi2=xi2+r(j)\*\*2

else

xi1=xi1+r(j)\*\*2

endif

30 continue

xi=dz\*(xi0+2.0d0\*xi2+4.0d0\*xi1)/3.0d0

vf=(xi\*cc)/(z\*es)

```
tb=z/(vf*60.0d0)
```

```
sr=(ri-r(1))/tb
```

```
print*, '-----'
```

```
print*, 'the moisture content (%)'
```

```
write(*,*)100.0d0*mc
```

```
print*, 'the combustion zone (m)'
```

```
write(*,*)z
```

```
print*, 'the shrinking rate (m/min)'
```

```
write(*,*)sr
```

```
print*, 'the burnout time (min)'
```

```
write(*,*)tb
```

```
print*, 'the migration velocity of the logs (m/min)'
```

```
write(*,*)vf*60.0d0
```

```
if((tb .eq. .0d0) .or. (sr .eq. .0d0))then
```

```
print*, '-----'
```

```
print*, 'check the grid size dz'
```

```
endif
```

```
print*, '-----'
```

```
write(11,5)ri,100.0d0*mc,z,sr,vf*60.0d0,tb
```

```
5 format(////////,
```

```
&20x, 'the initial radius (m) =',f6.5,/,/,
```

```
&20x, 'the moisture content (%) =',f6.2,/,/,
```

```
&20x, 'the combustion zone (m) =',f10.6,/,/,
```

```
&20x, 'the shrinking rate (m/min) =',f5.4,/,/,
```

```
&20x, 'the migration velocity (m/min) =',f5.4,/,/,
```

```
&20x, 'the burnout time (min) =',f10.6,/,/)
```

```
end
```

```
c$$$$$$$$$$$$$$$$$$$$$$$$$$$$$$$$$$$$$$$$$$$$$$$$$$$$$$$$$$$$$$$$$$$$$$$$$$$$$$$$$$$$
```

3 Transient moving boundary shrinking core model  
of "whole tree" combustion in a countercurrent  
fixed-bed reactor.\*

---

\* A short version of this work was submitted for publication in *Numerical Heat Transfer*, (1994).

## 3.1 Abstract

A transient shrinking core model of "whole tree" combustion in a one dimensional steady state fixed-bed reactor is developed and the results are compared with those of a quasi-steady model. The uniform core temperature and negligible heat of pyrolysis approximations commonly utilized in quasi-steady models are replaced by a transient moving pyrolysis front submodel. A modified *Variable Grid Method* called *Continuous Mapping Variable Grid Method (CMVGM)* is developed to solve the two-phase moving boundary problem in which in addition to the moving interface, the external boundary of the solid fuel is receding due to combustion. As anticipated and assumed in the quasi-steady model, the core temperature remains approximately constant during most of the combustion process, but close to the end, it rises steadily toward the interface temperature. The *CMVGM* scheme is found to be very stable and converge rapidly.

## 3.2 Introduction

In a recently published paper by Ouedraogo *et al.* [3.1], a steady state one dimensional model of "whole tree" combustion in a countercurrent fixed-bed combustor was presented. The bed which was modeled was designed to fire a "whole tree" burn boiler of a 100 MW net power plant [3.2] and to be loaded uniformly from the top at a rate of 75 ton / hr with a theoretical air wet fuel ratio of 5.5 kg / kg. Oxygen (air) is fed from the bottom at a preheated temperature of 260 °C. The quasi-steady model was formulated based on thin char layer and constant core temperature approximations. Also, the heat of pyrolysis was taken to be negligible. Although simple, the model was seen as an extension from previous formulations. First, the combustion of wood, particularly large wood specimens is assumed to be mostly diffusion rather than reaction kinetics controlled. Second, the appropriate combustion model is believed to be the shrinking core model. Third, an overall mass transfer coefficient comprising the effect of blowing is explicitly correlated, modified and incorporated into the combustion model. The results were found to be mostly in good agreement with those of an existing "whole tree" facility [3.2]. However, it has been speculated that the uniform core temperature assumption may be-

come critical especially toward the end of the combustion process. The present model uses the same bed characteristics but carries further the quasi-steady analysis by removing all the previous approximations. Therefore, both the core and shell temperatures become now unknown, function of the interface conditions. Hence, the problem is a two-phase moving boundary problem since the interface also changes its position continuously due to pyrolysis with the subsequent phase-change of active matter and moisture respectively to volatiles and water vapor. Yet another difficulty compared with the classical moving boundary type problem is that the external boundary of the solid fuel is receding due to combustion. Therefore, the solution of this problem requires not only tracking the position of both the interface and the external surfaces of the fuel elements but also tracking the position of the entire "whole tree" elements inside the bed. Computation starts from the top of the bed and the distance traveled by the fuel elements down to the fixed grate defines as before the residence time and bed depth. The bed is still a one dimensional steady combustor while unsteady conditions prevail inside each fuel element. The "whole tree" elements then undergo an unsteady overlapping phases of drying (preheat), pyrolysis and combustion.

The sequence of the actual "whole tree" process is believed to be as follows: 1) The exiting flue-gases dry and preheat the external layers of the fuel elements surfaces up to pyrolysis, with the subsequent formation of a char layer or shell surrounding an interior core which is still made of virgin wood. 2) The "whole tree" elements migrate to a area of the bed where the oxygen concentration is appropriate to cause combustion. 3) The heat released by the burning shell layers and pyrolysis products provides the necessary energy to further dry and pyrolyze the core so that all three processes overlap during most of the combustion process. This results in the formation of two distinct fronts : a) The combustion front, which is the driving force and which exchanges heat and matter with both the core and the gas phase and causes the recession of the external surface, b) the drying and pyrolysis front, which pyrolyzes the virgin wood (core) and causes the formation of the shell layer. The devolatilization of the wood layers is accomplished only as the pyrolysis front reaches these layers.

The complete model comprises then : First, the preheated process at the top of the bed, which is modeled by the heat equation with internal moisture convection and evaporation. This submodel is run until according to the experimental findings of Ragland *et al.* [3.3] on the combustion of green chunkwood, a char layer of approximately 6.00 mm thickness is formed. This submodel also provides the following set of inputs for the solid phase combustion model : core radius and shell thickness along with core and shell temperature profiles. Second the solid phase combustion model which itself comprises - The drying and pyrolyzing core submodel with internal moisture and pyrolysis gases convection, moisture evaporation and no internal heat generation - The burning shell layer submodel with convection of the exiting moisture and volatile gases. Heat is assumed to be generated only at the external boundary by the combustion of the shell and escaping volatile gases - The core and shell submodels cheer a common moving boundary. Third the gas phase model. The solid and gas phases combustion models are checked for temperatures convergence and specially for the convergence of the time step computed from the velocity of the pyrolysis front (moving boundary).

The objective of this study is to extend further the investigation carried out in the quasi-steady analysis by formulating a transient shrinking core model which removes all the previous assumptions. The work is divided in three parts : First the unsteady submodels of the fuel drying process, core recession and pyrolysis, fuel shell combustion along with steady state gas phase combustion equations are developed, second the numerical method for solving the two-phase moving boundary problem is formulated and presented, third, the results of the model are compared with those of the previous quasi-steady model.

### 3.3 Upper region modeling : Preheat submodel

"Whole tree" elements, assumed to be at uniform ambient temperature are loaded from the top of a continuously operating countercurrent fixed-bed. They are assumed to go through a pure drying (preheat) process which occurs at a much higher temperature and faster rate than usual timber drying reported by Plumb *et al.* [3.4]. This particular



type of drying actually only displaces moisture in the sapwood near the outer surface. Moisture from the inner layers then reaches the surface by diffusion over a period of time. When the trunk diameter is large as in the case of "whole tree" elements, it becomes more difficult for this process to occur. This may explain why such drying does not go to completion as in conventional drying. Instead the outer layers are dried first by the exiting flue-gases and their temperature increases to pyrolysis, while the interior layers remain practically virgin wood at ambient temperature.

The upper region is so close to the combustion zone that the initial gas temperature is assumed to be the exiting gas temperature from the combustion zone. The fuel elements are assumed to be made of fixed carbon (char called  $s$  here for shell to avoid confusion with the core  $c$ ), active matter which pyrolyzes to volatiles ( $v$ ), and moisture ( $m$ ) which evaporates to water vapor. Each phase represents a continuum governed by conservation laws and following Whitaker [3.5], a single governing equation is achieved which is valid throughout all phases by phase averaging. The equations are developed with the assumption that there is no viscous dissipation, the wood thermal conductivity is constant and only radial movement of moisture and volatiles occurs. The phase averaged energy equation of the preheat process is then

$$\phi_w \rho_w (\epsilon_s C_{ps} + \epsilon_v C_{pv} + \epsilon_m C_{pm}) \frac{\partial T}{\partial t} + \rho_w \epsilon_m C_{pm} V_g \frac{\partial T}{\partial r} = \frac{1}{r} \frac{\partial}{\partial r} (r K_w \frac{\partial T}{\partial r}) - Q \quad (3.1)$$

where  $Q = \epsilon_m (\rho_w - \rho_{dw}) (1 - \phi_w) h f g_m A_m \exp(-E_m / R T)$

$$\rho_w = S_g (1 + mc) \rho_{water} \quad \text{and} \quad 0 < r \leq r_0$$

$V_g$  is the velocity of the convective gases, given by the momentum equation or Darcy's law and is a function of the wood permeability, the viscosity of the gas mixture and the gas phase pressure gradient. The pressure is assumed to be the saturated vapor pressure  $P_{sv}$  given by Siau [3.6]. In S.I. units it is expressed as

$$P_g = p_{sv} = 11.66375 \times 10^{10} \exp(-43472 / RT)$$

and the momentum equation is written as

$$V_g = -\frac{k_{gc}}{\mu_g} \nabla P_g(r) < 0$$

The set of equations is subjected to the following initial and boundary conditions

$$T(r, t = 0) = T_i \quad , \quad 0 \leq r \leq r_o$$

where  $T_i$  is the ambient temperature.

$$\frac{\partial T}{\partial r} \Big|_{r=0} = 0 \quad , \quad t > 0$$

$$K_w \frac{\partial T}{\partial r} \Big|_{r=r_o} = h (T_g - T(r_o, t)) \quad , \quad t > 0$$

No heat is generated in the drying zone of the combustor and therefore, the energy equation of the gases as they pass upward through the steady-state upper regions of the combustor is

$$\rho_g C_{pg} V_{sg} \frac{\partial T_g}{\partial z} = h A_{av} (T_g - T(r_o, t)) \quad (3.2)$$

At  $z=z_1$  where  $z_1$  is the fuel elements inlet plane, the gas temperature  $T_g(z=z_1)$  is given by the quasi-steady model.  $T_g(z=z_1)=1010.0, 950.0, 900.0,$  and  $860.0$  °C for "whole tree" elements at 25, 30, 33.3 and 40 % moisture respectively.

In this zone of the combustor, the "whole tree" radius remains constant and equation (3.1) expresses the fact that the heat carried inside the elements by pure conduction plus

the heat carried by the inward convected moisture is equal to the heat accumulated plus the volumetric heat of evaporation. At the end of the preheat process, a shell layer of thickness  $b$  is formed surrounding a core of virgin wood of radius  $r_c$ .

### 3.4 Solid phase combustion

#### 3.4.1 Shell combustion submodel.

The "whole tree" elements migrate downward to a location of the bed where the oxygen concentration is such that combustion begins. The combustion of the shell (char) layer takes place at constant density. The volatiles and water vapor leaving the core convect through the porous shell into the bed environment. Heat is generated only by glowing combustion at the shell-gas interface. The phase averaged energy equation for the shell layer is

$$\epsilon_b \rho_s C_{ps} \frac{\partial T_s}{\partial t} + \rho_w V_g (\epsilon_v C_{pv} + \epsilon_m C_{pm}) \frac{\partial T_s}{\partial r} = \frac{1}{r} \frac{\partial}{\partial r} (r K_s \frac{\partial T_s}{\partial r}) \quad (3.3)$$

where  $r$  varies between the core-shell interface and the external fuel radius  $r_s$ , i.e.  $r_c \leq r \leq r_s$ . The shell thickness  $b$  is not modeled as in [3.7] but defined as

$$b(t) = r_s(t) - r_c(t)$$

Equation (3.3) is subjected to the following conditions. The shell temperature,

$$T_s(r, t = t_p) \quad , \quad r_c \leq r \leq r_s$$

at this location  $z_p$  of the bed, where  $t_p$  is the preheat time is given by the drying submodel described above. The convective boundary equation at the combustion front ( $r=r_s$ ) is written as

$$\rho_w (V_s \epsilon_s h_s + \alpha V_g \epsilon_v h_v) + h (T_g - T_s(r = r_s, t)) = K_s \frac{\partial T_s}{\partial r} \Big|_{r=r_s} \quad , \quad t > t_p$$

In this equation, the first term on the left represents the heat released by the shell combustion, the second represents the heat released by the combustion of a fraction  $\alpha$  of the volatiles and the third term is the convective heat exchange between the shell and gas phase. The term in the right is the heat conducted away from the combustion front and into the shell. The heat transfer coefficient  $h$  in the convective boundary relation has been correlated in previous studies by Ouedraogo *et al.* [3.1, 3.7] as

$$h = h_D \rho_g C_{pg}$$

where  $\rho_g C_{pg}$  is the volumetric heat capacity of the gases and  $h_D$  the mass transfer coefficient [3.1]. The shell recession velocity  $V_s$  in the convective boundary relation has been defined [3.1] as

$$V_s = -\dot{r} = \left(\frac{12}{16}\right) \frac{h_D C}{\rho_s}$$

where  $\rho_s$  is the constant shell (char) density and  $C$  the oxygen concentration inside the bed. The gases are assumed to convect at a much higher velocity, given as before by the momentum equation

$$V_g = -\frac{k_{gs}}{\mu_g} \nabla P(r) > 0$$

where  $k_{gs}$  is the permeability of the gases inside the shell layer. Since there is no moisture inside the shell, the pressure  $P(r)$  is modeled following a one dimensional steady state temperature distribution in a hollow cylinder of radius  $r$ . That is,

$$P(r) = P_g + (P_a - P_g) \frac{\ln(r/r_c)}{\ln(r/r_s)}$$

where  $P_g$  and  $P_a$  are respectively the saturated vapor pressure and the atmospheric pressure. They represent the limit of  $P(r)$  at the core-shell and shell-gas interfaces.

Finally, at the interface core-shell, the shell temperature is assumed to be equal to the interface temperature  $T_m^*$ . That is,

$$T_s(r = r_c, t) = T_m^* \quad , \quad t > t_p$$

### 3.4.2 Core drying and pyrolysis submodel

Part of the heat generated by the combustion front propagated inward and further dries (lost of moisture by the core) and pyrolyzes the core which is made of virgin wood. The conservation of energy in the core includes, heat conduction, internal convection of moisture and volatiles, heat of evaporation, and accumulation. No heat is generated and the pyrolysis is assumed to take place solely at a plane defined by the interface core-shell. The core energy equation is

$$\phi_w \rho_w (\epsilon_s C_{ps} + \epsilon_v C_{pv} + \epsilon_m C_{pm}) \frac{\partial T_c}{\partial t} + \rho_w V_g (\epsilon_v C_{pv} + \epsilon_m C_{pm}) \frac{\partial T_c}{\partial r} = \frac{1}{r} \frac{\partial}{\partial r} (r K_w \frac{\partial T_c}{\partial r}) - Q \quad (3.4)$$

$0 < r \leq r_c$ , where the convective gas velocity  $V_g$  is the same as in the preheat process and the equation of the volumetric evaporation has also been defined. The following conditions apply to equation (3.4). The core temperature

$$T_c(r, t = t_p) \quad , \quad 0 \leq r \leq r_c$$

at this particular location  $z_p$  of the bed is given by the preheat submodel. The boundary condition at the "whole tree" midplane ( $r=0$ ) is

$$\frac{\partial T_c}{\partial r} \Big|_{r=0} = 0 \quad , \quad t > t_p$$

At the interface core-shell, the core temperature is assumed to be equal to the interface temperature. That is,

$$T_c(r = r_c, t) = T_m^* \quad , \quad t > t_p$$

### 3.4.3 Core-shell interface modeling

Right at the boundary i.e. for  $r = r_c$  the temperatures of the core and shell are equal and equal to the interface (pyrolysis) temperature. That is,

$$T_c(r = r_c, t) = T_s(r = r_c, t) = T_m^* \quad , \quad t > t_p \quad (3.5)$$

Now the energy balance at the core-shell interface may be written as

$$K_s \frac{\partial T_s}{\partial r} - K_w \frac{\partial T_c}{\partial r} = -\rho_w \dot{r}_c \epsilon_s h_p \quad (3.6)$$

where  $-\dot{r} = V_c$  is the core recession velocity and  $h_p$  is the heat of pyrolysis. Assuming that the heat of evaporation of moisture at the interface has little influence on the propagation of the pyrolysis wave, the above equation expresses the fact that the heat conducted from the combustion front through the shell dries the core and pyrolyzes the active matter.

## 3.5 Gas phase combustion

The bed is assumed to be one dimensional and in a steady state and oriented upward. Now we shift our attention from the "whole tree" elements as such, to formulate what happens at a given location  $z$  of the bed. The axial oxygen mass balance is modeled as follows

$$V_{sg} \frac{dC}{dz} = -\dot{m}_{O_2}'' \left( \frac{A_{av}}{Vol} \right) \quad (3.7)$$

where  $A_{av} = 2 \frac{\epsilon_{sv}}{r}$  is the area to volume ratio and  $\dot{m}_{O_2}''$  is the oxygen mass flux defined [3.1] as

$$\dot{m}_{O_2}'' = -i [ \rho_s \dot{r}_s + (\rho_w - \rho_s) (1 - \frac{b}{r}) \dot{r}_c ]$$

Hence, equation (3.7) may be compactly written as

$$V_{sg} \frac{dC}{dz} = i [ \rho_s \dot{r}_s + (\rho_w - \rho_s) (1 - \frac{b}{r}) \dot{r}_c ] \frac{2 \epsilon_{sv}}{r}$$

where  $i$  is a stoichiometric index (12/16). The oxygen concentration at the beginning of the combustion process  $C(z=z_p)$  where  $z_p$  is the location of the bed where the combustion begins is estimated from the quasi-steady model to be  $0.040 \text{ kg/m}^3$  for all moisture and fuel elements size. The equation of energy conservation in the gas phase is a modified version of the quasi-steady model. That is,

$$\rho_g C_{pg} V_{sg} \frac{dT_g}{dz} = \dot{m}_{O_2}'' \frac{2 \epsilon_{sv}}{r} [ (\epsilon_s + \epsilon_v) \gamma H_{ag} - \sum_{j=1}^3 \epsilon_j C_{pj} (T_s - T_c) - (\epsilon_v hfg_v + \epsilon_m hfg_m) ] \left( \frac{1}{i} \right) \quad (3.8)$$

and  $H_{ag}$  is the average complete heat of combustion of the gases inside the bed given as

$$H_{ag} = \frac{[ (\epsilon_s H_s + \alpha \epsilon_v H_v) (1 - \beta) + (1 - \alpha) \epsilon_v H_v ]}{\epsilon_s + \epsilon_v}$$

The gas temperature  $T_g(z=z_p)$  is given by the preheat submodel.

### 3.6 Numerical method : Finite Difference Approximation

Because the set of equations to be solved are nonlinear due to the nonlinearity of the governing equations and boundary conditions (except for the boundary conditions in the gas and oxygen equations), their exact analytical solutions are in general not possible to obtain. Therefore, recourse is made here to numerical finite difference method. The flow problem being decoupled from the temperature problem, the radial velocity  $V_g$  becomes an input to the energy equation. Various schemes are available for the finite difference approximation of nonlinear diffusion problems. Here we make use of the combined

Crank-Nicolson method because of its versatility to yield the simple explicit, simple implicit and the simple Crank-Nicolson schemes.

Let us write the general form of the diffusion equation compactly as follows

$$\rho C_p \frac{\partial T}{\partial t} + \lambda(T) \frac{\partial T}{\partial r} = \frac{1}{r} \frac{\partial}{\partial r} (r K \frac{\partial T}{\partial r}) + Q(T) \quad (3.9)$$

Comparing relation (3.9) with equations (3.1), (3.3) and (3.4), the values of  $\rho C_p$ ,  $\lambda(T) = \chi V_g$  (where  $\chi$  is a constant for a given moisture),  $Q(T)$  and  $K$  are readily available.

### 3.6.1 Internal nodes

Applying the simple explicit forward differencing for the time derivative, the upwind and the central difference schemes to discretize respectively the convective terms and the second order derivatives, we get the following finite difference approximation of the diffusion equation (3.9) in the form of

$$\begin{aligned} & \Delta r (r \rho C_p)_i \frac{T_i^{n+1} - T_i^n}{\Delta t} + [r \lambda(T^n)]_i \Delta r \Theta \left( \frac{\partial T}{\partial r} \right)_i^{n+1} + [r \lambda(T^n)]_i \Delta r (1 - \Theta) \left( \frac{\partial T}{\partial r} \right)_i^n \\ & = \Theta \left[ (rK)_{i+1/2} \frac{T_{i+1}^{n+1} - T_i^{n+1}}{\Delta r} + (rK)_{i-1/2} \frac{T_{i-1}^{n+1} - T_i^{n+1}}{\Delta r} \right] + (1 - \Theta) \left[ (rK)_{i+1/2} \frac{T_{i+1}^n - T_i^n}{\Delta r} \right. \\ & \quad \left. + (rK)_{i-1/2} \frac{T_{i-1}^n - T_i^n}{\Delta r} \right] + r_i \Delta r Q(T_i^n) \end{aligned} \quad (3.10)$$

where the upwind scheme in the convection terms yields for the (n) time step

$$\left( \frac{\partial T}{\partial r} \right)_i^n = \frac{T_i^n - T_{i-1}^n}{\Delta r} \quad \text{for} \quad V_g > 0$$

$$\left( \frac{\partial T}{\partial r} \right)_i^n = \frac{T_{i+1}^n - T_i^n}{\Delta r} \quad \text{for} \quad V_g < 0$$



Similar relations may be written for the (n+1) time step. The sink relation and the coefficients of the convective terms are seen to be lagging by one time step i.e. when the computation is performed at the time level (n+1), these relations are evaluated at the previous time level (n). Assuming a positive convective velocity, expanding and collecting terms, equation (3.10) may be written more compactly as

$$\begin{aligned}
& - \left[ \frac{\Delta t \theta \lambda(T_i^n)}{(\rho C_p)_i \Delta r} + \frac{\Delta t \theta (rK)_{i-1/2}}{(r \rho C_p)_i \Delta r^2} \right] T_{i-1}^{n+1} + \left[ 1 + \frac{\Delta t \theta (rK)_{i+1/2}}{(r \rho C_p)_i \Delta r^2} + \frac{\Delta t \theta (rK)_{i-1/2}}{(r \rho C_p)_i \Delta r^2} + \frac{\Delta t \theta \lambda(T_i^n)}{(\rho C_p)_i \Delta r} \right] T_i^{n+1} \\
& - \frac{\Delta t \theta (rK)_{i+1/2}}{(r \rho C_p)_i \Delta r^2} T_{i+1}^{n+1} = \left[ \frac{\Delta t (1-\theta) \lambda(T_i^n)}{(\rho C_p)_i \Delta r} + \frac{\Delta t (1-\theta) (rK)_{i-1/2}}{(r \rho C_p)_i \Delta r^2} \right] T_{i-1}^n + \left[ 1 - \frac{\Delta t (1-\theta) (rK)_{i+1/2}}{(r \rho C_p)_i \Delta r^2} \right. \\
& \quad \left. - \frac{\Delta t (1-\theta) (rK)_{i-1/2}}{(r \rho C_p)_i \Delta r^2} - \frac{\Delta t (1-\theta) \lambda(T_i^n)}{(\rho C_p)_i \Delta r} \right] T_i^n + \frac{\Delta t (1-\theta) (rK)_{i+1/2}}{(r \rho C_p)_i \Delta r^2} T_{i+1}^n + \frac{\Delta t}{(\rho C_p)_i} Q(T_i^n)
\end{aligned} \tag{3.11}$$

$\theta$  ( $0 \leq \theta \leq 1$ ) is the weight factor representing the degree of implicitness, i. e. equation (3.11) reduces to the simple explicit form for  $\theta = 0$ , to the simple implicit scheme for  $\theta = 1$  and to the Crank-Nicolson method for  $\theta = 1/2$ . A more useful form of relation (3.11) is written as

$$A_i T_{i-1}^{n+1} + B_i T_i^{n+1} + C_i T_{i+1}^{n+1} = D_i T_{i-1}^n + E_i T_i^n + F_i T_{i+1}^n + \frac{\Delta t}{(\rho C_p)_i} Q(T_i^n) \tag{3.12}$$

where the coefficients of the node temperatures are clearly defined by equation (3.11). The simplest but sometimes less accurate method for computing the thermal properties is to lag their evaluation by one time step. A more accurate approach, however, is the extrapolation scheme, in fact a one order Taylor series expansion and may be found in the book by Ozisik [3.8]. Here, the thermal properties are assumed constant and the core density is only function of the moisture constant (mc). Assuming that the coefficients of the node temperatures are available, two separate cases have to be envisioned. First, by choosing an appropriate time step, the system (3.12) provides a complete set of equations for the determination of the fuel preheat unknown internal node temperatures when the temperatures at the boundary are prescribed. Second, in order to determine the core and shell internal node temperatures, additional technique has to be developed to handle the

moving boundary problem. In either case, since we are dealing with prescribed heat flux or convective boundary conditions, the boundary temperatures are unknown and additional relations are needed and described below.

### 3.6.2 Convective boundary nodes

For the convective boundary at the external surface of the "whole tree" elements, the diffusion equations (3.1) or (3.3) may be discretized with the Dupont-II scheme, Ozisik [3.8], or simply discretized as in equation (3.9). We start by evaluating the corresponding equations at the boundary  $s$ .

$$\rho C_p \frac{\partial T}{\partial t} \Big|_s + \lambda(T) \frac{\partial T}{\partial r} \Big|_s = \frac{1}{r} \frac{\partial}{\partial r} (r k \frac{\partial T}{\partial r}) \Big|_s + Q(T) \Big|_s$$

Expanding this relation, collecting terms and making use of the corresponding convective boundary relation i.e.,

$$\mathfrak{S}(T) \Big|_s = k \frac{\partial T}{\partial r} \Big|_s, \quad t > t_p$$

where  $\mathfrak{S}(T) \Big|_s = [\rho_w (V_s \epsilon_s h_s + \alpha V_g \epsilon_v h_v) + h (T_g - T_s(r, t))] \Big|_s$  or

$$\mathfrak{S}(T) \Big|_s = h (T_g - T(r, t)) \Big|_s$$

discretizing the final relation and utilizing a fictive node inside the bed yields

$$\begin{aligned} & \left[ 1 + \frac{2\Delta t k \Theta}{\rho C_p \Delta r^2} \right] T_i^{n+1} - \frac{2\Delta t k \Theta}{\rho C_p \Delta r^2} T_{i-1}^{n+1} = \left[ 1 - \frac{2\Delta t k}{\rho C_p \Delta r^2} (1 - \Theta) \right] T_i^n \\ & + \frac{2\Delta t k}{\rho C_p \Delta r^2} (1 - \Theta) T_{i-1}^n + \left( \frac{\Delta t}{\rho C_p} \right) \left[ \left( \frac{1}{r} \right)_i + \frac{2}{\Delta r} - \frac{\lambda(T_i^n)}{k} \right] \mathfrak{S}(T_i^n) + Q(T_i^n) \end{aligned} \quad (3.13)$$

where the index  $i$  identifies the boundary node and  $i-1$  the internal nearest node.

### 3.6.3 Centerline nodes

Since the same boundary conditions are applied to the external surface of the cylindrical shaped "whole tree" elements, the preheat and combustion processes are symmet-

rical about  $r=0$ . The finite difference equation is not applicable at this particular location because it has a singularity. A expression applicable at  $r=0$  can be developed by making use of the symmetry condition (zero heat and mass flux at midplane) in equation (3.9). Replacing the fictional temperature at the fictional node "-1" (in the region  $r$  negative) by the temperature at node "+1" due to symmetry, the discretization of the appropriate expression is straightforward and yields the temperature at  $i = 0$  i.e.  $T_0$ .

$$\begin{aligned} \left[ 1 + \frac{4 \Delta t \theta k_w}{\rho C_p \Delta r^2} \right] T_0^{n+1} - \frac{4 \Delta t \theta k_w}{\rho C_p \Delta r^2} T_1^{n+1} &= \left[ 1 - \frac{4 \Delta t (1-\theta) k_w}{\rho C_p \Delta r^2} \right] T_0^n \\ + \frac{4 \Delta t (1-\theta) k_w}{\rho C_p \Delta r^2} T_1^n + \frac{\Delta t}{\rho C_p} Q(T_0^n) \end{aligned} \quad (3.14)$$

### 3.6.4 Interface nodes

The interface although moving, has a prescribed temperature and therefore, is a boundary for both the shell and core. Applying equation (3.12) to Figure 3.1, where the core total number of grid points is  $N$ , the following relations are obtained for the temperature of the nearest nodes to the interface in each subdomain

$$\begin{aligned} A_{N-1} T_{cN-2}^{n+1} + B_{N-1} T_{cN-1}^{n+1} &= D_{N-1} T_{cN-2}^n + E_{N-1} T_{cN-1}^n \\ + (F_{N-1} - C_{N-1}) T_m^* + \frac{\Delta t}{\rho C_p} Q(T_{N-1}^n) \end{aligned} \quad (3.15)$$

$$\begin{aligned} B_{N+1} T_{sN+1}^{n+1} + C_{N+1} T_{sN+2}^{n+1} &= (D_{N+1} - A_{N+1}) T_m^* + E_{N+1} T_{sN+1}^n \\ + F_{N+1} T_{sN+2}^n + \frac{\Delta t}{\rho C_p} Q(T_{N+1}^n) \end{aligned} \quad (3.16)$$

### 3.6.5 Determination of the time step

At this point we will only say that the time step is obtained by discretizing equation (3.5) and making use of relation (3.6). Utilizing figure 3.1, it is written as

$$\Delta t_n = t_{n+1} - t_n = \frac{\rho_w \epsilon_v h_p \Delta r^2}{K_w [T_m^* - T_{cN-1}^{n+1}] - K_s [T_{sN+1}^{n+1} - T_m^*]} \quad (3.17)$$

and the core recession velocity  $V_c$  is inferred from relation (3.17). That is,

$$V_c = \left[ \frac{1}{\rho_w \epsilon_v h_p \Delta r} \right] [K_w (T_m^* - T_{cN-1}^{n+1}) - K_s (T_{sN+1}^{n+1} - T_m^*)]$$

### 3.6.6 Bed spatial grid

The migration velocity  $V_f$  of the "whole tree" inside the bed is defined as

$$V_f = \left( \frac{\dot{N}_i \Pi}{W \epsilon_{sv}} \right) r^2 = \frac{C^* r^2}{\epsilon_{sv}}$$

where  $C^* = \frac{\dot{N}_i \Pi}{W}$

This relation allows for the determination of the bed spatial grid as

$$\Delta z_k = \Delta t_n \frac{C^* r^2}{\epsilon_{sv}} \quad (3.18)$$

where k here is clearly the bed grid index. It also represents a closure of the model equations. As can be seen, for a given moisture content and bed characteristics, the bed grid size is a function of the time step and fuel radius. Therefore, the bed grid size is constant in the upper region of the bed, but becomes increasingly small as the "whole tree" elements shrink during the combustion process. Furthermore, relation (3.18) transforms the bed spatial grid into a virtual time step then allowing the incorporation of the steady state gas equations into the computation of the time-dependent fuel temperature.

## 3.7 Continuous Mapping Variable Grid Method: *CMVGM*

Relations (3.9) to (3.18) are now used to develop a new technique to solve the transient moving boundary shrinking core model. Various numerical methods for solving

moving boundary problems have been reported by many investigators in the literature, a classification of these methods can be found in the book by Osižik [3.8]. Here a modified version of the *Variable grid methods* called *Continuous Mapping Variable Grid Method (CMVGM)* is proposed to solve the transient shrinking core model of "whole tree" combustion in packed bed. Under the previous methods, usually a plane geometry domain "x-t" is subdivided into equal interval in one direction only. The corresponding grid size in the other direction is then determined so that the moving boundary always remains at a grid point. Murray and Landis [3.9] choose equal steps in time direction and keep the number of space intervals fixed for all times. In another example, Douglas and Gallie [3.10] divided the x-direction into equal intervals and choose time steps such that the moving boundary crosses exactly one mesh during that interval. Yet another method is due to Crank and Gupta [3.11] where the t-direction is divided into equal intervals and the space intervals are kept fixed.

The method proposed here is a modified version of the previous schemes (Murray and Landis and Douglas and Gallie) applied to a cylindrical domain. Consider a "whole tree" element of radius  $r$  at the end of the preheat process where a shell layer of thickness  $b$  is formed surrounding a core of virgin wood of radius  $r_c$  represented by the computational domain shown in Figure 3.2. As in Murray and Landis scheme, the "r-t" domain, as a matter of fact, the  $r_c$ -t and b-t subdomains at the beginning of the actual combustion process, are subdivided into equal interval by fixing the number of grid points for each subdomain, i.e.

$$dr_c(n=0)=d_s(n=0)=dr$$

Therefore, the mesh size changes from one time step to the next as the interface moves and both the external receding surface and the interface always remain at a grid point. In order to keep the dynamics of the computational domain as close as possible to that of the actual physical domain, a conformal mapping strategy is used to map in each subdomain the computational domain of time step  $(n+1)$  to that of the previous time step. To do so, each subdomain (core and shell) is identified by two radial grid sizes corresponding to time level  $n$  [ $dr(n)$ ] and  $n+1$  [ $dr(n+1)$ ]. The computation is then performed by continuously mapping in each subdomain, the radial grid points of time level  $n$  to those of

time level  $n+1$ . The transformation in the  $r_c$ - $t$  subdomain actually maps a cylindrical region of radius  $r_c(n)$  and length  $l$  at time  $n$  into a geometrically similar region at time  $n+1$ . Thus, at any grid point  $(i,n)$  of the computational domain at time level  $n$ ,

$$[ r_{ci}(n) = i dr_c(n), t_n ] \text{ maps into } [ r_{ci}(n+1) = i dr_c(n+1), t_{n+1} ]$$

i.e. a contraction ratio

$$\Gamma_c = \frac{dr_c(n)}{dr_c(n+1)} > 1$$

and where  $0 \leq i \leq N-1$  at any time  $n = 0, 1, 2, \dots$

For the  $b$ - $t$  subdomain, recall that the gas temperature has to be accounted for through the mean of the shell convective boundary condition. Hence, the "b-t" computational domain is now transformed into a "b-t,z" computational domain. But making use of relation (3.18), the "three dimensional" computational domain may be transformed back into a two dimensional computational domain. The mapping in this subdomain transforms a hollow cylinder of radius  $r$  and thickness  $b$  at time  $n$  into a geometrically similar region at time  $n+1$ . Thus, at any grid point  $(i-n,k)$  of the computational domain at time level  $n$ ,

$$[ b_i(n) = i dr_s(n) - t_n, z_k ] \text{ maps into } [ b_i(n+1) = i dr_s(n+1) - t_{n+1}, z_{k+1} ],$$

or a contraction ratio

$$\Gamma_s = \frac{dr_s(n)}{dr_s(n+1)} > 1$$

and  $N+1 \leq i \leq M$  at any time and bed location  $n = k = 0, 1, 2, \dots$  where  $M$  is the total grid number of the entire "whole tree" elements. Recall also that by setting these indexes equal to zero in both subdomains, we are quantifying only the combustion process.

Now as in Douglas and Gallie scheme, the time step in equation (3.17) is selected such that in the time interval from  $t_n$  to  $t_{n+1}$ , the interface moves exactly from the position  $r_c(n) = N dr_c(n)$  to the position  $r_c(n+1) = N dr_c(n+1)$ . If  $J$  is the total number of grid

of the shell layer, the following relations, therefore, always hold for the core and shell subdomains at each time step.

$$r_c(n+1) = r_c(n) - dr_c(n) = Ndr_c(n+1)$$

$$b(n+1) = r_s(n+1) - r_c(n+1) = Jdr_s(n+1)$$

$$[r_s(n) - r_s(n+1)] / \Delta t = V_s.$$

Hence, it is seen that contrary to the previous schemes, both the radial grid and the time step vary for all times and the computation is done by continuously tracking both the position of the interface and the external receding boundary. In addition, in solidification-freezing problems, the last time step is computed when there is only one phase left. Here, however, since for practical purposes neither  $r_c(n)$  nor  $r_s(n)$  ever go to zero, it is assumed that the problem is an infinite one i.e. the two-phase problem is always present.

The following algorithm summarizes the *CMVGM* procedure.

1. Approximate  $\Delta t_1^1$  by computing  $\Delta t_0$  as initial guess.

$$\Delta t_1^1 = \Delta t_0 = \frac{\rho_w \epsilon_v h_p \Delta r^2}{K_w [T_m^* - T_{cN-1}^0] - K_s [T_{sN+1}^0 - T_m^*]}$$

where  $T_{cN-1}^0$  and  $T_{sN+1}^0$  are respectively the core and shell node temperatures at the end of the preheat process.

2. Compute the core radius  $r_c(n+1) = r_c(n) - dr_c(n)$

3. Approximate the bed grid size. Apply the simple explicit forward differencing to discretize the burning rate and oxygen concentration equations and then iterates for the approximated values of the receding external radius  $r(n+1)$  or  $r_s(n+1)$  and bed oxygen concentration  $C(n+1)$ . Stop the computation when the difference between two consecutive iterations satisfies a specific convergence criteria. That is,

$$|r_1^{(l+1)} - r_1^{(l)}| \quad \text{and} \quad |C_1^{(l+1)} - C_1^{(l)}|$$

4. Approximate  $dr_s(n+1)=b(n+1)/J$ . With *CMVGM*, solve the finite difference equation (3.12) [approximation of the diffusion equation (3.3)] subject to appropriate boundary conditions [shell convective boundary (3.13) and equation (3.16)] and initial conditions i.e. conditions at  $(t_p, z_p)$ . Obtain an estimate for the shell node temperatures, holding the gas temperature  $T_g(k)$  constant.
5. Compute  $dr_c(n+1)=r_c(n+1)/N$ . As in step (4), solve the finite difference equation (3.12) [approximation of the diffusion equation (3.4)] subject to appropriate boundary conditions [symmetry condition (3.14) and equation (3.15)] and initial conditions i.e. conditions at  $(t_p, z_p)$ . Obtain an estimate for the core node temperatures.
6. Obtain  $\Delta t_1^1$  using equation (3.17), the new shell and core temperature profiles and  $\Delta r$  given by the average of the  $(n+1)$  radial grids computed in step (4) and (5).
7. Up-date  $r_s(n+1)$ ,  $C(n+1)$  and  $dr_s(n+1)$  in light of step (6)
8. Discretize the gas temperature as in step (3) and approximate  $T_g(k+1)$
9. Repeat step (3) to step (8) until the following quantities satisfy a convergence criteria i.e.

$$| T_{ci}^{(P+1)} - T_{ci}^{(P)} |, | T_{si}^{(P+1)} - T_{si}^{(P)} |, | T_{gk}^{(P+1)} - T_{gk}^{(P)} |$$

and  $| \Delta t_n^{(P+1)} - \Delta t_n^{(P)} |$

10. Continue marching by going back to step (2), then old  $\Delta t_1$  as approximation to  $\Delta t_2^1$  and repeat step (3) to step (8). Continue the process until burnout is reached defined as a given percentage of initial mass or radius loss.

## 3.8 Results and discussion

### 3.8.1 Preheat profile.



For  $0 \leq i \leq M$ , the finite difference equation (3.12) [diffusion equation (3.1)] together with appropriate boundary and initial conditions are solved using only the combine Crank-Nicolson scheme. This submodel is stopped following the experimental findings of Ragland *et al.* [3.3] when a shell layer of thickness  $b$  approximately equal to 6.00 mm is formed. As anticipated, the exiting flue-gas preheat progressively the external layers of the solid fuel surface to pyrolysis, Figures 3.3 and 3.4, while the interior still remains virgin wood at ambient temperature. This takes only about 2 to 4 min for fuel elements of 0.1016 and 0.2540 m radius respectively at 33.3 % moisture. The core and shell contours at this bed location estimated to be approximately equal to 94% of the corresponding total bed depth (measure from the bottom of the bed), are clearly shown by the temperature range in the previous figures. At the end of the preheat process, the core and shell temperature profiles and their respective radii serve as input for the combustion model.

### 3.8.2 *CMVGM* solution of the combustion model

The pyrolysis process of the "whole tree" elements surfaces according to Roberts [3.12], proceeds as follows. The hemicellulose is said to decompose first, largely between 200 and 260 °C, followed by the cellulose between 240 and 350 °C and finally the lignin between 280 and 500 °C. For practical purposes i.e. in order to have approximately the desired shell thickness in the appropriate temperature range, the interface temperature is set equal to about 200 °C. The set of equations of the combustion model is solved using *CMVGM* and the constant thermal properties shown in table 3.1. The weight factor is set equal to 0.75. Selected results are shown for "whole tree" elements at 33.3 % moisture and  $\alpha = \gamma = 60 \%$ . For computational purposes, the distances shown are measured from the top of the bed. The start of the combustion process is illustrated by the abrupt radial temperature difference between the core and shell shown in Figures 3.5 and 3.6. As the "whole tree" elements migrate downward, they shrink progressively with time and it is believed that the internal convection of moisture and volatiles inside the core tends to increase its internal pressure and temperature, Figures 3.7 and 3.8. This phenomenon which is sometimes called "cooking" is neglected in the quasi-steady model. As can be seen in the previous figures, the increase of the core tem-

perature is specially true close to the end of the combustion process, set equal to approximately 95% of initial radius reduction. This "cooking" effect, however, does not alter significantly the results of the quasi-steady model. It may explain on the other hand the results of tables 3.2 and 3.3 which display differences between 10 to 25 and 3 to 10 % respectively between the bed depth and burnout time computed from the two models. As we get closer and closer to the prescribed burnout time, it is found that not only the temperature of the core rises steadily toward the interface temperature but also the temperature of the interface and those of the nearest nodes are also becoming increasingly close. Accordingly, the time step is found to decrease in the same period. Since the "whole tree" elements have already shrunk to under 90% of their initial radii, the bed spatial grids calculated from relation (3.18) become even smaller with time. In another word, further computation beyond a certain burnout time will add little combustion time and almost no additional bed depth. Remember that the time step is the time necessary for the interface to move one radial grid size. But a reduced time step means that the process has slow down and ended, at the bottom of the bed, the core and shell radii tend to merge. As a matter of fact it has been found that for "whole tree" elements at 33.3 % moisture and 0.1016 m initial radius,  $r_c$  and  $r_s$  equal to 0.0087343 and 0.0087358 m respectively. The same phenomenon is true for their temperatures. Therefore, at that particular period, the all process behaves as an infinite two-phase moving boundary problem.

Table 3.4 shows a very good recovery of the preheated gas temperature and oxygen concentration at the end of the combustion process. Recall that, these are the bed prescribed inlet conditions and were used as boundary values of the gas combustion equations in the quasi-steady model as the computation was started from the bottom of the bed. Here, these quantities must be recovered in order to validate the boundary conditions of the gas and oxygen equations at the top of the bed. The number of time steps varies between 1400 and 7000 for "whole tree" elements of 0.075 and 0.2540 m radius. The radial grid size decreases from  $10^{-4}$  to about  $10^{-8}$  m at the end of the combustion process. Although a huge volume of computation is handle at each time step, the *CM-*

*VGM* scheme is found to be very stable and converges rapidly. Finally, the transient dies out very fast and shows no particular influence on the overall process.

It may be useful to add that, the model indirectly estimates the sign and magnitude of the heat of pyrolysis. The investigation of this property has been the subject of controversy over the years, not only about its magnitude but also about its sign. In some cases, the thermal decomposition has been formulated using the first order Arrhenius equation which is found inappropriate in modeling the combustion of large wood specimens. This model offers then, a novel approach in the investigation of the heat of pyrolysis, free from previous constraints such as the variation of the activation energy with temperature. The values presented in Table 3.5 are obtained solely as best fits in the computation of the appropriate time step. They range between 17 and 24 cal/g and are seen to remain practically constant for a given fuel radius but seem to vary with fuel moisture.

### 3.9 Conclusion

Depending on the accuracy needed, the results of the transient shrinking core model somehow validate the assumptions made in chapter 2 by showing that the quasi-steady model, although simple gives acceptable results. In particular, the assumption of a uniform core temperature is found to be appropriate during most of the combustion process but close to the end, the core temperature rises steadily toward the interface temperature. This is speculated to be due to the phenomenon of "cooking" believed to be caused by rising internal pressure and fuel temperature carried inward by convective moisture and pyrolysis gases. This may indeed explain the slight differences between the results of the two models. With variable time step and variable radial grid, the *CMVGM* method is found to be appropriate in solving this particular type of moving boundary problem by continuously tracking the position of both the interface and the receding external boundary. The scheme is found to be very stable and converges rapidly.

Table 3.1. Constant thermal properties

a. Quantities at the bottom are best fits

Properties	Values	Units	References
$A_m$	$1.08 \times 10^7$	$\text{sec}^{-1}$	3.13
$C_{ps}$	0.670	$\text{KJ/Kg} \cdot ^\circ\text{K}$	3.14
$C_{pv}$	1.10	$\text{KJ/Kg} \cdot ^\circ\text{K}$	3.14
$D$	$3.15 \times 10^{-4}$	$\text{m}^2/\text{sec}$	3.3
$d_w$	640	$\text{Kg/m}^3$	
$E_m$	$5.60 \times 10^4$	$\text{J/mol}$	3.13
$hfg_m$	2250	$\text{KJ/Kg}$	
$hfg_v$	200	$\text{KJ/Kg}$	
$H_s$	31,100	$\text{KJ/Kg}$	3.15
$H_v$	13,500	$\text{KJ/Kg}$	3.16
$K$	0.225	-	
$K_s$	$0.41 \times 10^{-4}$	$\text{KW/m} \cdot ^\circ\text{K}$	3.14
$K_w$	$1.254 \times 10^{-4}$	$\text{KW/m} \cdot ^\circ\text{K}$	3.14
$k_{gc}$	a { $56.0 \times 10^{-19}$ $5.00 \times 10^{-19}$	$\text{m}^2$	3.17
$k_{gs}$	a { $15.0 \times 10^{-17}$ $12.0 \times 10^{-16}$	$\text{m}^2$	3.17
$S_g$	0.64	-	3.2
$e_s$	95	$\text{Kg/m}^3$	3.3
$\phi_w$	0.45	-	3.18
$\mu_g$	a { $38.1 \times 10^{-6}$ $40.0 \times 10^{-6}$	$\text{Kgm}^{-1} \text{sec}^{-1}$	3.17

Table 3.2. Bed depth  $B_d$ (m) of the two Models

a. Percent difference

b. For a given  $r$ (m) and  $mc$ (%), the quantities at the top represent the Bed depth  $B_d$ (m) of the Quasi-steady Model.

c. The quantities at the bottom are the  $B_d$ (m) of the Transient Model.

$r$ (m)	$mc$ (%)				% <sup>a</sup>
—	25	30	33.3	40	—
.075	1.88 <sup>b</sup>	1.96	2.01	2.10	19 to 25
	1.41 <sup>c</sup>	1.51	1.61	1.69	
.1016	3.07	3.19	3.26	3.41	12 to 25
	2.30	2.46	2.60	2.74	
.1524	5.78	6.00	6.14	6.42	20 to 25
	4.34	4.60	4.84	5.08	
.2032	9.10	9.44	9.66	10.10	21 to 25
	6.80	7.20	7.56	7.94	
.2540	12.93	13.41	13.72	14.35	21 to 25
	9.65	10.20	10.72	11.23	

Table 3. 3. Burnout time  $t_b$ (min) of the two Models

a. Percent difference

b. For a given  $r$ (m) and  $mc$ (%), the quantities at the top represent the burnout time  $t_b$ (min) of the Quasi-steady Model.

c. The quantities at the bottom are  $t_b$ (min) of the Transient Model.

$r$ (m)	$mc$ (%)				$\sigma\%$ <sup>a</sup>
—	25	30	33.3	40	—
.075	23.88 <sup>b</sup>	24.88	25.52	26.80	-.8 to 7
	23.69 <sup>c</sup>	25.46	27.16	28.80	
.1016	38.86	40.42	41.42	43.50	1 to 10
	39.30	42.42	45.09	48.12	
.1524	73.24	76.10	78.00	81.92	3 to 11
	75.52	80.81	85.93	92.38	
.2032	115.26	119.76	122.74	128.90	3 to 12
	118.91	127.96	135.99	146.35	
.2540	163.86	170.20	174.45	183.20	3 to 12
	169.25	182.04	193.99	209.29	

Table 3.4. Oxygen concentration and preheated gas temperature at the bottom of the Bed.

- a. Percent difference for the Quasi-steady Model the oxygen concentration is  $.1365 \text{ Kg/m}^3$  and the preheated gas temperature  $260^\circ\text{C}$  for all mc.
- b. For a given  $r(\text{m})$  and  $mc(\%)$ , the quantities at the top represent the oxygen concentration ( $\text{Kg/m}^3$ ) of the Transient Model.
- c. The quantities at the bottom represent the preheated gas temperature of the Transient Model.

r (m)	mc (%)				% <sup>a</sup>
	25	30	33.3	40	
.075	.1359 <sup>b</sup>	.1333	.1298	.1313	.4 to 5
	260.65 <sup>c</sup>	259.82	260.32	260.69	-.06 to .2
.1016	.1363	.1333	.1302	.1314	1 to 5
	256.04	261.03	260.49	261.66	-2 to .6
.1524	.1360	.1344	.1311	.1326	.3 to 4
	260.66	259.81	257.64	255.11	-2 to .2
.2032	.1366	.1344	.1313	.1325	.07 to 4
	260.07	260.57	257.45	256.84	-1 to 2
.2540	.1366	.1344	.1310	.1322	.07 to 4
	260.12	260.63	260.78	259.86	-.05 to .3

Table 3.5. Heat of pyrolysis  $h_p$  (KJ/Kg) as a function of fuel properties

r (m)	mc (%)			
	25	30	33.3	40
—				
.1016	78.20	92.00	98.86	100.32
.1524	77.00	81.89	94.00	98.50
.2032	72.00	81.00	92.00	97.00
.2540	71.00	79.50	91.50	95.50



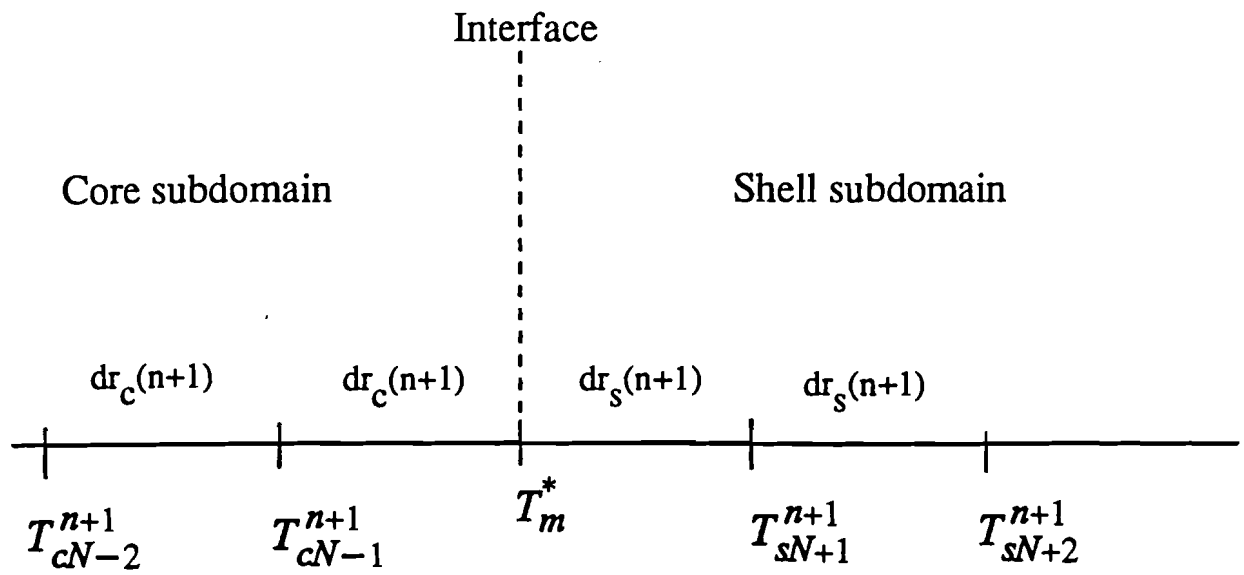


Fig. 3.1 : Interface and nearest core and shell nodes

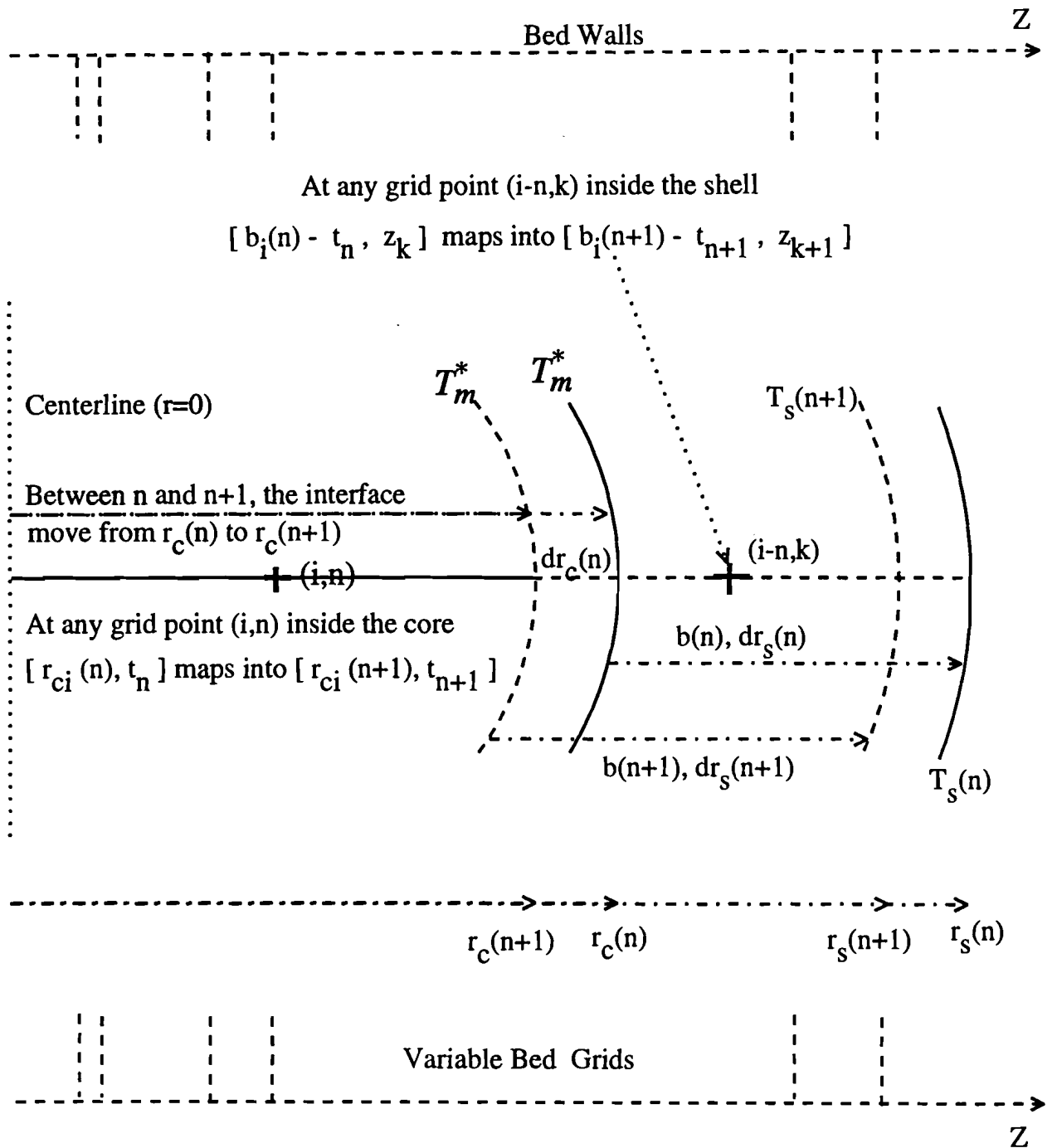


Fig. 3.2 : Computational domain : Variable fuel and bed grids

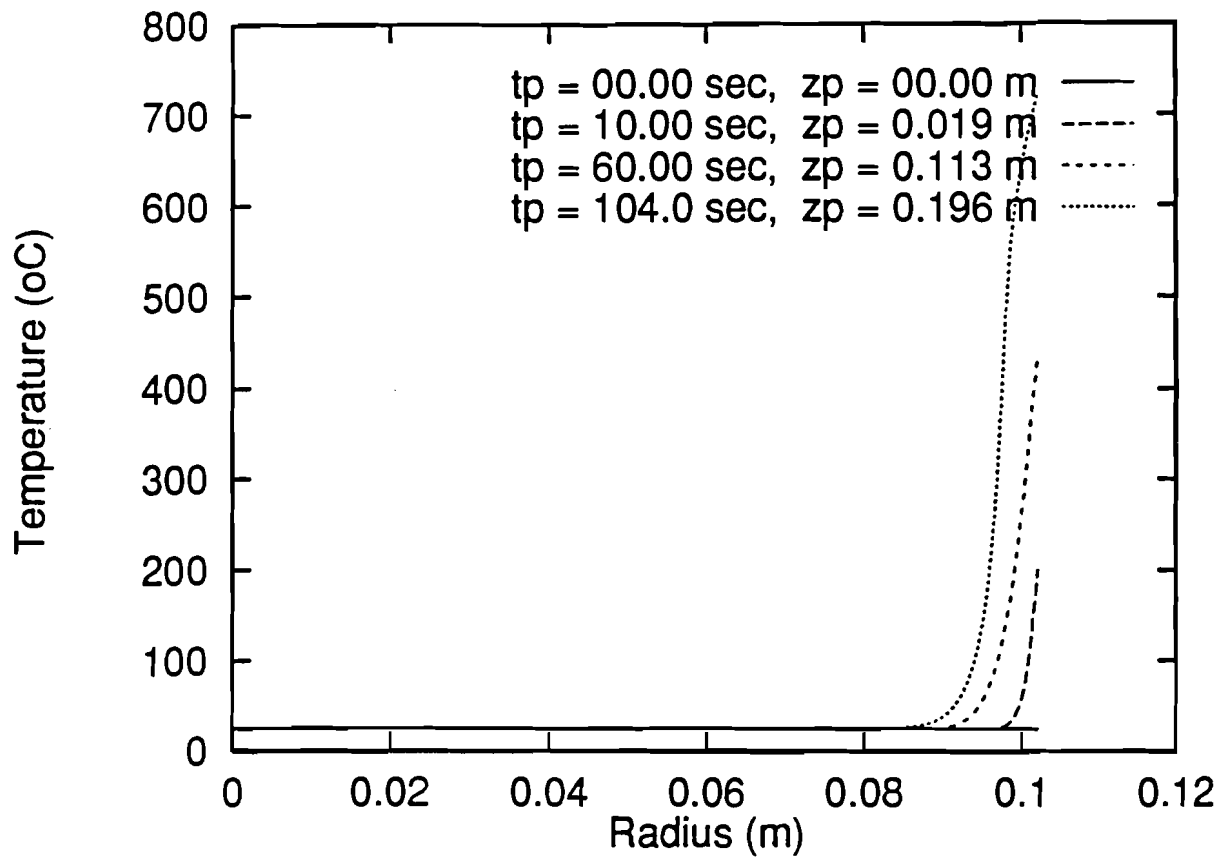


Fig. 3.3 : Preheat profiles,  $R_o = 0.1016$  m,  $m_c = 33.3$  %

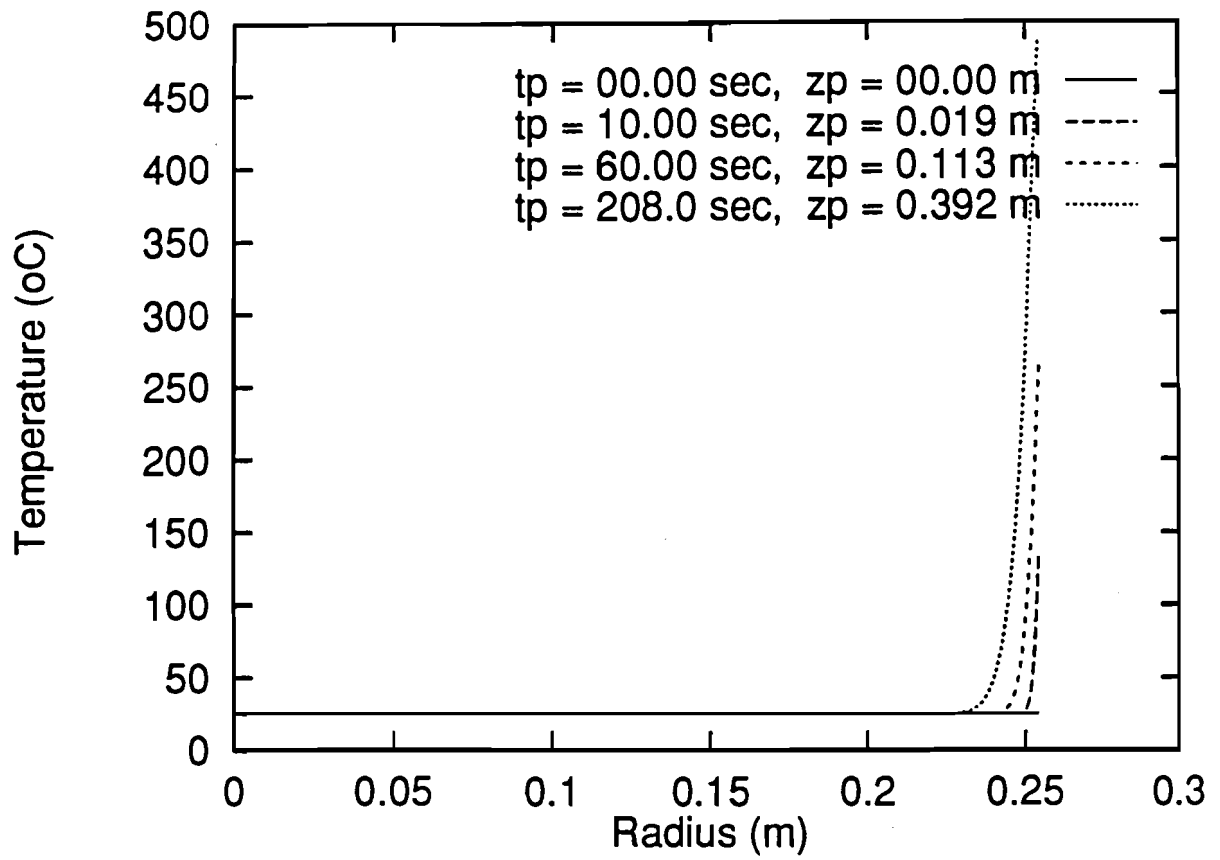
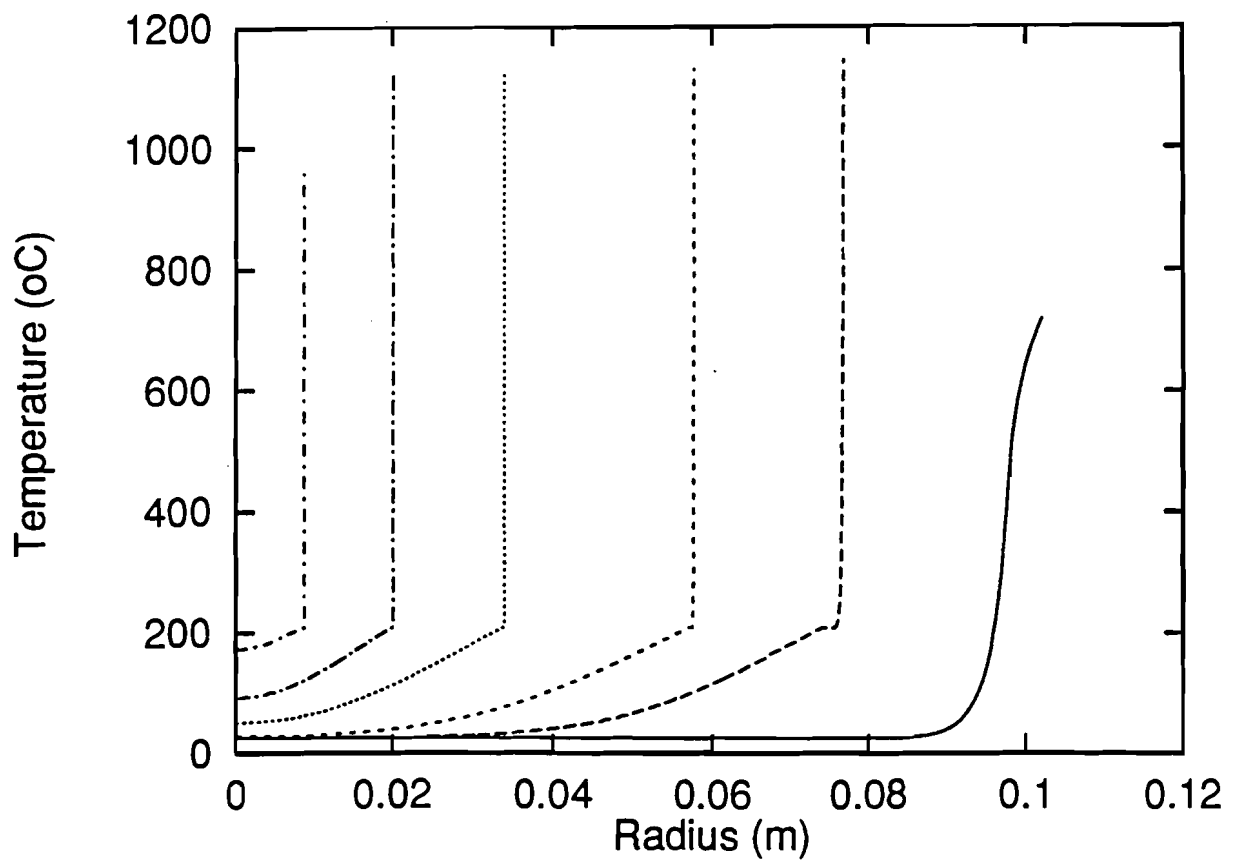
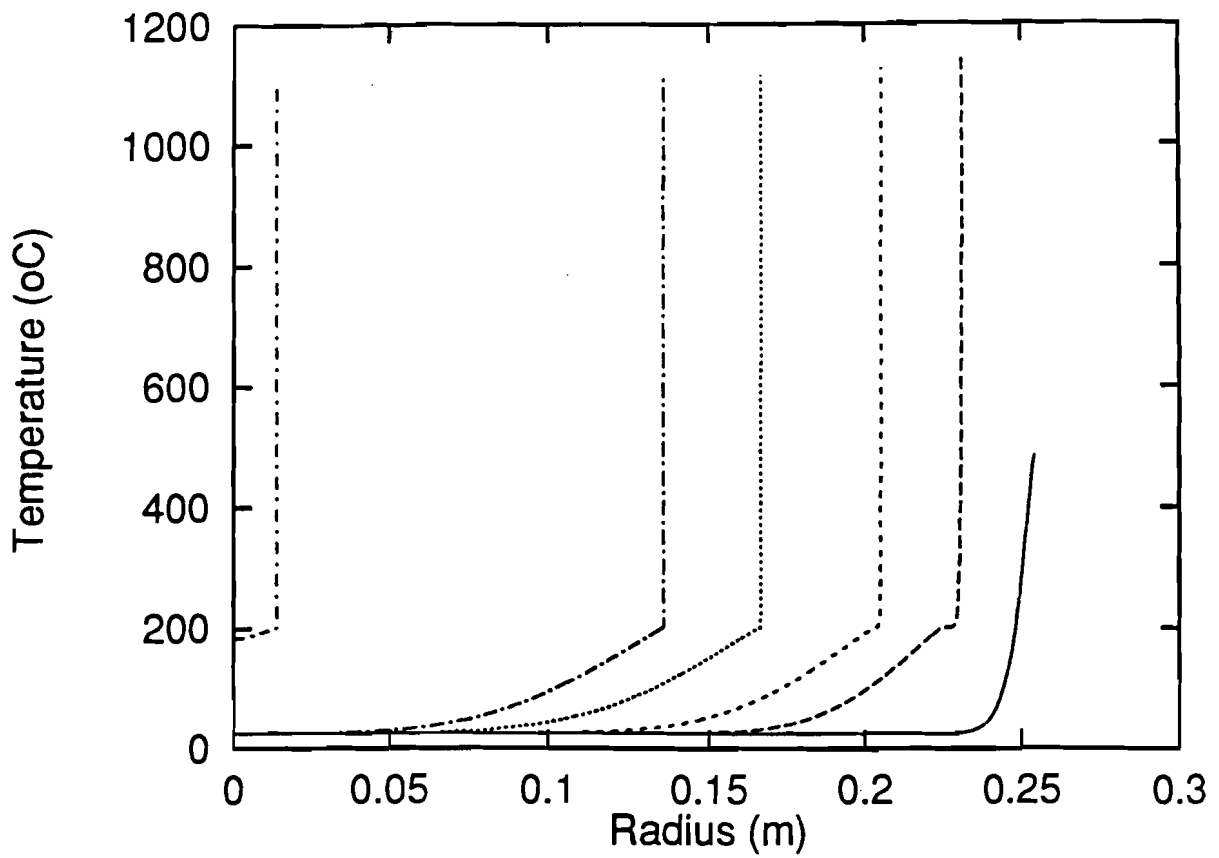


Fig. 3.4 : Preheat profiles,  $R_o = 0.2540$  m,  $mc = 33.3$  %



$t_p = 104.00 \text{ sec}, z_p = 0.196 \text{ m}$  ———  
 $t_b = 1240.5 \text{ sec}, B_d = 1.909 \text{ m}$  - - - - -  
 $t_b = 1783.3 \text{ sec}, B_d = 2.364 \text{ m}$  ·····  
 $t_b = 2279.5 \text{ sec}, B_d = 2.562 \text{ m}$  ·····  
 $t_b = 2511.7 \text{ sec}, B_d = 2.593 \text{ m}$  - · - · -  
 $t_b = 2706.6 \text{ sec}, B_d = 2.601 \text{ m}$  - · - · -

Fig. 3.5 : Core & Shell temperature profiles,  $Ro = 0.1016 \text{ m}$



$t_p = 208.000$  sec,  $z_p = 0.392$  m ———  
 $t_b = 2454.16$  sec,  $B_d = 4.283$  m - - - -  
 $t_b = 4300.20$  sec,  $B_d = 6.869$  m ·····  
 $t_b = 6396.21$  sec,  $B_d = 9.016$  m - - - -  
 $t_b = 7716.06$  sec,  $B_d = 9.906$  m - - - -  
 $t_b = 11639.2$  sec,  $B_d = 10.72$  m ·····

Fig. 3.6 : Core & Shell temperature profiles,  $R_o = 0.2540$  m

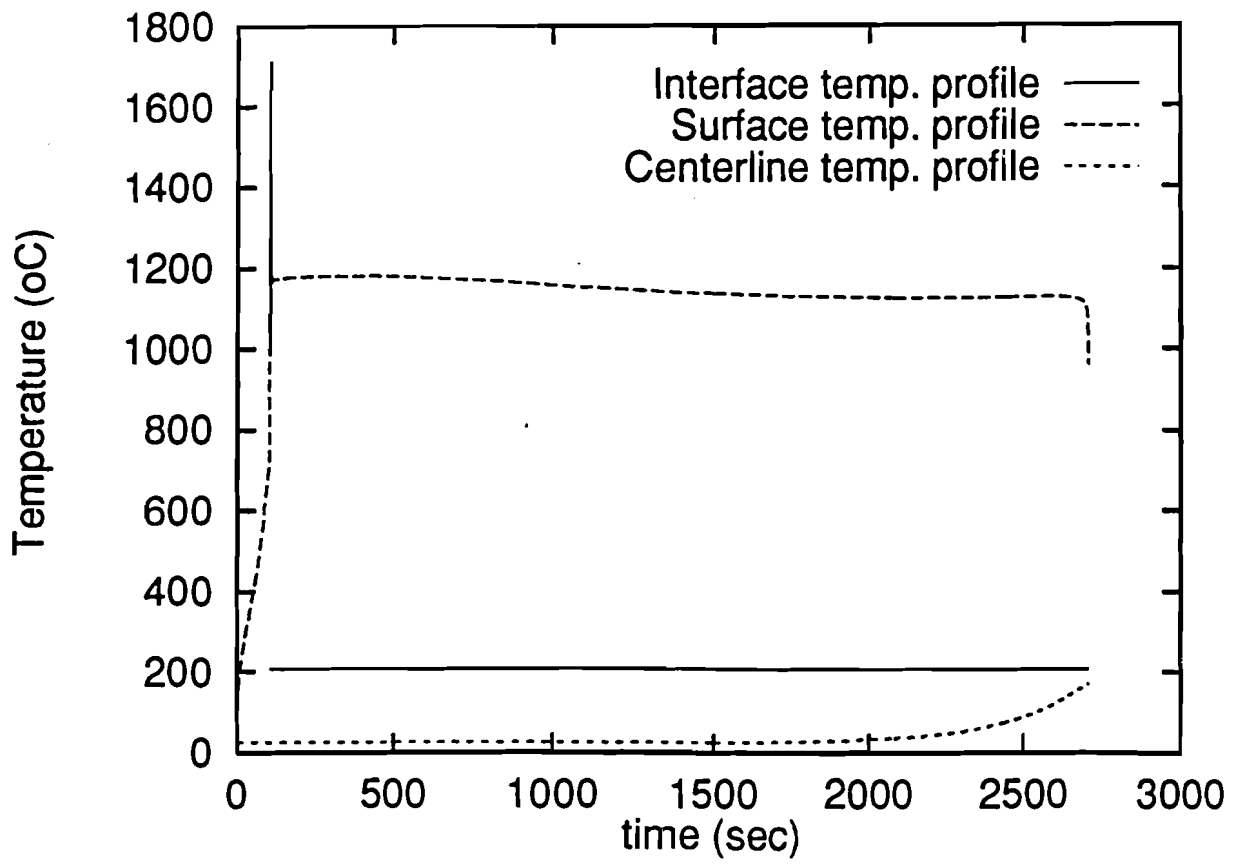


Fig. 3.7 : Selected temperature profiles,  $R_o = 0.1016$  m

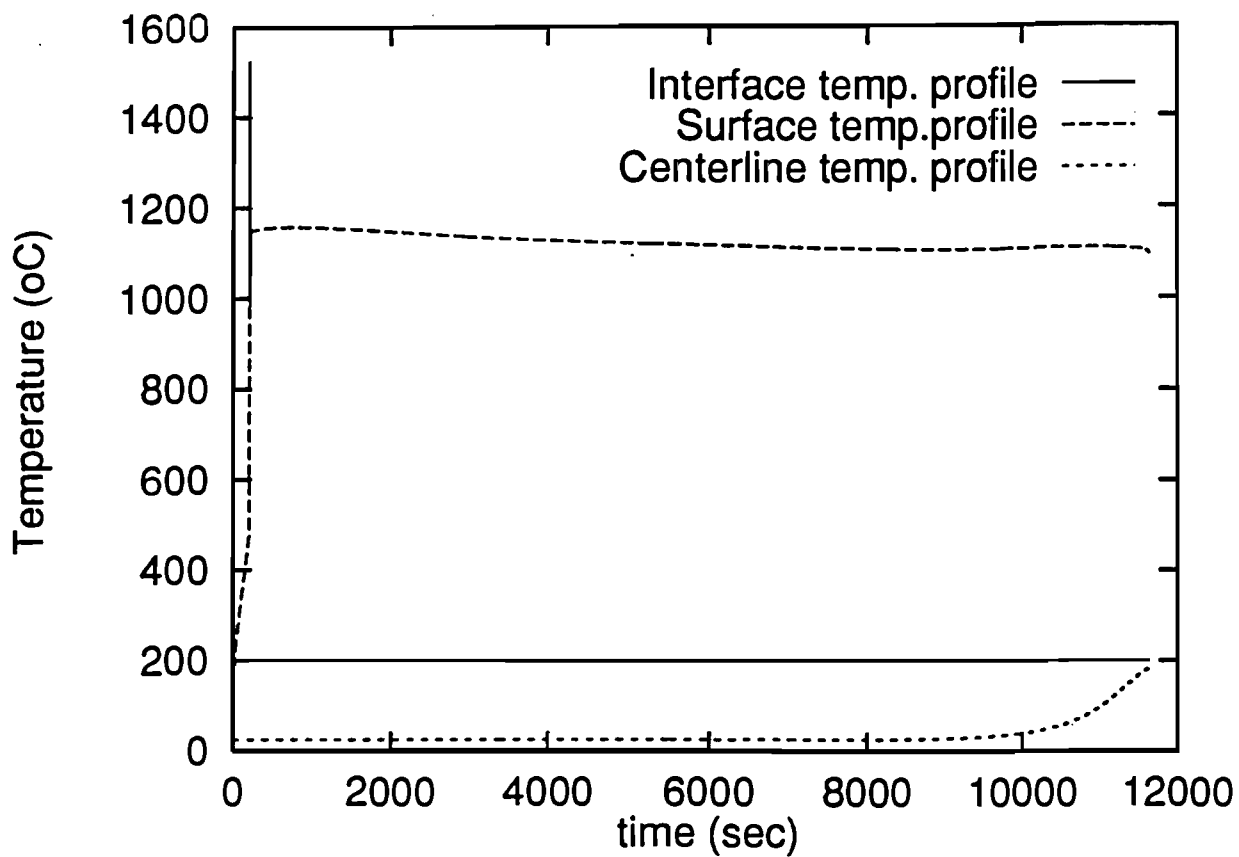


Fig. 3.8 : Selected temperature profiles,  $R_o = 0.2540$  m



## 3.10 References

- 3.1. A. Ouedraogo, J. C. Mulligan, and J. G. Cleland. A quasi-steady state shrinking core model of "whole tree" combustion in a countercurrent fixed-bed reactor. *Comb. Sc. and tech.*, (to be published), 1994.
- 3.2. Draft Final Report, EPRI Project RP 2612-15. Contractor Research Triangle Institute, Research Triangle Park , NC 27709, 1991.
- 3.3. K. W. Ragland, J. C. Boeger, and A. J. Baker. A model of chunkwood combustion. *Forest Products J.*, 38(2):27-32, 1988.
- 3.4. O. A. Plumb, G. A. Spolek, and B. A. Olmstead. Heat and mass transfer in wood during drying. *Int. J. Heat Mass Transfer*, 28 (9):1669-1678, 1985.
- 3.5. S. Whitaker. Simultaneous Heat, Mass and Momentum Transfer in Porous Media: A Theory of Drying. *Adv. Heat Transfer*, 9:119-203, 1977.
- 3.6. J. F. Siau. Transport Processes in Wood. In Springer Series in Wood Science (T. E. Timell, Ed.), 1-34, 1974.
- 3.7. A. Ouedraogo, J. C. Mulligan, and J. G. Cleland. A quasi-steady shrinking core analysis of wood combustion. *Combustion and Flame*, (to be published), 1994.
- 3.8. M. N. Ozisik. Finite Difference Methods in Heat Transfer. CRC Press, inc. Vol. 1, chap. 9 and 10, 249-305, 1994.
- 3.9. W. D. Murray and F. Landis. Numerical and machine solutions of transient heat conduction problems involving melting or freezing. *Transactions of the ASME*, 81:106-112, 1959.
- 3.10. J. Douglas Jr and T. M. Gallie Jr. On the numerical integration of a parabolic differential equation subject to a moving boundary condition. *Duke Math. JI*, 22:557-570, 1955.
- 3.11. R. S. Gupta and D. Kumar. Variable time step methods for one-dimensional Stefan problem with mixed boundary condition. *J. Heat and Mass Transfer*, 24:251-259, 1981.

- 3.12. A. F. Roberts. A Review of Kinetics Data for the Pyrolysis of Wood and Related Substances. *Combustion and Flame*, 14:261-272, 1970.
- 3.13. Wai-chun R. Chan, M. Kelbon, and B. B. Krieger. Modeling and experimental verification of physical and chemical processes during pyrolysis of a large biomass particle. *FUEL*, 64:1505-1513, 1985.
- 3.14. Hsiang-Cheng Kung and S. A. Kalelkar. On the heat of reaction in wood pyrolysis. *Combustion and Flame*, 20:91-103, 1973.
- 3.15. J. Diebold and J. Scahill. Ablative Pyrolysis of Biomass in Solid-Convective Heat Transfer Environments. in Fundamentals of Thermochemical Biomass Conversion (R. P. Overend, T. A. Milne and L. K. Mudge, Ed.), Elsevier Applied Science Publishers, 539-555, 1985.
- 3.16. W. J. Parker. Prediction of the Heat Release Rate of Wood. Ph.D. Thesis, The George Washington University, 1988.
- 3.17. B. Fredlund. A Model for Heat and Mass Transfer in Timber Structures during Fire. A theoretical, numerical and experimental study. Ph.D. Thesis, Institute of Science and technology, Lund University Sweden, 1988.
- 3.18. D. J. Aerta and K. W. Ragland. Pressurized downdraft combustion of woodchips. *Twenty-Third Symposium (International) on Combustion*. The Combustion Institute, 1025-1032, 1990.

### 3.11 Nomenclature

$A_{av}$	area to volume ratio ( $m^{-1}$ )
$A_m$	pre-exponential factor ( $sec^{-1}$ )
$b$	char thickness (m)
$B_d$	bed depth (m)
$C$	oxygen concentration ( $kg/m^3$ )
$C_{pj}$	specific heat of component j ( $KJ/kg^{\circ}K$ )
$E$	activation energy ( J/mol)

$h$	heat transfer coefficient ( $\text{KJ} / \text{m}^2\text{-sec-}^\circ\text{K}$ )
$h_D$	mass transfer coefficient (m/sec)
$hfg_m$	enthalpy of phase change of liquid water (KJ/kg)
$hfg_v$	enthalpy of phase change of active matter (KJ/kg)
$h_p$	heat of pyrolysis (KJ/Kg)
$H_{ag}$	average heat of combustion of gases inside the bed (KJ/Kg)
$H_j$	enthalpy of component j (KJ/kg)
$k_{gc}$	permeability of the gases in the core ( $\text{m}^2$ )
$k_{gs}$	permeability of the gases in the shell ( $\text{m}^2$ )
$K$	geometry correction factor
$K_s$	shell (char) conductivity ( $\text{KW/m-}^\circ\text{K}$ )
$K_w$	core (virgin wood) conductivity ( $\text{KW/m-}^\circ\text{K}$ )
$l$	wood thickness (m)
$m$	mass (kg )
$mc$	moisture content (%)
$\dot{m}$	mass loss rate (kg/sec)
$\dot{N}_i$	loading rate (log/sec)
$P$	pressure (Pascal)
$r$	radius (m)
$r_o$	initial radius ( $R_o$ in Figures) (m)
$\dot{r}$	rate of radius recession (m/sec)
$R$	gas constant ( $\text{J/mol-}^\circ\text{K}$ )
$t$	time (sec)
$T$	temperature ( $^\circ\text{C}$ )
$V_c$	rate of core recession (m/sec)
$V_f$	migration velocity (m/sec)
$V_g$	gas convective velocity (m/sec)
$V_s$	rate of shell recession (m/sec)
$V_{sg}$	superficial gas velocity (m/sec)
$W$	bed width (m)
$z$	bed coordinate (m)

## dimensionless variables

$Re_D$	Reynolds number
$S_g$	Specific gravity

## Greek Letters

$\alpha$	fraction of the volatiles which goes to incomplete combustion
$\beta$	ratio of the heat of combustion of C to CO to that of C to CO <sub>2</sub>
$\epsilon$	mass fraction
$\epsilon_b$	bed volume fraction
$\epsilon_{sv}$	solid volume fraction
$\rho$	density (kg/m <sup>3</sup> )
$\gamma$	fraction of the total gases that burn inside the bed
$\phi$	wood porosity
$\mu$	viscosity
$\Theta$	weighed factor

## Subscripts

a	atmospheric
b	burnout time
c	core
dw	dry wood
g	gas
i	initial (ambient), grid index
j	components (s, m, v)
m	moisture

s	shell (external radius)
sv	saturated vapor pressure
v	volatiles
w	virgin wood

## 3.12 Appendix







```

print*,'input the computational parameters'

print*,'-----'

print*,'ro is the fuel radius, mc its moisture content'

print*,'gt is the initial gas temperature,and hp is the'

print*,'heat of pyrolysis'

print*,'-----'

read*,ro,mc,gt,hp

c-----

c  Bed characterictics and computation of  $V_{sg}$ 

c-----

c  sg is the specific gravity of the wood.
c  rga and cpa are the density and specific heat of the gases
c  wi and he are the width and height of the bed.
c  db is the bulk density.
c  vsg is the superficial gas velocity-computed from the air
c  flow rate mi (5.5 kg air/kg fuel),the laoding rate lr (75
c  ton/hr) and the bed cross-section area (wi*le) where le
c  is the length of the bed.
c  tol is a convergence criteria.
c  ta is a weighted factor for the Crank-Nickolson scheme

      sg=.640d0
      rga=.650d0
      cpa=1.0340d0
      wi=4.5720d0
      db=240.0d0
      le=9.1440d0
      he=4.5720d0
      lr=75.0d0*907.20d0/3600.0d0
      mi=5.50d0
      vsg=(mi*lr)/(rga*le*wi)

c-----

c  physical properties of the fuel elements and gases

c-----

c  dw and dwd are the density of green and dry wood.
c  mc its moisture content (%)
c  dc is the char density
c  ec,em and ev are the mass fraction of the char, liquid

```

c water and volatile respectively.  
 c sv and bv are the solid void fraction and bed void fraction  
 c kw and kc are respectively the virgin fuel and char conductivity  
 c pew and pec the saturated fuel permeability and char permeability  
 c vis is the viscosity of the gases  
 c hp is the heat of pyrolysis  
 c pa the atmospheric pressure  
 c vof is the fuel porosity  
 c al and cq are pre-exponential factors  
 c el and eg are activation energy  
 c lni is the bed loading rate ( logs/sec ).

dw=sg\*(1.0d0+mc)\*1.0d3  
 dwd=sg\*1.0d-3

ec=dc/dw  
 em=mc/(1.0d0+mc)  
 ev=1.0d0-ec-em

sv=db/dw  
 bv=1.0d0-sv

kw=1.254000d-4  
 kc=.410d-4  
 pew=.500d-18  
 pec=15.0d-17  
 vis=40.0d-6

al=1.080d7  
 cq=1.3330d10  
 el=50.60d4  
 eg=43472.0d0  
 pa=1.013250d5  
 vof=.450d0

pi=4.0d0\*datan(1.0d0)  
 lni=lr/(pi\*dw\*le\*ro\*\*2)

c-----

c additional properties and computational constants

c-----

c cpv, cpm and cpc are respectively the specific heat of  
 c the volatile, moisture and char.  
 c ck1 is the negative stoichiometric ratio divided by dc.  
 c hfgv and hfgm are the enthalpy of phase change of the volatile  
 c and liquid water respectively.  
 c hc is the enthalpy of combustion of the char  
 c hv is the enthalpy of combustion of the volatiles  
 c alfa is the % of volatile that actually burn incompletely

c at the solid-gas interface  
 c gamma is the % of gas that actually burn inside the bed  
 c d is the molecular diffusivity.  
 c k is a correction factor, p1 and p2 are empirical coefficients  
 c ck is a constant time step for the preheat process  
 c rg is the gas constant

```
hw2=dw*(ev*cpv+em*cpm)
hw3=dw*em*cpm
cpw=(ec*cpc+ev*cpv+em*cpm)
ck1=-(12.0d0/16.0d0)/dc
k=.2250d0
ck=2.0d0
sf=.80d0
```

```
p1=.7660d0
p2=.5730d0
```

```
ck2=1.0d0/(rga*cpa*vsg)
ck3=((2.060d0*k*d/2.0d0)*(17400.0d0)**(.4250d0))/bv
cc=pi*lni/wi
```

```
alfa=.60d0
gamma=.60d0
```

```
ahc=((ec*hc + ev*hv*alfa)*(1.0d0-beta) + ev*hv*(1.0d0
&-alfa))*gamma/(ec + ev)
```

```
si=em*(1.0d0-vof)*(dw-dwd)*al*hfgm
```

```
cg=5.795d0*1.0d14*pew/(vis*rg)
cq=1.3330d10
```

c-----

c initial values : gas temperature, fuel radius and oxygen  
 c concentration

c-----

c ro is the fuel elements external radius prior to combustion  
 c r is the external shrinking radius  
 c rw the shrinking core radius  
 c co and cs are the oxygen concentration  
 c tg is the gas temperature

c at this stage no shell is formed so that the initial  
 c radius of the fuel ro is equal to the core radius rw(0).  
 c the values of tg and co are taken from the quasi-steady model



```

do 20 i=0,11

radius=dfloat(i)*dr

write( 1,* ) radius,tco(i)

20  continue
c-----
c  computation of the preheat temperature profile
c-----
c  heat and mass transfer coefficients

hd=ck3*(ro**(-.5750d0))*(p1*mc)/(dexp(p2*mc)-1.0d0)

h=hd*rga*cpa

n=1

cpw=(ec*cpc+ev*cpv+em*cpm)*vof
c-----
c  the ( known ) RHS variable matrix coefficients
c-----
c  tco and tc are the previous and the actual core temperature
1  a1(0)=1.0d0-4.0d0*(1.0d0-ta)*ck*kw/(dw*cpw*dr**2)

c1(0)=4.0d0*(1.0d0-ta)*ck*kw/(dw*cpw*dr**2)

d1(0)=- (ck/(dw*cpw))*si*dexp(-el/(rg*(tco(0)+273.0d0)))

do 30 i=1,11-1

vg=- (cg/((tco(i)+273.0d0)**2))*dexp(-eg/(rg*(tco(i)+273
&.0d0)))*((tco(i)-tco(i-1))/dr)

hw1=vg*hw3

a1(i)=1.0d0-ck*(1.0d0-ta)*hw1/(dw*cpw*dr)-ck*(1.0d0-ta)
&*kw*dr*(dfloat(i)+.50d0)/(dw*cpw*dfloat(i)*dr**3)-ck*
&(1.0d0-ta)*kw*dr*(dfloat(i)-.50d0)/(dw*cpw*dfloat(i)*dr**3)

b1(i)=ck*(1.0d0-ta)*hw1/(dw*cpw*dr)+ck*(1.0d0-ta)*kw*dr
&(dfloat(i)-.50d0)/(dw*cpw*dfloat(i)*dr**3)

c1(i)=ck*(1.0d0-ta)*kw*dr*(dfloat(i)+.50d0)/(dw*cpw*

```



```

&(dw*cpw*dfloat(i)*dr**3)+ck*ta*hw1/(dw*cpw*dr)

b(i)=-ck*ta*hw1/(dw*cpw*dr)-ck*ta*kw*dr*(dfloat(i)-
&.50d0)/(dw*cpw*dfloat(i)*dr**3)

c(i)=-ck*ta*kw*dr*(dfloat(i)+.50d0)/(dw*cpw*dfloat(i)*dr**3)
50  continue

a(11)=1.0d0+2.0d0*ck*ta*kw/(dw*cpw*dr**2)

b(11)=-2.0d0*ck*ta*kw/(dw*cpw*dr**2)

c-----

c  decompose the tridigonal matrix

c(0)=c(0)/a(0)

do 60 i=1,11

a(i)=a(i)-b(i)*c(i-1)

c(i)=c(i)/a(i)

60  continue

c  solve for the core temperature

tcn(0)=tcn(0)/a(0)

do 70 i=1,11

tcn(i)=(tcn(i)-b(i)*tcn(i-1))/a(i)

70  continue

c  back substitution

tc(11)=tcn(11)

do 80 i=11-1,0,-1

tc(i)=tcn(i)-c(i)*tc(i+1)

80  continue
c-----

c  output some selected quantities

c-----

```

```

c  output the fuel surface temperature ( / time )
      write ( 2,* ) tp,tco(11)
c  output the fuel centerline temperature ( / time )
      write( 3,* ) tp,tco(0)
c  output the shrinking radius ( / time )
      write ( 4,* ) tp,ro
c  output the gas temperature ( / dz )
      write ( 5,* ) -zp,tg(n-1)
c  output the fuel surface temperature ( /dz )
      write ( 7,* ) -zp,tco(11)
c  output the fuel centerline temperature ( / dz )
      write( 8,* ) -zp,tco(0)
c-----
c  compute the bed deep zp and corresponding total preheat
c  time tp
      dz=(cc*ck*ro**2)/sv
      zp=n*dz
      tp=n*ck
c-----
c  output the preheat temperature profile
c-----
      if ( n .eq. 5 ) then
          do 90 i=0,11
              radius=dfloat(i)*dr
              write( 9,* ) radius,tc(i)
90      continue
c

```



```

        write ( 10,15 ) ro,mc*100.0d0,zp,tp,n
15    format(//,
        &10x,'the initial radius           (m)      =',f6.5,/,
        &10x,'the moisture content         (%)       =',f6.2,/,
        &10x,'the bed depth                (m)       =',f6.5,/,
        &10x,'the preheat time              (s)       =',f6.2,/,
        &10x,'# of time step                =',I5  ,/)

        endif

c
        if ( tp .eq. 60.0d0 ) then

        do 100 i=0,11

        radius=dfloat(i)*dr

        write( 11,* ) radius,tc(i)

100    continue
c
        write ( 10,25 ) zp,tp,n
25    format(//,
        &10x,'the bed depth                 (m)       =',f6.5,/,
        &10x,'the preheat time               (s)       =',f6.2,/,
        &10x,'# of time step                 =',I5  ,/)

        endif

c
        if ( tc(1k+1) .ge. 200.0d0 ) then

        do 110 i=0,11

        radius=dfloat(i)*dr

        write( 12,* ) radius,tc(i)

110    continue
c
        write ( 10,35 ) zp,tp,n
35    format(//,
        &10x,'the bed depth                 (m)       =',f6.5,/,
        &10x,'the preheat time               (s)       =',f6.2,/,
        &10x,'# of time step                 =',I5  ,/)

        endif

c    output the heat and mass transfer coefficients

c        write ( 13,* ) tp,hd,h

c-----

```



```

c-----
c  the interface temperature ( tm ) is constant
      tm(0)=tc(lk+1)
c-----
c  the shell initial temperature profile ( tso )
      do 140 i=1,m
          tso(i)=tc(lk+1+i)
140  continue
c-----
c  output the core and shell temperature profiles
c-----
      do 150 i=0,lk
          radius=dfloat(i)*dr1(0)
          write( 14,* )radius,tco(i)
150  continue
c
      write ( 14,* )rw(0),tm(0)
c
      do 160 i=1,m
          radius=dfloat(i)*dr2(0)
          radius=rw(0)+radius
          write( 14,* )radius,tso(i)
160  continue
c-----
c  the average temperature of the shell ( tsm) and core ( tcm)
      summ=.0d0
      do 170 i=1,m
          summ=summ+tso(i)

```





```

c vs of the combustion front the char layer thickness bc is
c calculated from the quasi-steady formulation (if needed).
c the shell thickness rr is obtained by subtracting the
c actual core radius from the external fuel element radius.
c dz is the approximated bed depth at each time increment

```

```

c-----

```

```

    ji=n

```

```

c external radius and oxygen concentration at the beginning
c of each step

```

```

    rs(ji)=r(n-1)

```

```

    cs(ji)=co(n-1)

```

```

    ikk=1

```

```

4    hd=ck3*(rs(ji)**(-.5750d0))*(p1*mc*ro/rs(ji))
    &/ (dexp(p2*mc*ro/rs(ji))-1.0d0)

```

```

    h=hd*rga*cpa

```

```

    rs(ji)=r(n-1)-(12.0d0/16.0d0)*dt(n)*hd*cs(ji)/dc

```

```

    rr(n)=(rs(ji)-rw(n))

```

```

    vs=-hd*ck1*cs(ji)

```

```

    bc1=kc*(tsm-tcm)

```

```

    bc2=dw*vc*(ev*hfgv+em*hfgm)+bc1/(2.0d0*rs(ji))

```

```

    bc=bc1/bc2

```

```

    mo=vs*dc+(dw-dc)*(1.0d0-rr(n)/rs(ji))*vc

```

```

    dz=(dt(n)*cc*rs(ji)**2)/sv

```

```

    cs(ji)=co(n-1)+2.0d0*sv*mo*dz/(vsg*rs(ji))

```

```

    if ( ikk .eq. 1 ) then

```

```

        rs(ji+1)=rs(ji)

```

```

        cs(ji+1)=cs(ji)

```

```

        ji=ji+1

```

```

        ikk=ikk+1

```









```

hw1=vg*hw2
hc2=h*(tg(n-1)-tso(m))+(ec*dw*vs*hc+vg*ev*dw*alfa*hv)*beta
a1(m)=1.0d0-2.0d0*ck*(1.0d0-ta)*kc/(hc1*dr**2)
b1(m)=2.0d0*ck*(1.0d0-ta)*kc/(hc1*dr**2)
d1(m)=(ck/hc1)*(1.0d0/r(n-1)+2.0d0/dr-hw1/kc)*hc2
c  input the actual RHS vector
    tsn(1)=a1(1)*tso(1)+b1(1)*tso(0)+c1(1)*tso(2)-b(1)*ts(0)
    do 200 i=2,m-1
        tsn(i)=a1(i)*tso(i)+b1(i)*tso(i-1)+c1(i)*tso(i+1)
200  continue
    tsn(m)=a1(m)*tso(m)+b1(m)*tso(m-1)+d1(m)
c@@@@@@@@@@@@@@@@@@@@@@@@@@@@@@@@@@@@@@@@@@@@@@@@@@@@@@@@@@@@@@@@@@@@@@@@@@@@@@@@@@@@@@@@@@@@@@@@@@@@@@@@@@@@
c  the unknown ( LHS ) variable matrix coefficients
c-----
    dr=dr2(n)
    pg=cq*dexp(-eg/(rg*(tm(n)+273.0d0)))
    dp=(pa-pg)/(dlog(rs(ji)/rw(n))*(rw(n)+dfloat(1)*dr))
    vg=-pec*dp/vis
    hw1=vg*hw2
    z1=rw(n)+dr*(dfloat(1)+.50d0)
    z2=rw(n)+dr*(dfloat(1)-.50d0)
    z3=(rw(n)+dr*dfloat(1))*dr**2
    a(1)=1.0d0+ck*ta*kc*z1/(hc1*z3)+ck*ta*kc*z2/(hc1*z3)
    &+ck*ta*hw1/(hc1*dr)
    b(1)=-ck*ta*kc*z2/(hc1*z3)-ck*ta*hw1/(hc1*dr)
    c(1)=-ck*ta*kc*z1/(hc1*z3)

```

```

do 210 i=2,m-1

dp=(pa-pg)/(dlog(rs(ji)/rw(n))*(rw(n)+dfloat(i)*dr))

vg=-pec*dp/vis

hw1=vg*hw2

z1=rw(n)+dr*(dfloat(i)+.50d0)

z2=rw(n)+dr*(dfloat(i)-.50d0)

z3=(rw(n)+dr*dfloat(i))*dr**2

a(i)=1.0d0+ck*ta*kc*z1/(hc1*z3)+ck*ta*kc*z2/(hc1*z3)+
&ck*ta*hw1/(hc1*dr)

b(i)=-ck*ta*kc*z2/(hc1*z3)-ck*ta*hw1/(hc1*dr)

c(i)=-ck*ta*kc*z1/(hc1*z3)

210 continue

a(m)=1.0d0+2.0d0*ck*ta*kc/(hc1*dr**2)

b(m)=-2.0d0*ck*ta*kc/(hc1*dr**2)

c-----

c actual decomposition

c(1)=c(1)/a(1)

do 220 i=2,m

a(i)=a(i)-b(i)*c(i-1)

c(i)=c(i)/a(i)

220 continue

c solve for the shell temperature

tsn(1)=tsn(1)/a(1)

do 230 i=2,m

tsn(i)=(tsn(i)-b(i)*tsn(i-1))/a(i)

230 continue

```



```

d1(0)=- (ck/(dw*cpw))*si*dexp(-el/(rg*(tco(0)+273.0d0)))

do 250 i=1,11-1

  vg=- (cg/((tco(i)+273.0d0)**2))*dexp(-eg/(rg*(tco(i)+273
&.0d0)))*((tco(i)-tco(i-1))/dr)

  hw1=vg*hw2

  a1(i)=1.0d0-ck*(1.0d0-ta)*kw*dr*(dfloat(i)+.50d0)/(dw*
&cpw*dfloat(i)*dr**3)-ck*(1.0d0-ta)*kw*dr*(dfloat(i)-.
&50d0)/(dw*cpw*dfloat(i)*dr**3)-ck*(1.0d0-ta)*hw1/(dw*cpw*dr)

  b1(i)=ck*(1.0d0-ta)*kw*dr*(dfloat(i)-.50d0)/(dw*cpw*
&dfloat(i)*dr**3)+ck*(1.0d0-ta)*hw1/(dw*cpw*dr)

  c1(i)=ck*(1.0d0-ta)*kw*dr*(dfloat(i)+.50d0)/(dw*cpw*
&dfloat(i)*dr**3)

  d1(i)=- (ck/(dw*cpw))*si*dexp(-el/(rg*(tco(i)+273.0d0)))

```

250 continue

```

  vg=- (cg/((tco(11)+273.0d0)**2))*dexp(-eg/(rg*(tco(11)+
&273.0d0)))*((tco(11)-tco(11-1))/dr)

  hw1=vg*hw2

  a1(11)=1.0d0-ck*(1.0d0-ta)*kw*dr*(dfloat(11)+.50d0)/
&(dw*cpw*dfloat(11)*dr**3)-ck*(1.0d0-ta)*kw*dr*(dfloat
&(11)-.50d0)/(dw*cpw*dfloat(11)*dr**3)-ck*(1.0d0-ta)*
&hw1/(dw*cpw*dr)

  b1(11)=ck*(1.0d0-ta)*kw*dr*(dfloat(11)-.50d0)/(dw*cpw*
&dfloat(11)*dr**3)+ck*(1.0d0-ta)*hw1/(dw*cpw*dr)

  c1(11)=ck*(1.0d0-ta)*kw*dr*(dfloat(11)+.50d0)/(dw*cpw*
&dfloat(11)*dr**3)

  c(11)=-ck*ta*kw*dr1(n)*(dfloat(11)+.50d0)/(dw*cpw*
&dfloat(11)*dr1(n)**3)

  d1(11)=- (ck/(dw*cpw))*si*dexp(-el/(rg*(tco(11)+273.0d0)))

```

c input the actual RHS vector

```

tcn(0)=a1(0)*tco(0)+c1(0)*tco(1)+d1(0)

do 260 i=1,11-1

```

$$tcn(i)=a1(i)*tco(i)+b1(i)*tco(i-1)+c1(i)*tco(i+1)+d1(i)$$

260 continue

$$tcn(11)=a1(11)*tco(11)+b1(11)*tco(11-1)+c1(11)*tco(11+1) \\ \&-c(11)*tc(11+1)+d1(11)$$

cc

c the unknown variable matrix coefficients

c-----

$$dr=dr1(n)$$

$$a(0)=1.0d0+4.0d0*ck*ta*kw/(dw*cpw*dr**2)$$

$$c(0)=-4.0d0*ck*ta*kw/(dw*cpw*dr**2)$$

do 270 i=1,11-1

$$vg=- (cg/((tco(i)+273.0d0)**2))*dexp(-eg/(rg*(tco(i) \\ \&+273.0d0)))*((tco(i)-tco(i-1))/dr)$$

$$hw1=vg*hw2$$

$$a(i)=1.0d0+ck*ta*kw*dr*(dfloat(i)+.50d0)/(dw*cpw* \\ \&dfloat(i)*dr**3)+ck*ta*kw*dr*(dfloat(i)-.50d0)/(dw* \\ \&cpw*dfloat(i)*dr**3)+ck*ta*hw1/(dw*cpw*dr)$$

$$b(i)=-ck*ta*kw*dr*(dfloat(i)-.50d0)/(dw*cpw*dfloat \\ \&(i)*dr**3)-ck*ta*hw1/(dw*cpw*dr)$$

$$c(i)=-ck*ta*kw*dr*(dfloat(i)+.50d0)/(dw*cpw*dfloat(i)*dr**3)$$

270 continue

$$vg=- (cg/((tco(11)+273.0d0)**2))*dexp(-eg/(rg*(tco(11) \\ \&+273.0d0)))*((tco(11)-tco(11-1))/dr)$$

$$hw1=vg*hw2$$

$$a(11)=1.0d0+ck*ta*kw*dr*(dfloat(11)+.50d0)/(dw*cpw* \\ \&dfloat(11)*dr**3)+ck*ta*kw*dr*(dfloat(11)-.50d0)/ \\ \&(dw*cpw*dfloat(11)*dr**3)+ck*ta*hw1/(dw*cpw*dr)$$

$$b(11)=-ck*ta*kw*dr*(dfloat(11)-.50d0)/(dw*cpw*dfloat \\ \&(11)*dr**3)-ck*ta*hw1/(dw*cpw*dr)$$

$$c(11)=-ck*ta*kw*dr*(dfloat(11)+.50d0)/(dw*cpw*dfloat(11)*dr**3)$$

c-----







```

5      hd=ck3*(rs(ji)**(-.5750d0))*(p1*mc*ro/rs(ji))
      &/ (dexp(p2*mc*ro/rs(ji))-1.0d0)

      h=hd*rga*cpa

      rs(ji)=r(n-1)-(12.0d0/16.0d0)*dt(n)*hd*cs(ji)/dc

      rr(n)=(rs(ji)-rw(n))

      vs=-hd*ck1*cs(ji)

      bc1=kc*(tsm-tcm)

      bc2=dw*vc*(ev*hfgv+em*hfgm)+bc1/(2.0d0*rs(ji))

      bc=bc1/bc2

      mo=vs*dc+(dw-dc)*(1.0d0-rr(n)/rs(ji))*vc

      dz=(dt(n)*cc*rs(ji)**2)/sv

      cs(ji)=co(n-1)+2.0d0*sv*mo*dz/(vsg*rs(ji))

      if ( ikk .eq. 1 ) then

      rs(ji+1)=rs(ji)

      cs(ji+1)=cs(ji)

      ji=ji+1

      ikk=ikk+1

      go to 5

      else

      if((dabs(rs(ji-1)-rs(ji)) .gt. tol) .or. (dabs(cs(ji-1)
&-cs(ji)) .gt. tol )) then

      rs(ji+1)=rs(ji)

      cs(ji+1)=cs(ji)

      ji=ji+1

      ikk=ikk+1

      go to 5

```



```

c  as well as the time step
    do 330 i=0,11
        if( dabs( tc(i)-tci(i) ) .gt. tol ) go to 6
330  continue
        do 340 i=1,m
            if ( dabs ( ts(i)-tsi(i) ) .gt. tol ) go to 6
340  continue
            if ( dabs ( dtn(n)-dt(n) ) .gt. tol ) go to 6
            if ( dabs ( tgi(n)-tg(n) ) .gt. tol ) go to 6
            go to 7
c  there is no convergence - store these quantities
6    ik=ik+1
        dtn(n)=dt(n)
        tgi(n)=tg(n)
        do 350 i=0,11
            tci(i)=tc(i)
350  continue
        do 360 i=1,m
            tsi(i)=ts(i)
360  continue
c  return to compute new temperature profiles and time step
    go to 3
c-----
c  since there is convergence, Store the actual time step
c  and temperature profiles for the computation of the next step

```



```

390 continue
c
write ( 15,* ) rw(n),tm(n)
c
do 400 i=1,m

radius=dfloat(i)*dr2(n)

radius=rw(n)+radius

write( 15,* ) radius,tso(i)

400 continue
c
write ( 10,45 ) count1(n),count2(n),rs(ji),rw(n),n
45 format(/,
&10x,'the burnout time (s) =',f12.6,/,
&10x,'the bed depth (m) =',f7.4,/,
&10x,'the fuel external radius (m) =',f8.6,/,
&10x,'the core radius (m) =',f8.6,/,
&10x,'# of time step =',I5 ,/)

endif

if ( n .eq. 500 ) then

do 410 i=0,1k

radius=dfloat(i)*dr1(n)

write ( 16,* ) radius,tco(i)

410 continue
c
write ( 16,* ) rw(n),tm(n)
c
do 420 i=1,m

radius=dfloat(i)*dr2(n)

radius=rw(n)+radius

write( 16,* ) radius,tso(i)
420 continue
c
write ( 10,55 ) count1(n),count2(n),rs(ji),rw(n),n
55 format(/,
&10x,'the burnout time (s) =',f12.6,/,
&10x,'the bed depth (m) =',f7.4,/,
&10x,'the fuel external radius (m) =',f8.6,/,

```

```

&10x,'the core radius          (m)      =' ,f8.6,/,
&10x,'# of time step          =' ,I5 ,/)

endif

c
if ( n .eq. 1000 ) then

do 430 i=0,1k

radius=dfloat(i)*dr1(n)

write( 17,* ) radius,tco(i)

430 continue
c
write ( 17,* ) rw(n),tm(n)
c
do 440 i=1,m

radius=dfloat(i)*dr2(n)

radius=rw(n)+radius

write( 17,* ) radius,tso(i)

440 continue
c
write ( 10,65 ) count1(n),count2(n),rs(ji),rw(n),n
65 format(/,
&10x,'the burnout time          (s)      =' ,f12.6,/,
&10x,'the bed depth            (m)      =' ,f7.4,/,
&10x,'the fuel external radius (m)      =' ,f8.6,/,
&10x,'the core radius          (m)      =' ,f8.6,/,
&10x,'# of time step          =' ,I5 ,/)
endif

c
if ( n .eq. 1500 ) then

do 450 i=0,1k

radius=dfloat(i)*dr1(n)

write( 18,* ) radius,tco(i)

450 continue
c
write ( 18,* ) rw(n),tm(n)
do 460 i=1,m

radius=dfloat(i)*dr2(n)

```











```

if ( (ro .eq. .15240d0) .and. (n .eq. 3986 ) ) go to 8
if ( (ro .eq. .20320d0) .and. (r(n) .le. qb2) ) go to 8
if ( (ro .eq. .2540d0) .and. (r(n) .le. qb3) ) go to 8

c-----

n=n+1

count1(n)=count1(n-1)+dt(n)

count2(n)=count2(n-1)+dz

go to 2

c-----

c output the last core and shell temperature profiles

c-----

8 do 520 i=0,1k

radius=dfloat(i)*dr1(n)

write( 30,* ) radius,tco(i)

520 continue
c
write ( 30,* ) rw(n),tm(n)
c
do 530 i=1,m

radius=dfloat(i)*dr2(n)

radius=rw(n)+radius

write( 30,* ) radius,tso(i)
530 continue
c
write ( 10,85 ) count1(n),count2(n),rs(ji),rw(n),n
85 format(/,
&10x,'the burnout time (s) =',f12.6,/,
&10x,'the bed deep (m) =',f7.4,/,
&10x,'the fuel external radius (m) =',f8.6,/,
&10x,'the core radius (m) =',f8.6,/,
&10x,'# of time step =',I5 ,/)

c*****

```

```

c  this part of the program will be entirely conserved with
c  rearranging some outputs.
c-----
c  output the gas temperature ( / dz )
      do 540 i=1,n
      write ( 31,* ) -count2(i),tg(i)
540  continue
c  output the oxygen concentration ( / dz )
      do 550 i=1,n
      write ( 32,* ) -count2(i),co(i)
550  continue
c  output the fuel surface temperature ( /dz )
      do 560 i=1,n
      write ( 33,* ) -count2(i),st(i)
560  continue
c  output the interface temperatures ( / dz )
      do 570 i=1,n
      write ( 34,* ) -count2(i),tm(i)
570  continue
c  output the fuel centerline temperature ( / dz )
      do 580 i=1,n
      write( 35,* ) -count2(i),tcl(i)
580  continue
c  output the temperature of the core nearest node to the interface
      do 590 i=1,n

```

```

        write ( 36,* ) -count2(i),tcp(1k)
590  continue
c  output the temperature of the shell nearest node to the interface
        do 600 i=1,n
            write ( 37, * ) -count2(i),tsp(i)
600  continue
c-----
c  output the shell thickness
        do 610 i=1,n
            write( 38, * ) count1(i),rr(i)
610  continue
c-----
c  output the following selected quantities
c-----

        write(39,95)ro,100.0d0*mc,count2(n),r(n),rw(n),count1(n)
&/60.0d0
95  format(/////////,
&10x,'the initial radius           (m)      =',f6.5,/,/,
&10x,'the moisture content         (%)      =',f6.2,/,/,
&10x,'the combustion zone          (m)      =',f7.3,/,/,
&10x,'the external radius (r)      (m)      =',f12.9,/,/,
&10x,'the core radius      (rw)    (m)      =',f12.9,/,/,
&10x,'the burnout time             (min)    =',f9.3,/,/)

        write(39,105)co(n),tco(0),tco(1k),tm(n),tso(1),tso(m)
&,tg(n),n
105 format(//,
&10x,'the oxygen concentration     (Kg/m3) =',f6.5,/,/,
&10x,'the centerline ( cl ) temp.  (oc)    =',f9.4,/,/,
&10x,'temp.of core nearest node to cl (oc) =',f10.4,/,/,
&10x,'interface temperature        (oc)    =',f12.6,/,/,
&10x,'temp.of shell nearest node to cl(oc) =',f12.6,/,/,
&10x,'surface temperature          (oc)    =',f10.4,/,/,
&10x,'the gas temperature          (oc)    =',f10.4,/,/,
&10x,'# of time step               =',I5 ,/)

        write(39,115)gt,hp
115 format(//,

```



## ABSTRACT

OUEDRAOGO, ABDOULAYE. Investigation of "Whole Tree" Combustion in a Packed-Bed. (Under the direction of Dr. James C. MULLIGAN and DR. John G. CLELAND.)

A shrinking core model of the combustion of individual chunkwood and particle wood elements is developed and validated by comparison with literature data. The model is formulated on the physical evidence that large wood specimens inserted into a hot environment lose weight mostly over a relatively thin outside layer, while the interior (core) remains relatively undisturbed. The modeling of the complete process requires a correlation of the turbulent heat and mass transfer coefficients which includes the effects of transpiration of volatilized organic compounds and moisture, geometry, and shrinking radius. The model shows that under boundary layer diffusion control, the external boundary layer thickness and diffusional characteristics are constantly modified by the effects of blowing. Hence, for green wood specimens, the cooling effects of transpiration and the latent heat of evaporation do slow the burning rate contrary to earlier publications. The mass and heat transfer coefficients are then modified and incorporated into the analysis of a steady state one dimensional, packed-bed model of "whole tree" combustion. The bed is assumed to be loaded uniformly from the top, countercurrent to the preheated air stream of superficial velocity  $V_s$ . The preheat time of the fuel elements is assumed negligible. The mass loss rate is formulated in a quasi-steady shrinking core submodel with a uniform core temperature approximation and negligible heat of pyrolysis. The model is simple, and yet reliable enough to predict adequately the burnout time and the depth of the combustion zone of a 100 MW "whole tree" facility, by showing that fuel elements properties (size, moisture content), strongly influence combustion characteristics, especially that higher moisture produces depressed flame temperature, longer burnout time, and larger values of combustion zone. The uniform core temperature approximation and negligible heat of pyrolysis assumption of the quasi-steady model are latter replaced by a transient moving pyrolysis front submodel. A modified *Variable Grid Method* called *Continuous Mapping Variable Grid Method (CMVGM)* is developed to solve the two-phase moving boundary problem in which in addition to the

moving interface, the external boundary of the solid fuel is receding due to combustion. With variable time step and variable radial grid, the scheme continuously tracks the position of both moving boundaries together with the position of the entire "whole tree" elements inside the bed, by continuously mapping in the core and shell regions, the computational domain of time step (n+1) to that of the previous time step (n). The results of the transient model show that indeed, the preheat time is negligible. As anticipated, the core temperature also remains approximately constant during most of the combustion process, but close to the end, it rises steadily toward the interface temperature. This is speculated to be due to the effect of "cooking" believed to be caused by rising internal pressure and fuel temperature carried inward by convective moisture and pyrolysis gases. This phenomenon, however, does not alter significantly the results of the quasi-steady model which tends to give slightly lower burnout time (3 to 10 %) and higher depth of combustion zone ( 10 to 25 %).